Bacterial H_2S oxidation coupled to the reduction of MnO_2 studied on new isolated species of the genus *Sulfurimonas*

Dissertation

zur

Erlangung des akademischen Grades

Doctor rerum naturalium (Dr. rer. nat.)

Der Mathematisch-Naturwissenschaftlichen Fakultät

Der Universität Rostock

Vorgelegt von:

Jan Henkel, geb. am 28. Juni 1989 in Fulda

aus Rostock

Rostock, den _____

https://doi.org/10.18453/rosdok_id00002580

Gutachter:

Prof. Dr. Heide Schulz-Vogt, Leibniz- Institut für Ostseeforschung Warnemünde (IOW), Geomikrobiologie

Prof. Dr. Axel Schippers, Bundesanstalt für Geowissenschaften und Rohstoffe (BGR), Geochemie der Rohstoffe

Jun.-Prof. Dr. Mirko Basen, Universität Rostock, Mikrobielle Physiologie

Jahr der Einreichung: 2019
Jahr der Verteidigung: 2019

Content

Summary I

Zusammenfassung III

1 Introduction 1

2 Material and methods 11

2.1 Preparation of anoxic cultivation medium 11

2.2 Preparation of stock solutions 12

2.2.1 Manganese oxide (MnO_2) 12

2.2.2 Elemental sulfur (S^0) 13

2.2.3 Iron oxides 13

2.2.4 Sulfide (Na_2S) 13

2.3 Origin of the three *Sulfurimonas* species 13

2.3.1 *S. marisnigri* 13

2.3.2 *S. baltica* 14

2.3.3 *S. gotlandica* 14

2.4 Culture purity of *S. marisnigri* and *S. baltica* 15

2.4.1 16S rRNA sequencing and 16S rRNA clone libraries 15

2.5 Genome sequencing of *S. marisnigri* 16

2.5.1 DNA isolation 16

2.5.2 DNA sequencing 17

2.5.3 Genome assembly and annotation 17

2.6 Analysis of cell counts 17

2.6.1 DAPI stained epifluorescence microscopy 17

2.6.2 Flow-cytometry 18

2.7 Chemical analyses 20

2.7.1 Sulfur species 20

2.7.2 Metals and calcium (Ca) 21

2.7.3 Total inorganic carbon (TIC) 23

2.7.4 Cellular polyphosphate (polyP) 23

2.7.5 Nitrate (NO_3^-) and nitrite (NO_2^-) 24
2.8 Analysis of O_2, pH and H_2S with microsensors 24
2.9 Combined imaging and elemental quantification 24
2.9.1 Scanning electron microscopy (SEM) and energy dispersive X-ray spectroscopy (EDX) analysis 24
2.9.2 Nanoscale secondary ion mass spectrometry (NanoSIMS) 25
2.9.3 He- ion microscopy and secondary ion mass spectrometry (HIM-SIMS) 26
2.10 Rate calculations with exponential curve fitting 27
2.11 Numerical modeling 27
2.12 Experimental design, cultivation conditions and specific supplementation 29
2.12.1 Particle dynamics analyzed with NanoSIMS 29
2.12.2 Dynamic of Mn and S species during growth of *S. marisnigri* 29
2.12.3 *S. marisnigri* and *S. baltica* grown with NO_3^- and H_2S additions 31
2.12.4 *S. marisnigri* grown with MnO_2 and additions of H_2S or H_2S pre-reacted with MnO_2 31
2.12.5 Determination of H_2S oxidation rates of *S. marisnigri* 32
2.12.6 Dissimilatory metabolism – electron acceptors 33
2.12.7 Dissimilatory metabolism – electron donors 34
2.12.8 Disproportionation of S^0 and $S_2O_3^{2-}$ 35
2.12.9 SO_4^{2-} - reduction 35
2.12.10 Fermentation 35
2.12.11 Assimilatory metabolism 36
2.12.12 Abiotic factors influencing growth 36
3 Results 38
3.1 Chapter I: Reduction of MnO_2 coupled to the oxidation of $S_2O_3^{2-}$ and H_2S 38
3.2 Chapter II: Influence of a biological H_2S oxidation on the geochemical structure of the Black Sea suboxic zone 48
3.2.1 Estimation of a biological H_2S oxidation rate in the presence of MnO_2 48
3.2.2 Numerical modeling 50
3.3 Chapter III: Ecological niches of the newly isolated *Sulfurimonas* strains in comparison to *S. gotlandica*. 53

3.3.1 Dissimilatory metabolism - electron acceptors 53
3.3.2 Dissimilatory metabolism - electron donors 57
3.3.3 Disproportionation of S^0 and $S_2O_3^{2-}$ 59
3.3.4 Sulfate (SO_4^{2-}) - reduction 60
3.3.5 Fermentation 60
3.3.6 Assimilatory metabolism 61
3.3.7 Abiotic factors influencing growth 63
4 Discussion 70
4.1 Bacterial sulfur oxidation coupled to Mn reduction and a general view onto pelagic redoxclines with focus on the Black Sea 70
4.2 Mechanism of MnO_2 reduction and potential implications for $Mn(Ca)CO_3$ authigenesis 77
4.2.1 Biological MnO_2 reduction and competition with an abiotic reaction 77
4.2.2 Theoretical implications for the authigenesis of $Mn(Ca)CO_3$ 78
4.3 Ecological potential of *S. marisnigri*, *S. baltica* and *S. gotlandica* in comparison to other species of the genus *Sulfurimonas* 81
4.3.1 Electron acceptors 81
4.3.2 Disproportionation 85
4.3.3 Electron donors 86
4.3.4 Organic carbon oxidation, fermentation and sulfate reduction 88
4.3.5 Assimilatory metabolism 89
5 Conclusion and outlook 91
6 References 94
7 Acknowledgements V
Erklärung VII

Summary

Elevated primary production due to eutrophication of e.g. marginal seas like the Black Sea or the Baltic Sea leads to declining oxygen (O_2) concentrations and ultimately to anoxic conditions in and above sediments. The degradation of organic matter in the absence of O_2 by sulfate reducing bacteria fosters the accumulation of toxic sulfide (H_2S) in marine basins, also called “dead zones”. The reoxidation of H_2S has been observed in the pelagic redoxcline of the Black Sea in the absence of O_2, nitrate (NO_3^-) and light. In the respective water depth of H_2S removal, chemoautotrophic bacteria were fixing carbon dioxide (CO_2), which raises the question how these organisms generate energy for cellular activity. In this study two new species of the genus *Sulfurimonas*, namely *S. marisnigri* and *S. baltica* are described, originating from the Black Sea and the Baltic Sea, respectively. *S. marisnigri* and *S. baltica* reduce manganese oxide (MnO_2) with H_2S, elemental sulfur (S^0), thiosulfate ($S_2O_3^{2-}$) and hydrogen (H_2) as electron donors. The utilization of reduced sulfur compounds for the reduction of Mn was suggested since the late 1980s, but evidence was missing until now. *S. marisnigri* oxidizes H_2S and $S_2O_3^{2-}$ to SO_4^{2-}, thereby reducing the particulate MnO_2 to dissolved reactive Mn (putative Mn^{3+}) and Mn^{2+}, which ultimately precipitates as a Ca-rich manganese carbonate, here referred to as $Mn(Ca)CO_3$. It is hypothesized, that the energy metabolism of *S. marisnigri* is altering the chemical boundary conditions at the Mn particle surface, which fosters the authigenesis of $Mn(Ca)CO_3$ at the surface of MnO_2 particles, which was also observed in natural habitats, but the mechanism of formation is still under debate.

The H_2S oxidation rate per cell of *S. marisnigri* in the presence of MnO_2 was estimated and integrated into a numerical model to reconstruct the H_2S profile in the water column of the Black Sea. It is shown that the shape of the H_2S concentration profile and the depth of the ultimate removal of H_2S were depending on high local oxidation rates coinciding with the abundance of *Sulfurimonas* and the expression of the sulfide:quinone oxidoreductase gene

(*sqr*). The formation and maintenance of pelagic redoxclines with a separation of O_2 and H_2S of several meters is discussed with the Black Sea as an example.

S. marisnigri and *S. baltica* were cultivated along with the closely related species *S. gotlandica*. Potential electron acceptors and electron donors for growth, assimilatory C and N metabolism as well as the influence of the abiotic parameters temperature, salinity, pH and O_2 on growth were investigated. The results of these growth experiments and the genomic sequence data of *S. marisnigri* were discussed in comparison to other cultured species of the genus. As an example, it appeared that *S. marisnigri* and *S. baltica* are the first N_2 fixing strains of the genus, despite ammonia (NH_4^+) is usually available in sufficient amount in their natural habitat.

The results of this thesis showed the existence of a bacterial metabolism connecting the marine Mn and S cycles with implications on the water column biogeochemistry of euxinic basins. Further, the precipitation of $Mn(Ca)CO_3$ in pure culture experiments might offer a plausible explanation for sediment layers rich in Ca-rich manganese carbonate, which is discussed and hypothesized.

Zusammenfassung

Erhöhte Primärproduktion aufgrund der Eutrophierung von z.B. Randmeeren wie dem Schwarze Meer oder der Ostsee führen zu sinkenden Sauerstoffkonzentrationen (O_2) und letztendlich zu anoxischen Bedingungen an und in Sedimenten. Der Abbau von organischem Material in Abwesenheit von O_2 durch bakterielle Sulfatreduktion führt zu Anreicherung von giftigem Sulfid (H_2S) in sedimentnahen Wasserkörpern, die auch als "tote Zonen" bezeichnet werden. Die Reoxidation von H_2S wurde in der pelagischen Redoxkline des Schwarzen Meeres in Abwesenheit von O_2, Nitrat (NO_3^-) und Licht beobachtet. In der entsprechenden Wassertiefe der H_2S Oxidation fixieren autotrophe Bakterien Kohlenstoff-dioxid (CO_2), was die Frage aufwirft, wie diese Organismen metabolisch Energie generieren. In dieser Studie werden zwei neue Arten der Gattungen *Sulfurimonas*, *S. marisnigri* und *S. baltica*, beschrieben, die aus dem Schwarzen Meer bzw. der Ostsee isoliert wurden. *S. marisnigri* und *S. baltica* reduzieren Manganoxid (MnO_2) mit H_2S, elementarem Schwefel (S^0), Thiosulfat ($S_2O_3^{2-}$) und Wasserstoff (H_2) als Elektronendonatoren. Die Verwendung von reduzierten Schwefelverbindungen zur Reduktion von Mn wurde seit den späten 1980er Jahren vermutet, jedoch fehlten bis jetzt Beweise aus Kultivierungen. *S. marisnigri* oxidiert H_2S und $S_2O_3^{2-}$ zu SO_4^{2-}, wodurch das partikuläre MnO_2 zu gelöstem reaktivem Mn (Mn^{3+}) und Mn^{2+} reduziert wird, das schließlich als Ca-reiches Mangancarbonat ausfällt und in dieser Arbeit als $Mn(Ca)CO_3$ bezeichnet wird. Es wird diskutiert, dass der Energiestoffwechsel von *S. marisnigri* die chemischen Parameter an der Partikeloberfläche verändert und die Authigenese von $Mn(Ca)CO_3$ an der Oberfläche von MnO_2-Partikeln fördert.

Die H_2S-Oxidationsraten pro Zelle von *S. marisnigri* in Gegenwart von MnO_2 wurde bestimmt und in ein numerisches Modell zur Berechnung des H_2S Profils des Schwarzen Meeres integriert. Dabei wird gezeigt, dass die Form des H_2S Profils und die Tiefe der endgültigen Entfernung von H_2S von hohen lokalen Oxidationsraten abhängen, die mit der Häufigkeit von *Sulfurimonas* und der Expression des Sulfid:Quinone Oxidoreduktase-Gens

(*sqr*) zusammenfallen. Anhand dieser Ergebnisse wird die Bildung und Aufrechterhaltung von pelagischen Redoxklinen mit einer Trennung von O_2 und H_2S von mehreren Metern am Beispiel des Schwarzen Meeres diskutiert.

S. marisnigri und *S. baltica* sowie die nah verwandten Art *S. gotlandica* wurden kultiviert. Potentielle Elektronenakzeptoren und Elektronendonatoren, die Assimilation von C und N, sowie der Einfluss der abiotischen Parameter Temperatur, Salzgehalt, pH-Wert und O_2 auf das Wachstum der drei Stämme wurden untersucht. Die Ergebnisse dieser Wachstums-experimente und die genomischen Sequenzdaten von *S. marisnigri* wurden im Vergleich zu anderen kultivierten Arten der Gattung diskutiert. Beispielsweise scheinen *S. marisnigri* und *S. baltica* die ersten N_2-fixierenden Stämme der Gattung zu sein, obwohl Ammonium (NH_4^+) in ausreichender Menge in ihrem natürlichen Lebensraum vorhanden ist.

Die Ergebnisse dieser Arbeit zeigen die Existenz eines bakteriellen Metabolismus, der die marinen Mn- und S- Zyklen verbindet und Auswirkungen auf die Wassersäulenbiogeochemie von euxinischen Systemen hat. Darüber hinaus könnte die Ausfällung von $Mn(Ca)CO_3$ eine plausible Erklärung für Ca-reiche Mangancarbonat-haltige Sedimentschichten liefern.

1 Introduction

The conversion of inorganic nutrients like carbon dioxide (CO_2) or ammonia (NH_4^+) into organic molecules, organic matter or living matter like DNA or amino acids is called primary production. With carbon as the most important element as an example, the fixation of CO_2 and the conversion into organic molecules by light dependent oxygenic photosynthesis can be expressed as shown in Eq. 1.1.

$$CO_2 + H_2O \xrightarrow{\text{light}} [CH_2O] + O_2 \qquad 1.1$$

The assimilation of inorganic carbon as carbon source is called autotrophy and can also be light independent (dark CO_2 fixation). In this process, carbon is reduced from a +IV oxidation state in CO_2 to 0 in the organic molecule [CH_2O], which is crucial to form C-C polymers, thereby accepting 4 mole of electrons (e^-) per mole of CO_2 fixed. The degradation of organic carbon back to the inorganic nutrient CO_2 is called respiration and is performed by organotrophic organisms. The dissimilatory respiration of organic carbon to CO_2 in return is releasing 4 mole of e^-, transferred to an electron acceptor, which is oxygen (O_2) in the so called oxic respiration.

O_2 solubility in sea water is limited and depending on temperature as well as salinity and ranges from 456 µM (0 °C; 0 g/kg) to 231 µM (20 °C; 35 g/kg) (Ramsing & Gundersen, 2011). The depth profile of dissolved O_2 in the ocean or marginal seas is typically uniform and close to saturation in the mixed surface water layer and decreases below due to the oxic remineralization of sinking organic matter (Stramma et al., 2008). In systems with hampered deep water ventilation, i.e. lacking O_2 transport into deeper parts of the system, e.g. due to density stratification, the O_2 demand for the remineralization of organic matter can exceed the ambient concentrations of O_2 easily, which leads to low O_2 concentrations and ultimately to anoxia, with far reaching consequences for higher organisms. In the course of climate change, rising water temperatures decrease the O_2 solubility and hampers thermohaline circulation,

thereby reducing the amount of O_2 transported to the deep ocean (Schmidtko et al., 2017). Likewise, increased nutrient input from excessive agriculture stimulates primary production and ultimately O_2 demand in deeper waters (Diaz & Rosenberg, 2008).

In the absence of O_2, organic matter is degraded anaerobically by the utilization of alternative electron acceptors. Anaerobic degradation of organic matter follows a sequence of alternative electron acceptors (Fig. 1) based on the potential energy yield of the respective redox reaction (Froelich et al., 1979) as summarized in Tab. 1. Because the large availability of SO_4^{2-} with about 28 mM in sea water with a salinity of 35 (Jørgensen et al., 2019) exceeds the nano- to micromolar concentrations of nitrate (NO_3^-), MnO_2 and iron (Fe) oxides by orders of magnitude, SO_4^{2-} is the most important electron acceptor for anaerobic organic matter degradation. Consequently, 25 – 50% of the organic carbon may be remineralized by sulfate reducing bacteria in marine shelf sediments in the absence of O_2 (Jørgensen, 1982), despite

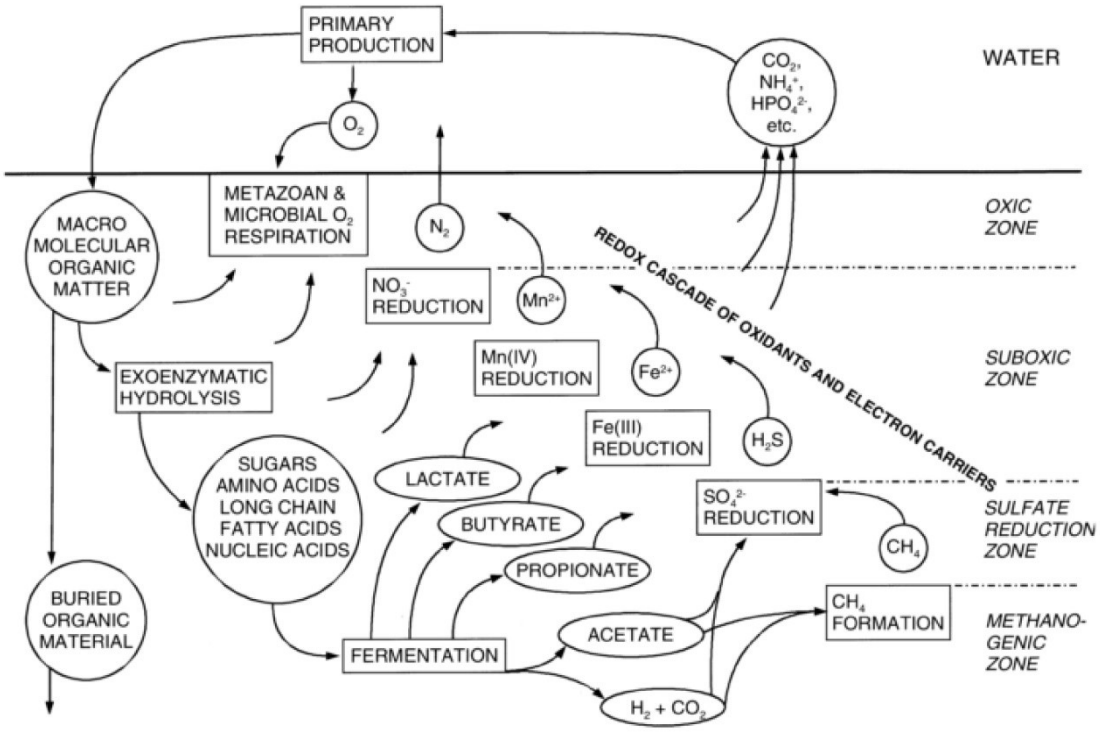

Figure 1: From Jørgensen (2000). Pathways of organic matter degradation in the water column and sediment. Degradation of organic matter to low molecular weight biogenic material like sugars, amino acids or fatty acids and finally inorganic compounds like CO_2, NH_4^+, HPO_4^{2-} etc. is consuming O_2 and a sequence of alternative electron acceptors as soon as O_2 becomes limited.

Table 1: Adapted from Jørgensen (2000). Data from Thauer et al. (1977), Conrad et al. (1986) and Fenchel & King (1998). Sequence of potential energy yield of organic matter respiration processes from oxic respiration to methanogensis. ΔG^0 values in kJ mol^{-1} [CH_2O].

Respiration process	e^- Acc.	Product	ΔG^0 (kJ mol^{-1})
Oxic respiration			
$[CH_2O] + O_2 \rightarrow CO_2 + H_2O$	O_2	H_2O	-479
Denitrification / Nitrate reduction			
$5\,[CH_2O] + 4\,NO_3^- \rightarrow 2\,N_2 + 4\,HCO_3^- + CO_2 + 3H_2O$	NO_3^-	N_2	-453
Manganese oxide reduction			
$[CH_2O] + 3\,CO_2 + H_2O + 2\,MnO_2 \rightarrow 2\,Mn^{2+} + 4\,HCO_3^-$	MnO_2	Mn^{2+}	-349
Iron oxide reduction			
$[CH_2O] + 7\,CO_2 + 4\,Fe(OH)_3 \rightarrow 4\,Fe^{2+} + 8\,HCO_3^- + 3\,H_2O$	$Fe(OH)_3$	Fe^{2+}	-114
Sulfate reduction			
$2\,[CH_2O] + SO_4^{2-} \rightarrow H_2S + 2\,HCO_3^-$	SO_4^{2-}	H_2S	-77
Methanogenesis			
$CH_3COO^- + H^+ \rightarrow CH_4 + CO_2$	CH_3COO^-	CH_4	-28

the low energy yield (ΔG^0 = -77 kJ mol^{-1} [CH_2O]) compared to aerobic respiration (ΔG^0 = -479 kJ mol^{-1} [CH_2O]) or Mn reduction (ΔG^0 = -349 kJ mol^{-1} [CH_2O]) (Tab. 1).

Anaerobic respiration results in the formation of reduced compounds of N, Mn, Fe, S and C; NH_4^+, Mn^{2+}, Fe^{2+}, sulfide (H_2S here referred to as $\sum H_2S$, HS^- and S^{2-}) and methane (CH_4), respectively (Tab. 1, Fig. 1). Next to the demand for O_2 and the oxidized forms of the above mentioned elements for organic matter degradation, also the reoxidation of the reduced compounds requires oxidation potential. As pointed out above, SO_4^{2-} reduction is by far the most important process for anaerobic organic matter degradation. Consequently, H_2S is a common end product that is toxic to higher organisms even in low concentrations (Evans, 1967). As long as the reoxidation of H_2S (Tab. 2) is equally effective as the concurrent sulfate reduction, H_2S remains undetectable (Jørgensen et al., 2019). Next to an effective reoxidation, H_2S is also trapped in iron mono-sulfide precipitates (FeS) with Fe^{2+} ions, which also prevents the formation of free H_2S and the release out of the sediment (Rickard & Luther III, 2007). As soon as sulfate reduction rates exceed the concurrent reoxidation and binding capacitvy of the Fe pool, free H_2S will be detectable, which is described as euxinic condition (King, 2004;

Table 2: Electron acceptors for the oxidation of H_2S and the respective potential free energy at standard conditions and pH7 ($\Delta G^{0'}$) per mole H_2S or per electron transferred. Values for the calculation were taken from Thauer et al. (1977) and Stumm & Morgan (1996).

Electron acceptor for H_2S oxidation (1 atm, 25 °C, pH7)	$\Delta G^{0'}$ (kJ mol^{-1} H_2S)	$\Delta G^{0'}$ (kJ mol^{-1} e^-)
Oxygen		
$HS^- + 2\,O_2 \rightarrow SO_4^{2-} + H^+$	-797	-100
Nitrate (Denitrification)		
$5\,HS^- + 8\,NO_3^- + 3\,H^+ \rightarrow 5\,SO_4^{2-} + 4\,N_2 + 4\,H_2O$	-744	-93
Manganese oxide		
$HS^- + MnO_2 + 3\,H^+ \rightarrow S^0 + Mn^{2+} + 2\,H_2O$	-130	-65
$HS^- + 4\,MnO_2 + 7\,H^+ \rightarrow SO_4^{2-} + 4\,Mn^{2+} + 4\,H_2O$	-478	-60

Rickard & Luther III, 2007). The former sedimentary redoxcline, as the depth boundary to waters with detectable free H_2S, can move into the water column by leakage of H_2S out of the sediment and form a pelagic redoxcline.

Pelagic redoxclines in marine systems are frequently reported from semi enclosed basins and/or water systems with a strong density stratification like the Black Sea (Murray et al., 1989), the Baltic Sea (Grote et al., 2007; Dellwig et al., 2010; Jost et al., 2010), the Cariaco Basin (Taylor et al., 2001), the Saanich Inlet (Zaikova et al., 2010) or the Framvaren Fjord (Mandernack & Tebo, 1999). High nutrient load together with limited ventilation fosters severe accumulation of free H_2S formed by SO_4^{2-} reduction in bottom waters. A lower cellular abundance of 10^4 - 10^6 cells mL^{-1} in pelagic redoxclines compared to 10^8 - 10^{10} cells cm^{-3} (Canfield et al., 2005) in sedimentary redoxclines with accordingly lower reaction rates results in less steep concentration gradients and spreads this zone of intensive element cycling from centimeter to meter scale, allowing high resolution sampling and investigation of the underlying processes. A frequently studied system with a permanent stratified water column and pelagic redox transition zone is the Black Sea.

With a maximum depth of about 2200 m, an area of 4.2 x 10^5 km^2 and a volume of 5.3 x 10^5 km^3, the Black Sea is the largest semi enclosed basin in the world (Özsoy & Ünlüata, 1997). Inflow of high saline waters from the Mediterranean Sea through the Bosporus strait and

inflow of freshwater from rivers causes vertical density stratification due to a shift in salinity from 18 in the freshwater effected surface waters to a salinity of 22 in bottom waters (Dellwig et al., 2012). This density gradient restricts the mixing of the surface waters to a maximum depth between 60 and 80 m water depth, below turbulent diffusion controls fluxes (Murray et al., 1991; Gregg & Yakushev, 2005; Yakushev et al., 2006). The lacking deep water renewal and organic matter degradation by SO_4^{2-} reduction fosters severe accumulation of H_2S in bottom waters starting approximately 50 m below the mixing depth of 60 – 80 m, resulting in the accumulation of 4.6 x 10^{15} g H_2S due to bacterial SO_4^{2-} reduction in the water body of the Black Sea (Lev N. Neretin, PhD thesis cited in Neretin et al., 2006), leaving just 13% of the total volume with oxic conditions (Özsoy & Ünlüata, 1997). Murray et al. (1989) reported for the first time the existence of a up to tens of meters thick zone lacking O_2 and H_2S, a so called suboxic zone (Fig. 2A).

At the bottom boundary of this suboxic zone at the chemocline, H_2S is disappearing (Fig. 2A and B) more than 10 meters below detectable concentrations of NO_3^- and O_2 (Murray &

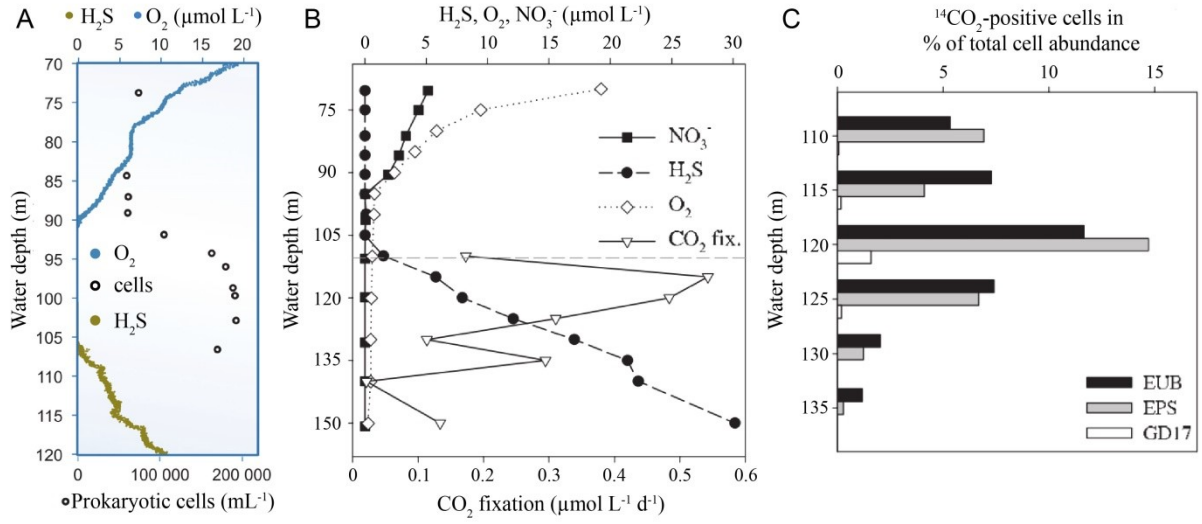

Figure 2: Chemical profile, chemolithoautotrophic activity and involved bacterial groups of the Black Sea suboxic zone. A, O_2 and H_2S concentration profiles together with total prokaryotic abundance (from Schulz-Vogt et al., 2019). NO_3^- is approaching 0 at a water depth of 94 m. B, Black Sea suboxic zone together with CO_2 fixation rates. C, Percentage of autotrophic bacteria ($^{14}CO_2$-positive cells) of the total bacterial community and importance of the group *Epsilonbacteraeota* (EPS). B and C from Grote et al. (2008).

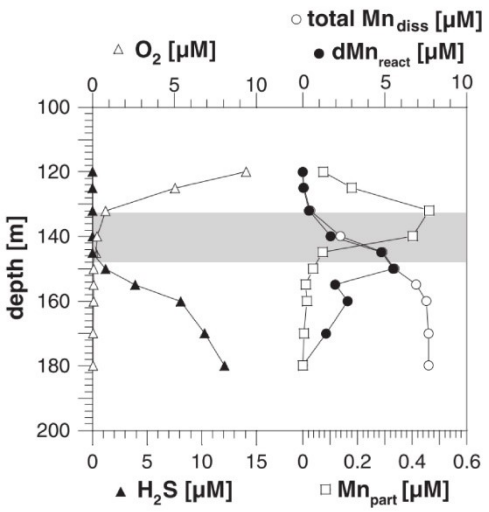

Figure 3: From Dellwig et al., 2012. Mn cycling across the Black Sea suboxic zone. Cycling of particulate Mn (Mn_{part}) to dissolved (total Mn_{diss}) reactive Mn (dMn_{react}) with active transformation at the upper and lower boundary of the suboxic zone and act as a trap for Mn thereby reaching concentrations of about 9 µM.

Yakushev, 2006; Canfield & Thamdrup, 2009; Schulz-Vogt et al., 2019) raising the question of which compound is oxidizing H_2S. Based on the bacterial abundance in the suboxic zone compared to overlying and underlying waters (Fig. 2A) together with high dark CO_2 fixation rates at and below the chemocline (Fig. 2B) it could be suggested that autotrophic bacteria are responsible for the oxidation of H_2S. However, phototrophic oxidation of H_2S has been shown to be of minor importance in the Black Sea (Overmann et al., 1992) and the established electron acceptors for bacterial H_2S oxidation, NO_3^- and O_2, are absent in the respective depth of H_2S removal (Fig. 2A and B). Oxidation of H_2S could be coupled to Mn (Fig. 3). Mn is a redox sensitive trace metal, which is particulate in the oxidized form MnO_2 (+IV) and typically dissolved in the reduced ion form Mn^{2+}. The reduced and dissolved Mn^{2+} is transported upwards by turbulent mixing and is reoxidized biologically and chemically with O_2 to particulate MnO_2 at the upper boundary of the suboxic zone, which is again transported via gravitational sinking towards the sulfidic bottom waters (Burdige & Nealson, 1985, 1986; Lewis & Landing, 1991; Tebo, 1991; Tebo et al., 2004). This cycle effectively traps Mn in the suboxic zone and the total concentrations reaches concentrations of about 9 µM (Fig. 3).

Sulfur transformation processes are manifold including inorganic fermentation (disproportionation), oxidation and reduction reactions with a huge variety of electron donors and acceptors as well as redox and equilibrium reactions between sulfur species of different oxidation state (Fig. 4), including abiotic and biotic modes (Siu & Jia, 1999; Jørgensen et al., 2019). The oxidation of H_2S with MnO_2 can be a purely chemical process, but some obser-

vations speak up against a pure abiotic scenario in the water column of the Black Sea. The abiotic reaction is reported to be fast and complete within minutes in chemical experiments with high concentrations of both reactants (>0.5 M MnO_2; 150 µM H_2S - Burdige & Nealson, 1986). The speed of the chemical H_2S oxidation by MnO_2 in sea water depends on the pH, the surface area of the MnO_2 particle and the concentration of H_2S (Yao & Millero, 1993, 1996; Herszage & dos Santos Afonso, 2003). The products of the chemical H_2S oxidation by MnO_2 in sea water depend on the pH and the ratio between H_2S and MnO_2 (Yao & Millero, 1996; Herszage & dos Santos Afonso, 2003).

Based on these chemical studies elemental sulfur (S^0), thiosulfate ($S_2O_3^{2-}$), sulfite (SO_3^{2-}) and SO_4^{2-} are the oxidation products of a chemical oxidation with MnO_2 in sea water, with S^0 as the dominant reaction product. A low MnO_2 to H_2S ratio and higher pH fosters the formation of elemental sulfur as oxidation product (Yao & Millero, 1996; Herszage & dos Santos Afonso, 2003). The speed of the chemical reaction is maximal at pH 5 and decreasing towards lower and higher pH values (Yao & Millero, 1996). At the redoxcline of Black Sea approximately 20 nM MnO_2 and < 5 µM H_2S were reported at near neutral pH (Fig. 2 and 3). Under these conditions elemental sulfur should be the almost exclusive reaction product at the chemocline of Black Sea, but no major accumulation of this or other intermediate compounds have been reported (Jørgensen et al., 1991; Luther III et al., 1991; Glazer et al., 2006). In con-

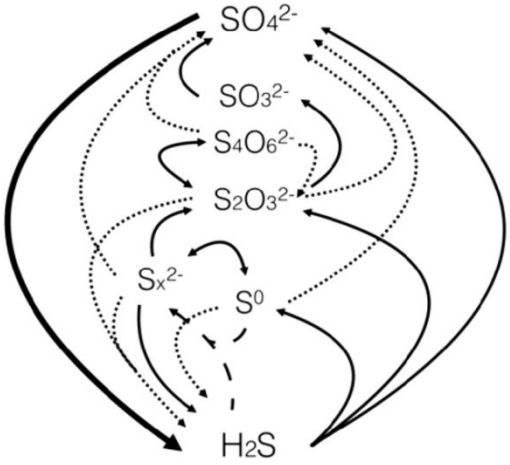

Figure 4: from Zopfi et al. (2004) modified from Jørgensen et al. (2019). Transformation processes of the important inorganic species of the sulfur cycle. Large black arrow represents sulfate reduction, thin black arrows oxidation reaction and dotted lines disproportionations. Dashed lines represent equilibrium reaction to form polysulfides (S_x^{2-}). Mean oxidation state of S are as follows: H_2S (-2), elemental sulfur S^0 (0), thiosulfate $S_2O_3^{2-}$ (+2), tetrathionate $S_4O_6^{2-}$ (+2.5), sulfite SO_3^{2-} (+4) and SO_4^{2-} (+6).

trast, biological H_2S oxidation by lithotrophic bacteria is typically complete to SO_4^{2-} [e.g. S oxidation coupled to denitrification by *Sulfurimonas gotlandica* GD1 (Grote et al., 2012) or S oxidation coupled to O_2 by *Beggiatoa* sp. (Nelson et al., 1986)] which would explain the absence of accumulating sulfur intermediates.

Even though the reaction of H_2S and MnO_2 is reported to be fast in chemical studies, it is emphasized, that the speed of the reaction is depending on the pH and the concentrations of both reactants. At the redoxcline of the Black Sea, concentrations of H_2S and MnO_2 are low (Fig. 2 and 3) which should result in overall low reaction rates (Yao & Millero, 1993) and should affect the overall concentration profile of H_2S. This was shown by Nelson et al. (1986) in culture experiments (Fig. 5). Depending on the absence (Fig. 5A) or presence (Fig. 5B) of *Beggiatoa*, the depth profiles of O_2 and H_2S were completely different. Biological H_2S oxidation coupled to the reduction of O_2 by *Beggiatoa* sp. is 10,000 to 100,000 times faster compared to the corresponding chemical reaction (Jørgensen & Revsbech, 1983). These high reaction rates result in the increased fluxes of both reactants (Fig. 5, Jørgensen & Revsbech,

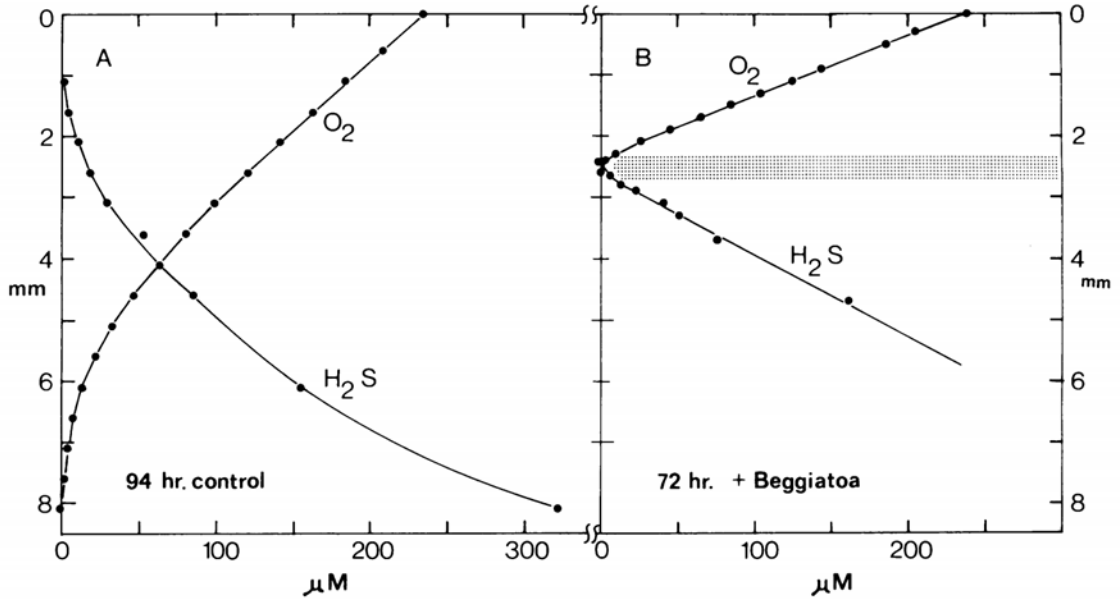

Figure 5: From Nelson et al. (1986). Depth profile of O_2 and H_2S in a marine sediment, either with or without a *Beggiatoa* mat. Without the fast biological H_2S oxidation rates by *Beggiatoa* (B), concentration profiles of the reactants O_2 and H_2S overlap in control sediment cores (A). Higher oxidation rates did also result in steeper concentration gradients and thereby in higher fluxes of both, H_2S and O_2.

1983; Nelson et al., 1986) and to a pronounced change from a curved (Fig. 5A, abiotic) to a linear concentration gradient (Fig. 5B, biological) of both, O_2 and H_2S. Due to the high reaction rates, the depth horizon of active H_2S oxidation with O_2 is diminished from 6.7 mm (Fig. 5A) to 0.3 mm (Fig. 5B), resulting in the apparently linear concentration gradients in the upper centimeter of the cultivation tube. Similarly, also the oxidation rates of H_2S in pelagic redoxclines will shape the form of the gradient in situ and thus the observed linear concentration gradient (Fig. 2A and B) indicates a fast H_2S oxidation rate in a narrow zone. It can be assumed that the faster the reaction, biological, chemical or both, the smaller the overlap of oxidant and reductant and consequently the more linear the concentration gradient appears in the depth profile.

The reduction of MnO_2 for the degradation of organic matter is known for species of e.g. the genera *Shewanella* and *Geobacter* (Myers & Nealson, 1988; Lovley, 1991) but so far no isolate existed that couples the oxidation of H_2S to the reduction of MnO_2. However, indirect evidence for a bacterially mediated H_2S oxidation with MnO_2 came from marine sediments. Aller & Rude (1988) and King (1990) reported the formation of SO_4^{2-} when MnO_2 was added to anoxic sediment slurries, which was inhibited by the addition of 2,4-dinitrophenol and sodium azide, indicating a biological mode of SO_4^{2-} formation. Interestingly, SO_4^{2-} formation could not be stimulated by the addition of Fe-oxides. Thus, the formation of SO_4^{2-} was unlikely a combination of an abiotic oxidation of H_2S to S^0 and subsequent bacterial disproportionation to H_2S and SO_4^{2-}, because S^0 would also form with Fe-oxides (Yao & Millero, 1996). In any case, unambiguous evidence for a biologically mediated oxidation of H_2S with MnO_2 can only be drawn from experiments with isolated pure cultures.

In the present work, two new species of the genus *Sulfurimonas* were investigated. The strains *Sulfurimonas marisnigri* and *S. baltica* were enriched and isolated with MnO_2 provided as the sole electron acceptor. With *S. marisnigri*, originating from the lower boundary of the Black Sea suboxic zone, studies on biological Mn reduction coupled to the oxidation of reduced

sulfur compounds, dynamics of Mn and S during the growth phase of *S. marisnigri* and estimations of biological H_2S oxidation rates were done. *S. baltica*, originating from a turbulent redoxcline of the central Baltic Sea after salt water inflow from the North Sea, was cultured as well as *S. marisnigri* and *S. gotlandica* to examine the metabolic potential of the two new isolated strains in comparison to a well-documented species of the genus. Results of the growth experiments from *S. marisnigri* and *S. gotlandica* were further compared and discussed with the annotated genomes of both species.

2 Material and methods

2.1 Preparation of anoxic cultivation medium

The Standard medium for cultivation and experiments, if not mentioned otherwise, was prepared following the technique described by Widdel & Pfennig (1981) based on sulfate free artificial seawater with a salinity of 21, 14, or 10 for *S. marisnigri*, *S. baltica* or *S. gotlandica*, respectively. Artificial seawater of the different salinities was prepared by dissolving the dry chemicals in 1 L of MilliQ water (Tab. 3).

The artificial seawater was filled into a special glass vessel, colloquially called "Widdelkolben", autoclaved and subsequently cooled under a constant flow of N_2 gas with 10 to 30% CO_2 to purge O_2 to achieve anoxic conditions. After 10 minutes of gas flow, the glass vessel was closed and a slight overpressure was maintained to avoid contamination of air and to speed up the pH adjustment by the formation of carbonic acid. After cooling, the components listed in Tab. 4 were added. Solutions of $NaHCO_3$ and NH_4Cl were prepared with Ar purged MilliQ water and autoclaved under Ar atmosphere. Components of the trace elements solution SL7 and the vitamin solution are listed in Tab. 5 and 6, respectively. No resazurin was added to the medium because growth of *S. marisnigri* with particle metal oxide electron acceptors was apparently suppressed by the redox indicator.

Table 3: Components of sulfate free artificial seawater with different salinities for the three *Sulfurimonas* strains.

Dry chemical	g L^{-1}		
	Sal. 21	**Sal. 14**	**Sal. 10**
NaCl	17.7	11.8	8.5
$MgCl_2 \cdot 6\ H_2O$	3.2	2.2	1.5
$CaCl_2 \cdot 2\ H_2O$	0.4	0.3	0.2
KCl	0.7	0.4	0.3

Table 4: Solutions added to artificial seawater for the preparation of standard anoxic medium.

solution	mL L^{-1}
1 M $NaHCO_3$	30
100 mM NH_4Cl	0.2
Trace elements solution SL7 (Tab.5)	1
10 mM Na_2HPO_4	1
Vitamin solution (Tab.6)	0.42

Further, no reducing agent was added to the standard medium. The pH of the medium was adjusted to approximately 7.5 by the exposure time to the anoxic N_2 gas mixture containing 10 to 30% CO_2. After the pH was reached, the medium was dispensed into 100 mL or 150 mL sterile serum bottles, with a small headspace volume of 10 – 20 mL, which was exchanged by the respective anoxic gas mixture several times and closed with gas tight butyl rubber stoppers. All additions and bottling were performed in a sterile working bench. Bottles were stored in the dark at 10 °C. Substrates were added to the prepared medium before inoculation.

2.2 Preparation of stock solutions

Stock solutions were prepared by adding the respective chemical to anoxic MilliQ water, purged with Ar or N_2, in serum bottles closed with butyl rubber stoppers. Solution and headspace were purged for at least 1 hour with Ar or N_2 gas by penetrating the rubber stopper with two cannulas, one to the ground of the bottle and one to provide a gas outflow. Afterwards, stock solutions were heat sterilized in closed bottles and stored in the refrigerator.

2.2.1 Manganese oxide (MnO_2)

Technical MnO_2 was purchased as powder from Merck (Darmstadt, Germany) and additionally grinded with an agate ball mill. The ground MnO_2 was added to Ar/N_2 purged MilliQ

Table 5: Components of the trace elements solution SL7 from Widdel and Pfennig (1981) filled to 1 L with MilliQ water.

Solution or dry chemical	Added amount
25% HCl	10 mL
$FeCl_2 \cdot 4\ H_2O$	1.5 g
$CoCl_2 \cdot 6\ H_2O$	0.19 g
$MnCl_2 \cdot 4\ H_2O$	0.1 g
$ZnCl_2$	0.07 g
H_3BO_3	0.062 g
$Na_2MoO_4 \cdot 2\ H_2O$	0.036 g
$NiCl_2 \cdot 6\ H_2O$	0.024 g
$CuCl_2 \cdot 2\ H_2O$	0.017 g

Table 6: Components of the vitamin solution dissolved in MilliQ water.

Vitamin	g L^{-1}
B 12	0.1
Inositol	0.1
Biotin	0.1
Folic acid	0.1
4-Aminobenzoic acid	1
Nicotinic acid	10
d-pantothenate	10
Thiamine	20

water with different final molarities and used as stock solution. Final suspension was again purged with Ar or N_2 as described above and autoclaved under O_2 free atmosphere. Extraction of MnO_2 from the MnO_2 suspension was done with syringes under constant shaking. All experiments shown in this work were conducted with MnO_2 of the same batch.

2.2.2 Elemental sulfur (S^0)

Elemental sulfur was prepared as colloidal S^0 according to Blumentals et al. (1990) with a final concentration of approximately 0.4 M or slightly lower due to minimal losses during washing steps. The final suspension was purged with Ar or N_2 as described earlier and applied as a non-sterile suspension to the respective experiments.

2.2.3 Iron oxides

Amorphous FeOOH and goethite (α-FeOOH) were precipitated as described by Lovley & Phillips (1986). The resulting precipitates were washed with Ar or N_2 purged MilliQ water until the salinity decreased below 10, which was measured with a refractometer. The suspensions of amorphous FeOOH and goethite were purged with Ar or N_2 as described above and autoclaved under O_2 free atmosphere.

2.2.4 Sulfide (Na_2S)

Crystals of Na_2S were dissolved in anoxic MilliQ water, transferred into a serum bottle, purged with Ar or N_2 as described above and autoclaved under O_2 free atmosphere.

2.3 Origin of the three *Sulfurimonas* species

2.3.1 *S. marisnigri*

S. marisnigri originates from the Black Sea (44°-16.7586 N and 36°-18.9567 E) at the lower boundary of the suboxic zone (σ_θ = 16.145) where H_2S was just detectable [see Fig. 1 in (Henkel et al., 2019)]. Initial water sampling and enrichment was done by Prof. Dr. Heide N. Schulz-Vogt. Water was sampled at the 21th of November 2013 and filled into a gas tight

Figure 6: Dilution to extinction series with MnO_2 and $S_2O_3^{2-}$ to isolate *S. marisnigri*. From left to right: sterile control, dilution of 1:10^4, dilution of 1:10^5, and dilution of 1:10^6 from the previous culturing series.

serum bottle. MnO_2 was provided as sole electron acceptor and H_2S was added daily in small amounts out of a Na_2S stock solution resulting in concentrations of 10-20 µM. After this pre-enrichment for the metabolism of interest, cultivation was continued with $S_2O_3^{2-}$ instead of H_2S as electron donor in artificial standard medium prepared as described in chapter 2.1. Isolation was performed by repeated series of dilution-to-extinction transfers. Because MnO_2 particles might have harbored bacteria of different species, dilution series were done with the supernatant of a shortly centrifuged sample from the respective previous culturing series. The highest dilution with positive growth as indicated by the change in color was used for dilution and re-cultivation (Fig. 6).

2.3.2 *S. baltica*

Initial water sample was taken by Prof. Dr. Klaus Jürgens at the 14th of June 2016 in the Gotland Basin of the Baltic Sea at station TF271 (57°-9.2 N and 20°-03 E) at a water depth of 220-225 m after salt water inflow from the North Sea in November 2015 and January-February 2016. Culture enrichment and isolation was performed as described for *S. marisnigri*.

2.3.3 *S. gotlandica*

Cryo-preserved culture stocks of *S. gotlandica* GD1^T from 2014 were thawed and re-cultivated in anoxic media as described in chapter 2.1.

2.4 Culture purity of *S. marisnigri* and *S. baltica*

Cultures were inspected with 4′6-diamidino-2-phenylindole (DAPI) stained epifluorescence and phase contrast microscopy. Plating on heterotrophic marine broth agar medium at ambient oxygen conditions and room temperature did not result in the formation of cell colonies. Analysis of 16 S ribosomal RNA (rRNA) sequenced were performed as described below.

2.4.1 16S rRNA sequencing and 16S rRNA clone libraries

For the phylogenetic classification of the Mn reducing isolates from the Black and Baltic Sea, 16S rRNA sequences were analyzed. As an additional indicator for a successful isolation of the respective species, 16S rRNA clone libraries were prepared and sequenced.

DNA extraction

DNA was extracted using QIAamp DNA Mini Kit (Cat. No. 51306) following the manual.

Amplification of the 16S rRNA gene with the polymerase chain reaction (PCR)

PCR was performed using Taq DNA Polymerase (native with bovine serum albumin (BSA) – Thermo Fisher Scientific, Germany). The protocol was as follows using the reagents sent with the Polymerase. A 50 µL PCR was prepared with 32.1 µL of diethyl dicarbonate (DEPC) H_2O; 5 µL 10x PCR buffer; 1 µL BSA; 5 µL $MgCl_2$; 1 µL 10 mM deoxynucleotides(dNTP)-mix (Thermo Scientific R0192); 2 µL Primer 27f (5′-AGA GTT TGA TCC TGG CTC AG-3′); 2 µL Primer 1492r (5′-GGT TAC CTT GTT ACG ACT T-3′) and 0.27 µL Taq Polymerase. To this mastermix 0.5 µL of a DNA template was added. Samples were placed in a thermocycler with the following temperature protocol: 1 min 94 °C; 30x [1 min 94 °C; 1 min 50 °C; 1.5 min 72 °C]; 10 min 72 °C; 10 °C till samples were taken out and stored at minus 20 °C.

Purification of the PCR product

The PCR products were washed using Agentcourt AMpure XP (Beckman Coulter GmbH, Germany) magnetic beads. 72 µL of AMpure Reagent per 50 µL PCR product was added to a

1.5 mL microcentrifuge tube, gently mixed, shortly centrifuged and incubated at room temperature for 5 minutes. The tube was placed in a magnetic bead separator (drawer) until the solution was clear (about 2-3 minutes). The supernatant was discarded, 200 µL ethanol (80%) were added and the solution was incubated for 30 seconds. This step was done twice while the tube remained in the drawer. The tube was removed from the drawer and placed with an open lid at 37 °C for 10 minutes. 17 µL TRIS/EDTA (TE) buffer were added, gently mixed, centrifuged briefly and incubated for 2 minutes at room temperature. The tube was again placed in the drawer for 2-3 minutes and 17 µL supernatant were transferred into a 0.5 mL PCR tube.

Preparation of clone libraries

Purified PCR amplicons were cloned into the vector pSC-A-amp/kan (StrataClone PCR Cloning Kit – competent cells Strataclone SoloPack) following the manual and plated onto ampicilin-containing (10 mg ampicilin per 100 mL lysogeny broth (LB) medium) LB agar plates (17.5 g LB Agar in 500 mL MilliQ) with 40 µL 2% X-galactosidase (X-Gal) on top. A 96 well microtiter plate with ampicillin-containing LB agar was picked. Clones were sequenced (LGC, Germany) forwards and backwards using vector primers T3 and T7prom.

Sequence analysis

The sequence reads were analyzed with SeqMan (Seqman II 5.06, DNASTAR Inc.). Sequences were quality trimmed with high stringency, quality checked by eye, assembled and cut with 27f and 1492r primers. Sequence data from the clone library of *S. marisnigri* was deposited at the Genbank sequence database from NCBI (refs. MF563385-MF563475).

2.5 Genome sequencing of *S. marisnigri*

2.5.1 DNA isolation

S. marisnigri was cultivated with $S_2O_3^{2-}$ as electron donor and NO_3^- instead of MnO_2 as electron acceptor to avoid negative interference of high Mn particle loads on DNA isolation and downstream application. About 4 L of a grown *S. marisnigri* culture were filtered onto

0.2 µm polycarbonate filter, cut into pieces and used as template for DNA isolation with the innuPREP Bacteria DNA Kit (Analytik Jena AG) following the manual. The yield was of 200 µL with ~ 1µg μL^{-1} DNA, quantified by spectrophotometric quantification with NanoDrop.

2.5.2 DNA sequencing

DNA sequencing was performed by BaseClear B.V. (Leiden, The Netherlands) using the Illumina HiSeq2500 system.

2.5.3 Genome assembly and annotation

Genome assembly and annotation was performed by Dr. Thomas Schott. Paired Illumina reads were assembled using SPAdes (Nurk et al., 2013) v 3.10.1 (k-mers 57, 65, 77, 85, 89, 95, 101, 105, 109). In addition, a subset of 875000 randomly selected read pairs was assembled using mira (Chevreux et al., 1999) v4.9.4 with default settings. Contigs resulting from both assemblies with a minimum average coverage of 40x and a minimum length of 500 nucleotides were manually merged using Gap5 (Bonfield & Whitwham, 2010) of the Staden package. The final contigs were uploaded to The RAST Server (Aziz et al., 2008) for automated annotation.

2.6 Analysis of cell counts

2.6.1 DAPI stained epifluorescence microscopy

Sample fixation was done with glutaraldehyde (2.5% final concentration) for 1 h at room temperature. Fixed samples containing Mn particles were diluted with at least 5 times the sample volume of a hydroxylamine solution (1.5 M $NH_2OH \cdot HCl$ dissolved in 0.25 M HCl) and treated for 5 minutes in an ultrasonic bath before the samples were filtered onto 0.2 µm polycarbonate filters. Fixed samples without metal particles were treated the same way, but phosphate buffered saline (1x PBS) instead of hydroxylamine was used for dilution. Filters were washed with 0.2 µm filtered MilliQ water, dried in the dark and embedded in DAPI contain-

ing fluorescence oil (1.1 mL Citifluor, 0.2 mL Vecta-shield, 0.1 mL 1x PBS including 1.4 µg DAPI). Cell counts were enumerated at 1000x magnification.

2.6.2 Flow-cytometry

Staining for flow-cytometry was done with nucleic acid stain SYBR Green I (Molecular Probes) following the technique of Marie et al. (1997). A subsample of a Mn containing glutaraldehyde fixed sample was diluted in tenfold the volume of a hydroxylamine solution and treated for 5 minutes in an ultrasonic bath. Subsequently, half the volume of the hydroxylamine solution of a 2.3 M 4-(2-hydroxyethyl)-1-piperazineethanesulfonic acid (HEPES - in MilliQ water) buffer solution was added to raise the pH to neutral condition. Samples without Mn were treated in the same way, but 1x PBS instead of hydroxylamine and HEPES was used instead. A subsample of this solution was filled up to 400 µl with sterile filtered MilliQ water and 50 µl sterile (0.2 µm) filtered staining solution (Tab. 7) together with 10 µl bead solution (1:2 x 10^{10} dilution in sterile filtered MilliQ water of 0.86 µm FL3 beads, Duke Scientific Corp., Cat. No. R900) were added. Chemical blanks of MilliQ water, PBS and hydroxylamine with HEPES were treated as described for the samples. Final samples were incubated in the dark at room temperature for at least 30 minutes. Samples were analyzed using FACSCalibur (Beckton Dickinson) in medium flow rate and excitation wavelength of 488 nm (blue) with a 15 mW air cooled argon-ion laser. Forward scatter (FSC – 488/10 nm), side scatter (SSC – 488/10 nm), FL1 (530/30 nm) and FL3 (>670 nm) were recorded. Within the run time of 188 s per sample, 105 µL were analyzed according to flow rate measurements. To account for fluctuating flow rates, a daily mean bead count was calcu-

Table 7: Components of the SYBR Green I staining solution.

Solution	Volume	Final concentration
Potassium citrate	1200 µL	2.4 M
Dimethyl sulfoxide (DMSO)	245 µL	0.2 M
SYBR Green I (10000x)	5 µL	-

lated from all measurements at the respective day and was used to correct the bacterial cell count according to Eq. 2.2.

$$\text{corrected cell counts} = \text{cell counts} * \frac{\text{mean bead count at respective day}}{\text{bead count in respective sample}} \quad 2.2$$

Data analysis was done with Flowing Software version 2.5.1 (Perttu Terho, Turku Centre for Biotechnology, Finland; www.flowingsoftware.com). Gates for cells and beads were chosen on the basis of dot plots of FL3 against FL1 on logarithmic scales. Cell counts were calculated with Eq. 2.3.

$$\text{Cells counts mL}^{-1} = \frac{\text{Events}_{\text{cells}} - \text{Events}_{\text{blank}}}{\text{V}_{\text{analyzed}}} * \text{DF}_{\text{fix}} * \text{DF}_{\text{proc}} * \text{DF}_{\text{cyt}} \quad 2.3$$

With $\text{Events}_{\text{cells}}$ = event counts within cell gate, $\text{Events}_{\text{blank}}$ = event counts within the cell gate in blank, $V_{analyzed}$ = analyzed sample volume in mL, DF_{fix} = dilution factor due to sample fixation, DF_{proc} = dilution factor due to sample processing and DF_{cyt} = dilution factor due to preparation for flow cytometry.

Dilution factors (DF) were calculated according to Eq. 2.4, 2.5 and 2.6.

$$\text{DF}_{\text{fix}} = \frac{\text{V}_{\text{fix}} + \text{V}_{\text{sample}}}{\text{V}_{\text{sample}}} \quad 2.4$$

$$\text{DF}_{\text{proc}} = \frac{\text{V}_{\text{acid/PBS}} + \text{V}_{\text{fix.sample}} + \text{V}_{\text{HEPES/PBS}}}{\text{V}_{\text{fix.sample}}} \quad 2.5$$

$$\text{DF}_{\text{cyt}} = \frac{\text{V}_{\text{proc.sample}} + \text{V}_{\text{MQ}} + \text{V}_{\text{beads}} + \text{V}_{\text{SYBR}}}{\text{V}_{\text{prep.sample}}} \quad 2.6$$

With V_{fix} = volume fixative added, V_{sample} = volume sample added, $V_{acid/PBS}$ = volume of hydroxylamine solution or 1x PBS added, $V_{fix.sample}$ = volume of fixed sample added, $V_{HEPES/PBS}$ = volume of buffer or 1x PBS added, $V_{proc.sample}$ = volume of sample added processed with hydroxylamine and HEPES or 1x PBS, V_{MQ} = volume MilliQ water added, V_{beads} = volume bead solution added and V_{SYBR} = volume SYBR Green I staining solution added.

2.7 Chemical analyses

2.7.1 Sulfur species

Sulfate (SO_4^{2-})

Sulfate was quantified by precipitation as $BaSO_4$ and photometry against a standard series. A 1 mL sterile filtered subsample was added to 1 mL $BaCl_2$ solution for $BaSO_4$ precipitation. The $BaCl_2$ solution was a mixture of two components. Component 1 was a mixture of MilliQ water and glycerine with a ratio of 2:3 (vol.%), respectively. Component 2 was 40.95 mM $BaCl_2$ solution in MilliQ water. Components 1 and 2 were mixed with a ratio of 3:2 (vol.%), respectively. Samples were stored at 4 °C. Samples were shaken thoroughly and treated with ultrasonic prior to turbidity measurement against a calibration series using the TECAN infinite M200 PRO plate reader with photometric measurement at 436 nm wavelength. The samples were shaken for 10 minutes prior to the beginning of the measurements and additionally 10 seconds before each measurement.

Thiosulfate ($S_2O_3^{2-}$) and sulfite (SO_3^{2-})

Thiosulfate and sulfite were analyzed by derivatization with monobrombimane against a standard series. A 0.5 mL 0.2 µm filtered subsample was added to 25 µL of HEPES/EDTA buffer (200 mM/50 mM in MilliQ, respectively) and 25 µL of a monobrombimane solution (48 mM in acetonitrile). The mixture was kept in the dark at room temperature for 30 minutes for derivatization. Derivatization was stopped by the addition of 25 µL methanesulfonic acid (324 mM in MilliQ water). Samples were diluted with MilliQ water and measured daily. Samples and calibration series were analyzed using BioTek high pressure liquid chromatography (HPLC) system with pump 525 (1 mL min^{-1}), oven 582 (40 °C), column LiChrospher 60 RP-Select B (5 µm) 125x4 and a Jasco FP 1520 detector (excitation at 380 nm, emission at 480 nm). Data were analyzed with the program Geminyx III Version 1.10.3.7. Eluent A: 0.25% acetic acid; Eluent B: 100% methanol. Gradient protocol: 0 min 100% A, 2 min 100% A, 5.5

min 92% A, 8 min 68% A, 12 min 68% A, 13 min 0% A, 18 min 0% A, 19 min 100% A, 23 min 100% A. With these adjustments, the $S_2O_3^{2-}$ peak appeared after 10 minutes and the SO_3^{2-} peak after 8 minutes.

Elemental sulfur (S^0)

Samples were immediately fixed by adding zinc acetate (0.5% w/v final concentration) to precipitate H_2S as ZnS to avoid chemical oxidation to S^0. Chloroform was added and intensively mixed for several minutes to dissolve S^0 in the chloroform phase. The chloroform phase at the bottom was transferred into a new tube and stored at -80 °C until HPLC measurements. 100 µL of the chloroform extract were diluted with 400 µL methanol and measured with HPLC against a standard series. S^0 was analyzed using BioTek HPLC System with pump 525 (1 mL min^{-1}), oven 582 (25 °C), column LiChrospher 100 RP-18 B (5 µm) 125x4 and DAD 545V detector (wavelength 265 nm and 6nm bandwidth). Data analysis was done with the program Geminyx III Version 1.10.3.7. An isocratic gradient with 100% methanol was applied. With these adjustments, the S^0 peak appeared after 4.4 min.

Hydrogen sulfide (H_2S)

Total H_2S was determined photometrically with the Cline method (Cline, 1969) against a standard series at a wavelength of 670 nm.

2.7.2 Metals and calcium (Ca)

After distinct sample preparation (see below) dissolved and particulate concentrations of Fe, Mn, S and Ca were determined by inductively coupled plasma optical emission spectrometry (ICP-OES - iCAP 7400 Duo, Thermo Fisher Scientific) using an external calibration ranging from 0.18 – 146 µM for Mn and from 0.012 – 2 mM for Ca. The Mn wavelength 260.6 nm and the Ca wavelength 318.1 nm were used in radial mode. Sc (316.4 nm) was used as internal standard to compensate matrix effects and instrument fluctuations. If necessary, samples were diluted with 2 vol.% HNO_3 to fit within the calibration ranges of Mn and Ca. Precision

and accuracy were checked by using acid digestions of the international reference material green river shale (SGR-1b) from U.S. Geological Survey (USGS) and were below 2%.

Total dissolved Fe, Mn, S and Ca

0.5 mL of a 0.2 µm filtered subsamples were filled in preconditioned (filled and stored with 2% HNO_3) microcentrifuge tubes, acidified with 10 µL 65% HNO_3 and stored at 4 °C.

Dissolved reactive Mn (Mn_{react})

Dissolved reactive Mn was analyzed according to the protocol of Schnetger and Dellwig (2012). Leftovers of 0.2 µm filtrated subsamples were stored in sterile microcentrifuge tubes at oxic conditions for 48h at room temperature and filtered again with 0.2 µm. Total dissolved Mn of the filtrate was quantified as described above. Dissolved reactive Mn was calculated with Eq. 2.7.

$$\text{Diss. reactive Mn} = \text{total diss. Mn at sampling time} - \text{total diss. Mn after 48h} \qquad 2.7$$

Particulate Fe, Mn, S and Ca

Unfiltered subsamples were centrifuged in a Beckman Coulter X15R System with a SX4750 rotor at 3200 rpm for 15 min at 10 °C. The supernatant was discarded and the pellet was dispersed in MilliQ water, shaken and centrifuged as described above. This washing step was done twice. After the second washing step, the supernatant was discarded and the residue was dried at 60 °C and stored at room temperature. The pellet was dissolved with a hydroxylamine solution (1.5 M NH_2OH • HCl dissolved in 0.25 M HCl) and analyzed as described above.

Calculation of reduced Mn in the particulate Mn phase

During precipitation of reduced Mn(II) as $Mn(Ca)CO_3$, the particulate Mn phase comprised new reduced and previously present oxidized Mn. Because precipitated rhombohedral shaped $Mn(Ca)CO_3$ contains exclusively reduced Mn, the amount of reduced Mn in the particulate phase can be quantified with Eq. 2.8.

$$\mathrm{Mn}_{part.(red)} = \mathrm{Mn}_{part.} * \frac{\left(\frac{\mathrm{Ca}}{Mn}\right)_{total}}{\left(\frac{Ca}{Mn}\right)_{rhomb}} \quad 2.8$$

Total particulate Ca to Mn ratio was analyzed with ICP-OES as described above. Starting Ca content of the respective experiment was subtracted and treated as a blank value. About 20-30 rhombohedral $Mn(Ca)CO_3$ precipitates of the respective sample were analyzed by SEM-EDX punctual measurements to determine the molar ratio of single $Mn(Ca)CO_3$ precipitates (see chapter 2.9.1).

2.7.3 Total inorganic carbon (TIC)

Direct TIC analysis was applied on dried material with a multi-EA 4000 (Analytic Jena). Samples were treated with 40% H_3PO_4 and the released CO_2 was analyzed by an infrared detector. Pure standard $CaCO_3$ (12.0% TIC) was used for calibration.

2.7.4 Cellular polyphosphate (polyP)

Glutaraldehyde fixed cells of *S. marisnigri* were enriched by centrifugation in a Beckman Coulter X15R System with a SX4750 rotor at 3200 rpm for 15 min at 10 °C. The supernatant was discarded. Particulate Mn was removed by dissolution in three consecutive series of hydroxylamine addition (see chapter 2.6), centrifugation and discarding of the supernatant. The Mn-particle free cell pellet was rinsed with PBS, centrifuged and the supernatant was discarded. Polyphosphate staining with tetracyclin was performed following the protocol of Koch et al. (2013). Cells were identified by forward and sideward scatter and separated by either positive (polyP+) or negative (polyP-) staining with tetracyclin by fluorescence activated cell sorting (FACS) with FACSARIA III (Becton Dickinson, Heidelberg, Germany). In a subsample, the cell concentration of the sorted cell solutions was enumerated by flow cytometry. The P content of the sorted samples was analyzed by quadrupol ICP-MS (iCAP Q, Thermo Fisher Scientific) in KED mode. The collision cell was filled with He with 8% H_2 to eliminate putative interference of $^{15}N^{16}O$. ^{62}Ni was detected next to ^{31}P to account for signal

interferences due to double ionized $^{62}Ni^{++}$. System calibration was performed with an ICP P standard (Alfa Aesar) from 1 to 100 ppb. The amount of P accumulated as polyP by *S. marisnigri* was calculated by subtracting the mean cellular P content of polyP- cells from polyP+ cells.

2.7.5 Nitrate (NO_3^-) and nitrite (NO_2^-)

NO_3^- and NO_2^- were analyzed following the protocol of García-Robledo et al. (2014) with a little modification. NO_3^- reduction with vanadium chloride was performed overnight without heating in a cooling bath.

2.8 Analysis of O_2, pH and H_2S with microsensors

Equipment used for micosensor analysis was purchased from Unisense (Denmark). Calibration and analysis were performed according to the manual and recorded with the soft-ware SensorTrace Logger provided by the manufacturer.

2.9 Combined imaging and elemental quantification

2.9.1 Scanning electron microscopy (SEM) and energy dispersive X-ray spectroscopy (EDX) analysis

Imaging and element analysis were performed with a Merlin Compact SEM (variable pressure, in-lens SE and HE-SE2 detectors) from Zeiss and elemental semi-quantification with an equipped EDX (Oxford Instruments).

SEM imaging

Samples were prepared on 0.2 µm polycarbonate filters and sputter coated with a 10 nm chromium layer for imaging of bacterial cells. Imaging was done with the HE-SE2 detector, aperture adjusted between 10 and 30 µm and 3 kV electron beam intensity. For high quality images, 2048 x 1536 px were recorded with line averaging of 8.

EDX analysis

Samples were prepared on 0.2 µm polycarbonate filters and sputter coated with a 10 nm elemental carbon layer for element analysis with EDX. Element analysis was performed with the HE-SE2 detector, 15 kV beam current and 60 µm aperture. EDX data were recorded in mass% and was transformed to molar ratios by dividing the value with the respective atomic weight. C was excluded from analysis.

Automated particle analysis

Samples for automated particle analysis shown in this work were prepared as described for NanoSIMS analysis. Automated particle analysis was performed with the program Inca (V. 5.05, Oxford Instruments). Particle identification was done at 1000x magnification and 2048 x 1526 px resolution by contrast and grey values, which were adjusted to 110 – 255. Particles smaller than 0.1121 µm (ECD 1.79 μm^2 ≙ 800 px) were excluded from analysis. 1000 particles per sample were analyzed within fields of 1000 μm^2 at an electron beam intensity of 10 kV and a pixel dwell time of 10 µs. A particle threshold of 25 per field was chosen. With this adjustments, a minimum of 40 fields at different filter locations were analyzed. Each particle was analyzed in full area with two runs, the first with 3 s and the second with 5 s and a process time of 5 s. Co was used for drift compensation. Au was excluded for analysis data were exported as mass% and transformed as described before.

2.9.2 Nanoscale secondary ion mass spectrometry (NanoSIMS)

Samples for NanoSIMS analysis were prepared on 0.2 µm polycarbonate filter material. Dried filters were sputter coated with a 30 nm gold layer for electrical conductivity. SIMS imaging was performed by Dr. Angela Vogts using a NanoSIMS 50 L from Cameca (Gennevilliers, France). Samples were implemented for 200 s with a $^{133}Cs^+$ ion beam at a beam current of 600 pA. Secondary ions were detected using mass detectors equipped with electron multipliers (Hamamatsu, Hamamatsu City, Japan). For analysis, the secondary ions $^{16}O^-$, $^{12}C^{14}N^-$, $^{31}P^-$,

Table 8: Area analyzed with Nano-SIMS at the respective sample days shown in Fig. 14.

Day	Ion source	Raster µm
0	Cs^+	47 x 47
	O^{2+}	36 x 36
3	Cs^+	45 x 45
	O^{2+}	36 x 36
6	Cs^+	48 x 48
	O^{2+}	36 x 36
13	Cs^+	48 x 48
	O^{2+}	36 x 36
17	Cs^+	47 x 47
	O^{2+}	35 x 35

$^{32}S^-$ and $^{55}Mn^{16}O^-$ were generated with a $^{133}Cs^+$ ion beam and the secondary ions $^{39}K^+$ and $^{40}Ca^+$ were generated with an O^{2+} ion beam at a beam current of 1 pA and a pixel dwell time of 125 µs px^{-1}, each. SIMS analysis was done with a resolution 1024 x 1024 px in varying sample areas (Tab. 8). 30 planes were recorded for each analysis. Data were evaluated with Look@NanoSIMS software (Polerecky et al., 2012). Recorded planes were drift-corrected and accumulated. To assemble SIMS analyses from both ion sources, images from $^{16}O^{2+}$ were aligned on $^{133}Cs^+$ images. Thereby, overlays are cropped to the lower size of the $^{16}O^{2+}$ derived images.

2.9.3 He- ion microscopy and secondary ion mass spectrometry (HIM-SIMS)

Glutaraldehyde fixed samples for HIM-SIMS analysis were prepared on 0.2 µm polycarbonate filters rinsed with MilliQ water and analyzed by Jelena Lovric at Luxembourg Institute of Science and Technology (LIST), Advanced Instrumentation for Ion Nano-Analytics (AINA), Materials Research and Technology Department 41, rue du Brill, L-4422 Belvaux. Analytical information and secondary electron images were obtained with a Secondary Ion Mass Spectrometry (SIMS) system specifically developed at LIST for Zeiss ORION NanoFab Helium Ion Microscope (HIM) (Wirtz et al., 2015; Dowsett et al., 2017). The secondary electron images were acquired with a helium ion beam at a beam energy of 20 keV in a matrix of 2048 × 2048 pixels with a dwell time of 20 µs px^{-1} and line averaging (8 lines). The field of view was 16 × 16 µm and ion dose was 7.73×10^{15} ions cm^{-2}. The spectrometer was tuned for the simultaneous detection of the $^{40}Ca^+$, and $^{55}Mn^+$ signals in the positive polarity. The $^{16}O^-$ and $^{12}C^{14}N$- ion cluster signals have been detected in negative polarity. Secondary ion images were acquired with a neon beam at 20 keV in a matrix of

512 × 512 pixels and a beam dwell time of 3 ms px^{-1}. In positive polarity, the field of view was 15 × 15 µm and ion dose was 1.42 × 10^{19} ions cm^{-2}. In negative polarity, the field of view was 14 × 14 µm and ion dose was 1.63 × 10^{19} ions cm^{-2}. Laplacian pyramid image fusion of the secondary electron micrograph and secondary ion images of Mn^+ and CN^- was performed after (Vollnhals et al., 2017).

2.10 Rate calculations with exponential curve fitting

The chemical reaction of MnO_2 and H_2S (Tab. 2) was forced from a reaction of second order type to a pseudo-first order type by adding large amounts of MnO_2 (10-20 mM) and single small additions of H_2S (20-40 µM) as it is done in chemical studies (e.g. Yao & Millero (1993). The concentration decrease of H_2S against time was used to calculate H_2S oxidation rates by fitting Eq. 2.9 to concentrations of H_2S with the nonlinear least square fit (nls) function in R by adjusting k and a.

$$\frac{C_{H2S(t)}}{C_{H2S(0)}} = e^{(a+kt)} \qquad 2.9$$

With $C_{H2S(t)}$ = H_2S concentration at time t, $C_{H2S(0)}$ = H_2S concentration added initially, k the reaction rate coefficient, t the time in minutes and a the variable to adjust for the y-intercept. The reaction rate coefficient k (min^{-1}) can be multiplied with the concentration of H_2S to receive H_2S oxidation rates.

2.11 Numerical modeling

With a numerical model the influence of bacterial H_2S oxidation at the lower border of the Black Sea suboxic zone onto the depth related concentration profile of H_2S was visualized. In the modeling approach from Schulz (2006) the differential equation for diffusive transport (Fick's second law – Eq. 2.10),

$$\frac{\Delta c}{\Delta t} = D \cdot \frac{\Delta^2 c}{\Delta x^2} \qquad 2.10$$

with D = diffusion coefficient, c = concentration, t = time and x = distance coordinate is solved by using the explicit numerical solution which was adapted from Schulz-Vogt et al. (2019) shown in Eq. 2.11.

$$C_{H2S(x,t+\Delta t)} = C_{H2S(x,t)} + \Delta t \cdot D_x \cdot \frac{C_{H2S(x+\Delta x,t)} - 2 \cdot C_{H2S(x,t)} + C_{H2S(x-\Delta x,t)}}{\Delta x^2} + \Delta t \cdot k_{bio(A\ or\ P)} \cdot C_{H2S(x,t)} \cdot Epsilonbact._{(x)} \quad 2.11$$

With C_{H2S} = concentration of H_2S at a given depth x and time t, D_x = diapycnical diffusivity constant at the depth x as determined by (Gregg & Yakushev, 2005), $k_{bio(A\ or\ P)}$ = cell specific H_2S oxidation rate as determined described in chapter 2.10 and *Epsilonbact.* = cellular abundance of *Epsilonbacteraeota* at the respective depth x.

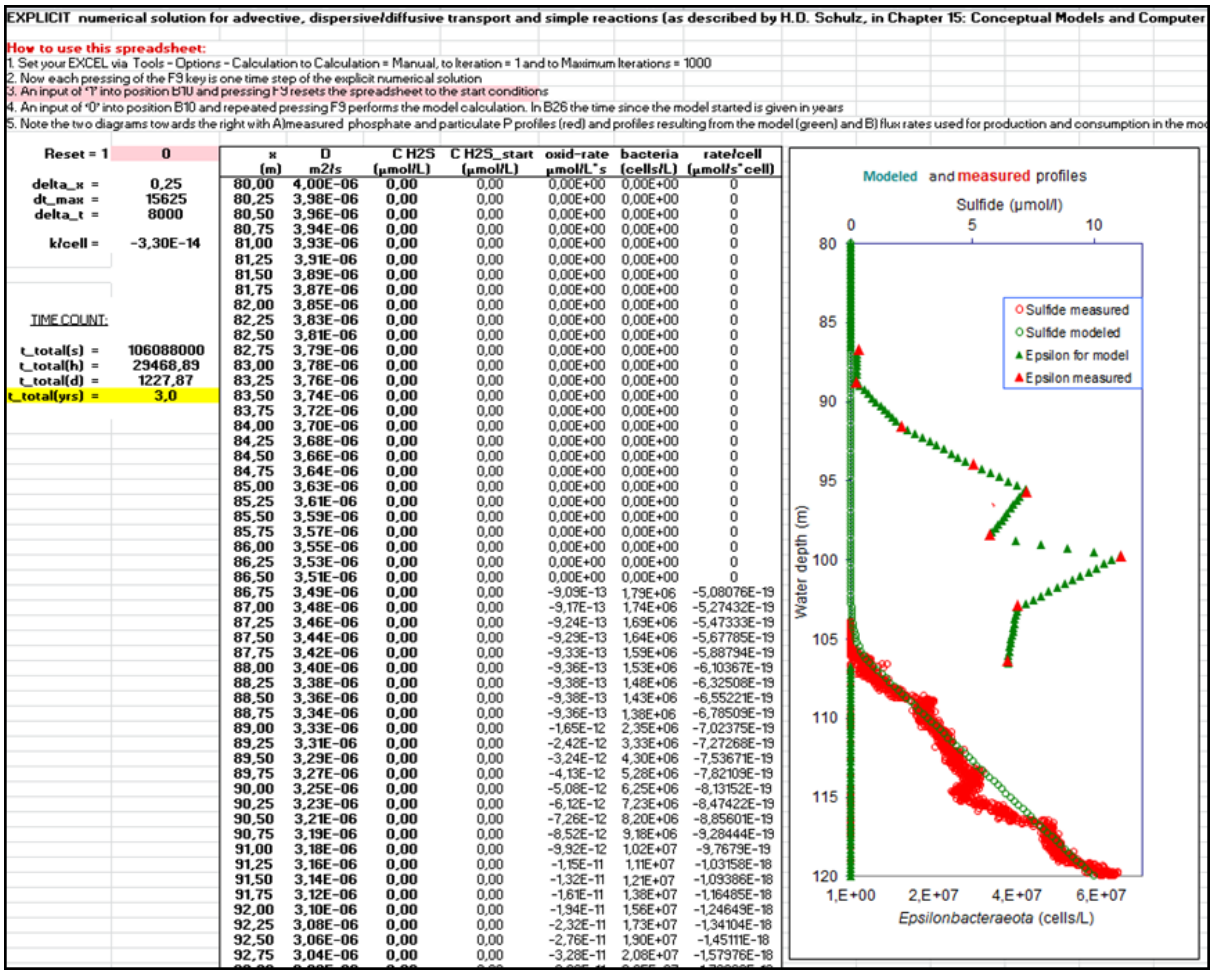

Figure 7: Screenshot of the numerical model used for the calculation of H_2S profiles with different oxidation rates. Modeling results with the value $k_{bio(A)}$ = -3.16 x 10^{-14} L $cell^{-1}$ s^{-1} after 3 years of model run in steady state are shown.

As starting condition, 10 µM H_2S are implemented in 120 m depth which represents in situ concentrations (Fig. 2A). In each calculation interval of $\Delta t = 8000$ s, the concentration of H_2S is calculated in the depth range from 80 to 120 m with an integrated depth for each cell of $\Delta x = 0.25$ m. The calculated H_2S concentrations after a calculation interval are the basis for the next calculation. Different oxidation rates per cell for *Epsilonbacteraeota* are implemented and steady state conditions were displayed. If no steady state was achieved after 3 years of modeling, the concentration profile after 3 years were displayed (Fig. 7).

2.12 Experimental design, cultivation conditions and specific supplementation

In the present work, experimental conditions were adjusted based on the respective question. If not mentioned otherwise, medium was prepared as described in 2.1. Experimental design and growth conditions are listed as they appear in the results section. To avoid any misunderstandings, the following details should be read along with the respective passage in the results part.

2.12.1 Particle dynamics analyzed with NanoSIMS

For NanoSIMS analysis focusing on the dynamics of Mn particles, *S. marisnigri* was cultivated with the additions listed in Tab. 9.

2.12.2 Dynamic of Mn and S species during growth of *S. marisnigri*

S. marisnigri cultivated with MnO_2 and $S_2O_3^{2-}$

S. marisnigri was cultivated in triplicates with one sterile control in 500 mL medium with MnO_2 as electron acceptor and $S_2O_3^{2-}$ as electron donor. Sampling was performed by ex-

Table 9: Concentration of added electron acceptors and donors and basic information for growth of *S. marisnigri* for the Nano-SIMS time series shown in Fig. 14.

e^- acceptor	$C_{e^-\ acceptor}$	e^- donor	$C_{e^-\ donor}$	Volume	Cell counting
MnO_2	6.7 mM	$S_2O_3^{2-}$	1.7 mM	150 mL	Microscopy

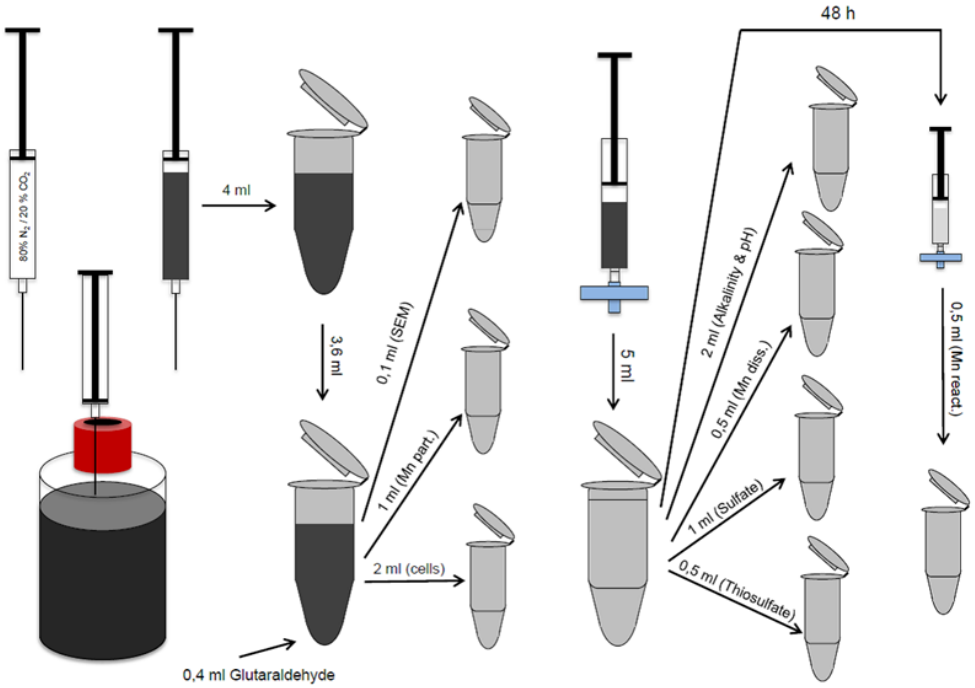

Figure 8: Sampling scheme for the experiments shown in Fig. 15 and 16.

changing the extracted sample volume with N_2 gas mixture containing 20% CO_2. Syringes were flushed several times with the gas mixture before sampling. 10 mL samples were extracted under constant shaking and divided into 0.2 µm filtered and unfiltered subsamples for the respective analyses as displayed in Fig. 8.

S. marisnigri cultivated with MnO_2 and continuous addition of H_2S

Three 1 L glass bottles were filled with 500 mL medium prepared after standard protocol with prolonged headspace flushing. Bottles were closed with butyl rubber stoppers pierced with several glass pipes, either connected to the liquid phase or the headspace (Fig. 9, scheme).

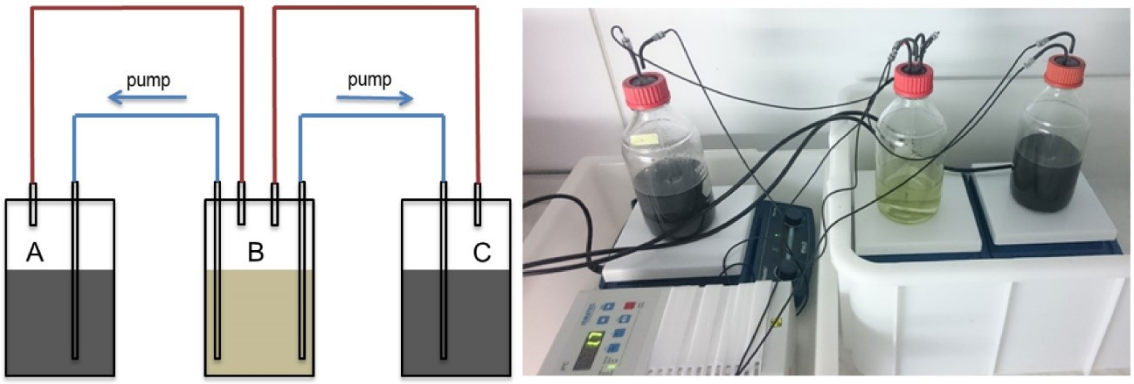

Figure 9: Setup for continuous addition of H_2S to MnO_2 to the bottle containing *S. marisnigri* or abiotic control.

Bottles were connected with gas tight iso-versinic tubing and autoclaved. 10 mL 1 M MnO_2 solution were added to bottle A and C, and 5 ml 1 M Na_2S stock solution were added to bottle B (Fig. 9). H_2S was added continuously with a peristaltic pump (ISMATEC, IPC-N) from bottle B to bottle A and C with a pump speed of 3 µL min^{-1}. The experiment was running for two days before cells were added (day 0). Pump speed was increased to 7.5 µL min^{-1} at day 12. All bottles were constantly stirred. Sampling for SO_4^{2-}, S^0, diss. reactive Mn, diss. Mn, part. Mn and cell numbers was performed as described earlier.

2.12.3 *S. marisnigri* and *S. baltica* grown with NO_3^- and H_2S additions

S. marisnigri and *S. baltica* together with sterile controls were cultivated with 6.7 mM NO_3^- as electron acceptor in serum bottles with 150 mL medium. Small additions of 100 µL, 200 µL or 300 µL out of a 10.79 mM Na_2S stock solution resulting in 7.2 µM, 14.4 µM or 21.6 µM, respectively, were made several times per day. Samples for cell numbers and sulfide were taken every second day. Cell numbers were enumerated with epifluorescence microscopy.

2.12.4 *S. marisnigri* grown with MnO_2 and additions of H_2S or H_2S pre-reacted with MnO_2

Two parallels with triplicates each were prepared in serum bottles containing 150 mL medium, 6.7 mM MnO_2 and *S. marisnigri*. Small additions of 100 µL, 200 µL or 300 µL out of either stock solution 1 (H_2S) or 2 (Mn/H_2S) were added several times per day. Stock solution 1 was prepared by adding 1.5 mL 1 M Na_2S stock solution to ~150 mL anoxic and sterile medium. Stock solution 2 was prepared by adding 3 mL 1 M MnO_2, 1.5 mL 1 M Na_2S

Table 10: S-composition of stock solution 1 (H_2S) and 2 (Mn/H_2S). n.d. = not detectable; n.q. = not quantifiable.

Stock solution	H_2S	S^0	$S_2O_3^{2-}$	SO_4^{2-}	Sum
H_2S	10.8 mM	n.q.	n.d.	0.1 mM	10.9 mM
Mn/H_2S	n.d.	9.17 mM	0.34 mM	<0.01 mM	9.5 mM

and 0.3 mL 30% HCl to ~150 mL anoxic and sterile medium. HCl was added in 3 steps of 100 µL to keep the pH at 7.5, which rose by the chemical reaction of H_2S and MnO_2. Sulfur composition of stock solution 1 (H_2S) and 2 (Mn/H_2S) are depicted in Tab. 10.

2.12.5 Determination of H_2S oxidation rates of *S. marisnigri*

Six glass bottles were filled with 500 mL medium and 10 mL 1 M MnO_2 were added. To three bottles 5 mL 200 mM $Na_2S_2O_3$ and *S. marisnigri* were added (Culture parallels); the others remained unchanged (control). The addition of $S_2O_3^{2-}$ to control bottles had to be omitted. Preliminary tests showed a pH dependent H_2S oxidation activity, which stopped at approximately pH 8, which is consistent with the chemical oxidation of H_2S with $S_2O_3^{2-}$ according to the work of Siu & Jia (1999). In culture parallels, $S_2O_3^{2-}$ was completely consumed after 12 days of growth, which was measured prior to the additions of H_2S. Bottles were opened, placed in a 10 °C water bath and a pH and H_2S microsensor were placed in the medium as shown in Fig. 10. The medium was constantly stirred and the headspace was flushed with a low Ar stream during the time of the experiment to avoid O_2 contaminations. Bottles were treated with sodium azide (20 mM final concentration, 1h incubation) or heat (pasteurization, 80 °C for 1 h) after 8 (culture) or 5 (sterile control) additions of H_2S. Then another 3 additions of H_2S were made. Data were analyzed as described in 2.10.

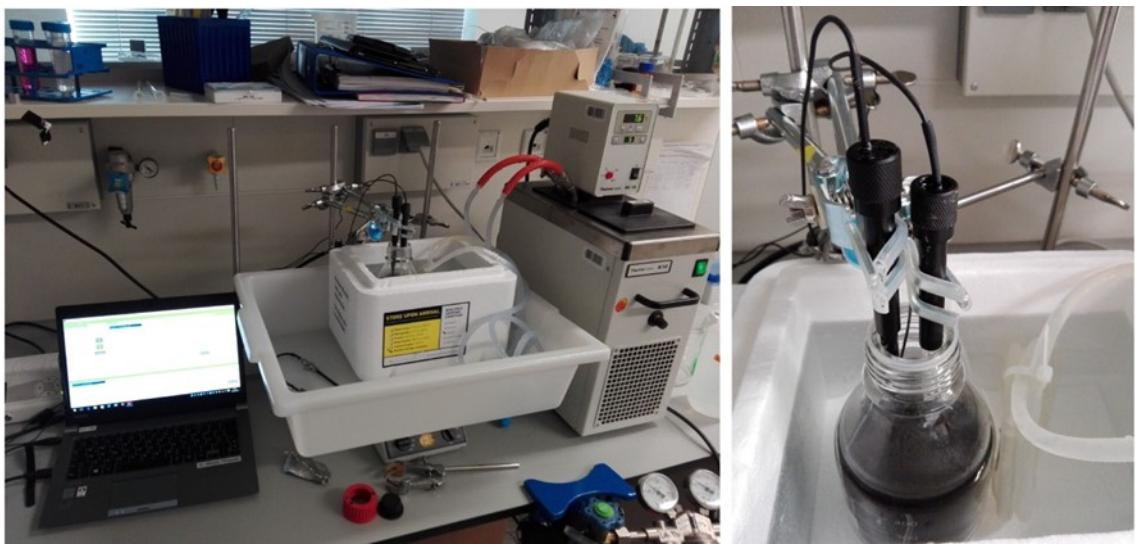

Figure 10: Setup for the determination of H_2S oxidation rates with a pH and a H_2S microsensor.

2.12.6 Dissimilatory metabolism – electron acceptors

As potential electron acceptors for the oxidation of $S_2O_3^{2-}$, O_2, NO_3^-, nitrite (NO_2^-) and a variety of metal oxides were tested. Additionally, the ability for SO_4^{2-} - reduction, disproportionation of $S_2O_3^{2-}$ and S^0 and fermentation of organic C was investigated.

O_2

Bottles were prepared as described in 2.12.12 – oxygen tolerance, but no electron acceptor was added.

NO_3^-

Medium was supplemented as listed in Tab. 11. In a second experiment, *S. marisnigri*, pregrown with NO_3^- as electron acceptor, was cultivated in triplicates in 500 mL medium containing 4 mM $NaNO_3$ and 3.5 mM $Na_2S_2O_3$. After 22 days of growth, MnO_2 was added to a final concentration of 3.5 mM. Cell numbers were enumerated with epifluorescence microscopy.

NO_2^-

Medium was supplemented as listed in Tab. 12.

Metal oxides

To ~150 mL medium containing 2.7 mM $Na_2S_2O_3$, 670 µM Fe_2O_3 or $FeCl_3$ were added twice a week, because (Labrenz et al., 2013) suggested potentially toxic effects of high iron concentrations. Ability of *S. gotlandica* to reduce MnO_2 was performed with 2.7 mM $Na_2S_2O_3$ and

Table 11: Concentration of added electron acceptors and donors and basic information to test for NO_3^- reduction.

e- acceptor	$C_{e\text{- acceptor}}$	Volume	e- donor	$C_{e\text{- donor}}$	Cell counting	Transfers
NO_3^-	10 mM	100 mL	$S_2O_3^{2-}$	10 mM	Flow cytometry	2

Table 12: Concentration of added electron acceptors and donors and basic information to test for NO_2^- reduction.

e- acceptor	$C_{e\text{- acceptor}}$	Volume	e- donor	$C_{e\text{- donor}}$	Cell counting	Transfers
NO_2^-	5 mM	100 mL	$S_2O_3^{2-}$	10 mM	Flow cytometry	2

6.7 mM MnO_2 as it is applied by default for *S. marisnigri* and *S. baltica*. As control experiments, two bottles were prepared as described in 2.1, but 1.7 µM resazurin as redox indicator were added. One bottle was treated with 3.8 mM cystein 7 days before inoculation to eliminate putative O_2 contaminations, the other remained unchanged. Both were inoculated with cells and 2.7 mM $Na_2S_2O_3$. Cells were enumerated with epifluorescence microscopy. Amorphous FeOOH and goethite were added as electron acceptor in batch type cultivation with concentrations below 10 mM together with 5 mM $Na_2S_2O_3$.

2.12.7 Dissimilatory metabolism – electron donors

As potential electron donors (e^- - donors) for the reduction of either MnO_2 or NO_3^-, elemental sulfur (S^0), sulfite (SO_3^{2-}), hydrogen (H_2) and organic carbon (C- org.) were tested. Experimental conditions are summarized in Tab. 13.

S^0

Stock solution of colloidal S^0 was prepared anoxic and non-sterile as described in 2.2.2.

SO_3^{2-}

In the third transfer of *S. gotlandica*, 10 mM instead of 5 mM Na_2SO_3 were added as electron donor.

H_2

Growth with H_2 as electron donor or in the presence of H_2 was done with a negative (no H_2, no $Na_2S_2O_3$) and a positive control (H_2 and $Na_2S_2O_3$). H_2 was applied by flushing the headspace (~ 20 ml) with 0.2 µm filtered H_2 gas for 30 s generated with a H_2 generator (Horiba STEC 3200C).

Organic carbon (C- org.)

Organic carbon was added as an equal mix of acetate ($C_2H_4O_2$), propionate ($C_3H_6O_3$) and succinate ($C_4H_6O_4$). Two transfers were made with *S. marisnigri* and three transfers were made with *S. baltica* and *S. gotlandica*.

Table 13: Concentration of added electron acceptors and donors and basic information to test for potential electron donors.

e^- donor	$C_{e- donor}$	Volume	e^- acceptor	$C_{e- acceptor}$	Cell counting	Transfers
S^0	~4 mM	100 mL	MnO_2/NO_3^-	5 mM	Flow cytometry	2
Na_2SO_3	5 (10) mM	100 mL	MnO_2/NO_3^-	5 mM	Flow cytometry	2 (3)
H_2	H_2 gas	150 mL	MnO_2/NO_3^-	6.7 mM	Microscopy	1
C- org. mix	7.5 mM	100 mL	MnO_2/NO_3^-	5 mM	Flow cytometry	2 (3)

2.12.8 Disproportionation of S^0 and $S_2O_3^{2-}$

Disproportionation was tested by adding solely $S_2O_3^{2-}$ or S^0 as energy source to cultivation medium with bacteria as listed in Tab. 14.

2.12.9 SO_4^{2-} - reduction

Organic carbon was added as an equal mix of acetate ($C_2H_4O_2$), propionate ($C_3H_6O_3$) and succinate ($C_4H_6O_4$) as listed in Tab. 15.

2.12.10 Fermentation

Organic carbon was added as an equal mix of acetate ($C_2H_4O_2$), propionate ($C_3H_6O_3$) and succinate ($C_4H_6O_4$) shown in Tab. 16.

Table 14: Concentration of added electron acceptors and donors and basic information to test S^0 and $S_2O_3^{2-}$ disproportionation.

S- component	$C_{S-component}$	Volume	Cell counting	Transfers
S^0	4 mM	100 mL	Flow cytometry	3
$S_2O_3^{2-}$	10 mM	100 mL	Flow cytometry	3

Table 15: Concentration of added electron acceptors and donors and basic information to test SO_4^{2-} reduction.

e^- acceptor	$C_{e- acceptor}$	e^- donor	$C_{e- donor}$	Volume	Cell counting	Transfers
SO_4^{2-}	10 mM	C- org. mix	7.5 mM	100 mL	Flow cytometry	2

Table 16: Added components and basic information to test for fermentation of organic carbon compounds. One transfer was made for *S. marisnigri* and two for *S. baltica* and *S. gotlandica*.

C- component	$C_{C-component}$	Volume	Cell counting	Transfers
C-org. mix	7.5 mM	100 mL	Flow cytometry	1(2)

2.12.11 Assimilatory metabolism

The potential of the three *Sulfurimonas* species to fix molecular nitrogen (N_2) and to grow with organic carbon (C- org.) as carbon source was investigated.

N_2 – fixation

Medium was prepared without NH_4Cl as N-source. NO_3^- was omitted as electron acceptor for *S. gotlandica*, instead, O_2 was provided by flushing the ~ 15 mL headspace with sterile filtered breathing air (Tab. 17).

Organic carbon (C- org.)

Medium was prepared with HEPES as pH buffer and Ar gas instead of N_2 with 20% CO_2 was used for de-oxygenation. The pH was adjusted to 7.5 with NaOH and HCl. Acetate ($C_2H_4O_2$), propionate ($C_3H_6O_3$) or succinate ($C_4H_6O_4$) was added prior to inoculation in concentrations specified in Tab 18.

2.12.12 Abiotic factors influencing growth

Added components to cultivation medium to test for abiotic growth factors are listed in Tab. 19.

Table 17: Concentration of added electron acceptors and donors and basic information to test for N_2-fixation. Two transfers were made for *S. gotlandica* and *S. marinsigri* and three transfers were made for *S. baltica*.

Experiment	Volume	e- acceptor	$C_{e\text{- acceptor}}$	e- donor	$C_{e\text{- donor}}$	Cell counting	Transfers
N_2 – fixation	100 mL	MnO_2/O_2	10 mM/gas	$S_2O_3^{2-}$	5 mM	Flow cytometry	2(3)

Table 18: Concentration of added electron acceptors and donors and basic information to test for heterotrophic growth on a variety of organic carbon sources. 4 mM $S_2O_3^{2-}$ was added for *S. marisnigri* and *S. gotlandica*. 5 mM $S_2O_3^{2-}$ was added for *S. baltica*.

C- source	$C_{C\text{-source}}$	Volume	e- acceptor	$C_{e\text{- acceptor}}$	e- donor	$C_{e\text{- donor}}$	Cell counting
HCO_3^- (pos. C.)	10 mM	100 mL	MnO_2/NO_3^-	10 mM	$S_2O_3^{2-}$	4(5) mM	Microscopy
Neg. C	-	100 mL	MnO_2/NO_3^-	10 mM	$S_2O_3^{2-}$	4(5) mM	Microscopy
Acetate	15 mM	100 mL	MnO_2/NO_3^-	10 mM	$S_2O_3^{2-}$	4(5) mM	Microscopy
Propionat	15 mM	100 mL	MnO_2/NO_3^-	10 mM	$S_2O_3^{2-}$	4(5) mM	Microscopy
Succinate	15 mM	100 mL	MnO_2/NO_3^-	10 mM	$S_2O_3^{2-}$	4(5) mM	Microscopy

Table 19: Concentration of added electron acceptors and donors and basic information to test for abiotic factors influencing growth of the three *Sulfurimonas* species.

Experiment	Volume	e- acceptor	$C_{e\text{- acceptor}}$	e- donor	$C_{e\text{- donor}}$	Cell counting
Temperature	100 mL	MnO_2/NO_3^-	10 mM	$S_2O_3^{2-}$	5 mM	Microscopy
Salinity	100 mL	MnO_2/NO_3^-	10 mM	$S_2O_3^{2-}$	5 mM	Flow cytometry
pH	100 mL	MnO_2/NO_3^-	10 mM	$S_2O_3^{2-}$	5 mM	Flow cytometry
O_2 tolerance	50 mL	MnO_2/NO_3^-	10 mM	$S_2O_3^{2-}$	5 mM	Flow cytometry

Temperature

Bottles were placed in dark, temperature controlled rooms or climate cabinets. Bottles at 0 °C were placed in an isolated box filled with ice and water in a 4 °C climate controlled room. Ice was refilled frequently. Temperatures were documented with temperature-loggers.

Salinity

Different salinities were achieved by adding more or less salts listed for the preparation of artificial seawater (chapter 2.1) by the rule of proportions.

pH

pH was tested from 4 to 9 (4.0, 5.0, 6.0, 6.5, 7.0, 7.5, 8.0, 9.0). Instead of HCO_3^-, sodium acetate (pH 4-5), MES (pH 6-6.5), HEPES (pH 7-8) and TRIS (pH 9) were used for pH buffering. Artificial seawater was prepared with 10 mM of the respective buffer substance and the pH was adjusted before and after autoclaving by the addition of NaOH or H_2SO_4. Ar or N_2 was used for de-oxygenation. 2.5 mL L^{-1} 1 M $NaHCO_3$ was added as carbon source before bottling.

O_2 tolerance

The effect of different O_2 levels onto growth of *S. marisnigri*, *S. baltica* and *S. gotlandica* were investigated. 150 mL serum bottles were filled with 50 mL medium and the remaining 100 mL headspace was flushed with the anoxic gas mixture used for the preparation of anoxic medium (2.1) for 1 minute. No volume (0 Vol% O_2), 5 mL (1%), 20 mL (4%) or the headspace (21%) was exchanged with 0.2 µm filtered breathing air (~ 21% O_2). Complete exchange was done by flushing the headspace with air for 1 minute.

3 Results

3.1 Chapter I: Reduction of MnO_2 coupled to the oxidation of $S_2O_3^{2-}$ and H_2S

The original water sample from the Black Sea was supplied with MnO_2 and daily small additions of H_2S to enrich for the metabolism of interest. Subsequently, $S_2O_3^{2-}$ was used as electron donor, because it is not toxic even in higher concentrations non-reactive with the MnO_2 used in this work and a suitable electron donor for most sulfur oxidizing bacteria, which can be grown with batch type cultivation. Batch type cultivation with MnO_2 and $S_2O_3^{2-}$ was accompanied by a color change of the medium from black to brownish-gray (Fig. 11A and B, bottle photographs). By microscopic inspection of DAPI-stained culture samples, cells appeared to be mostly associated to particles (Fig. 12, 13 and 14). The colonization of particles by *S. marisnigri* ranged from single cells and cell plugs (Fig. 12A) to large-scale occupation (Fig. 12B and C) with sometimes biofilm-like structure (Fig. 12D). Analysis with HIM-SIMS and NanoSIMS showed that the particles covered with bacteria consist of Mn (Fig. 13 and 14).

Detailed imaging of the particulate phase before and after growth of the culture revealed that the change in color is concurrent with a change in the shape and mineralogy of the Mn con-

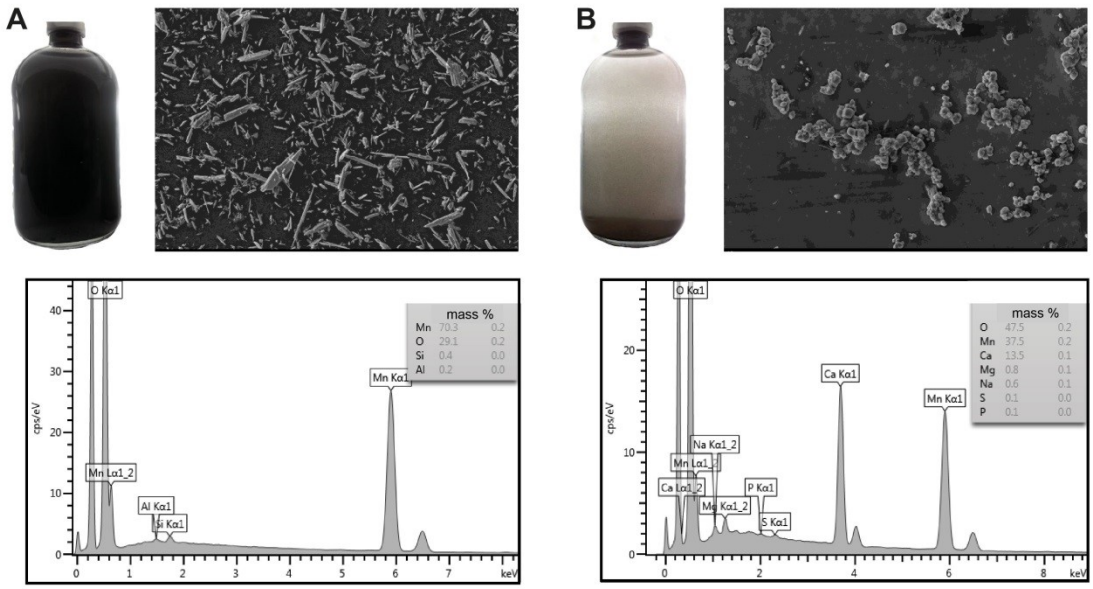

Figure 11: Bottle photographs, scanning electron micrographs and EDX spectra of the particulate phase before (A) and after growth (B) of *S. marisnigri* cultivated with MnO_2 and $S_2O_3^{2-}$.

taining particles. Technical MnO_2 added as electron acceptor had a needle like shape (Fig. 11A, scanning electron micrograph) with no detectable Ca content (Fig. 11A, EDX spectrum), while the particulate phase at the end of bacterial growth consisted of rhombohedral shaped Mn particles (Fig. 11B, scanning electron micrograph) with a high Ca-content (Fig. 11B, EDX spectrum). TIC analysis of the particulate phase after bacterial growth revealed a high content of carbonate (Tab. 20) here referred to as $Mn(Ca)CO_3$.

In a time course experiment, the transition of MnO_2 to $Mn(Ca)CO_3$ together with the spatial localization of *S. marisnigri* and the elements Mn and Ca was documented using NanoSIMS (Fig. 14). The elements ^{55}Mn, ^{40}Ca and the combined mass of $^{12}C^{14}N$ (as indicator for a biological origin) were detected and color coded in green, red and blue, respectively. Cell numbers increased which could be seen by direct cell counting (Fig. 14A) and by higher visual abundance e.g. day 0 compared to day 13 (in Fig. 14, $^{12}C^{14}N$ signal, blue).

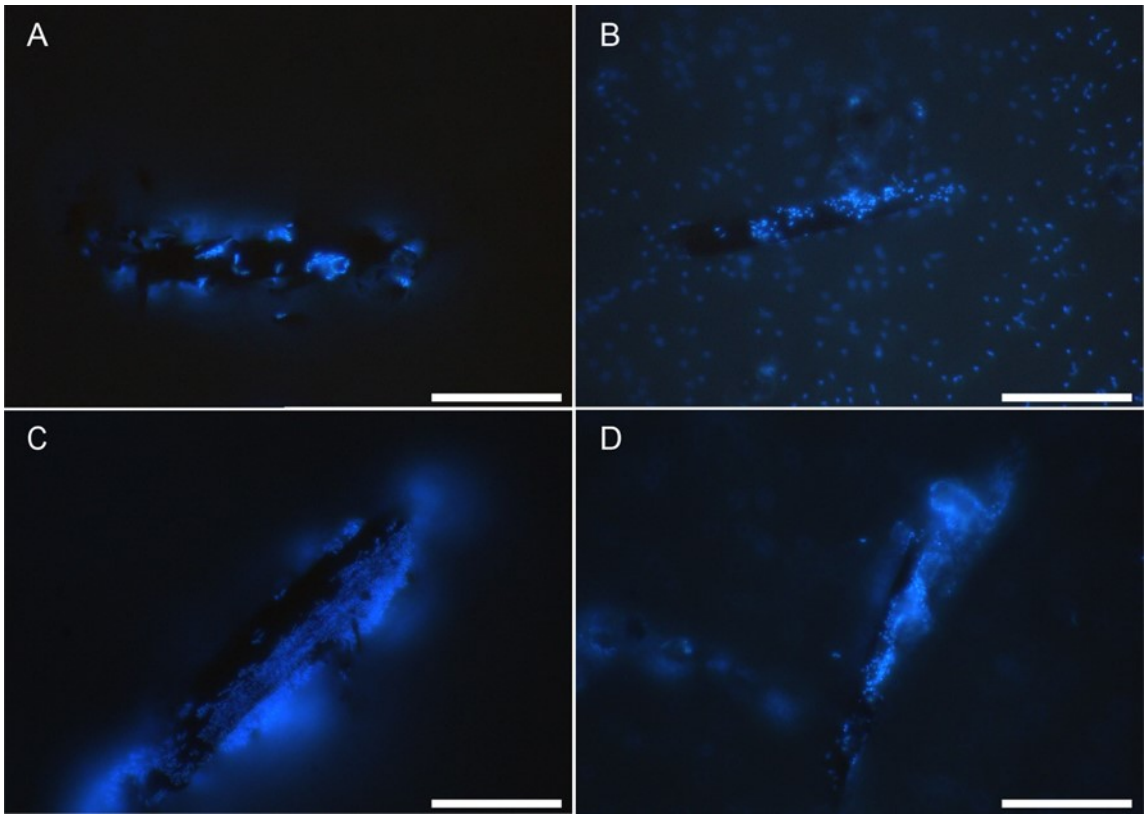

Figure 12: Epifluorescence images of a *S. marisnigri* culture grown with MnO_2 stained with the DNA dye DAPI at 630x magnification. Scale bars: 20 µm.

S. marisnigri was mostly located at or in the proximity of manganese particles (Fig. 14, day 6). At day 0, no mixed signal of red and green could be seen, which indicated the absence of reduced Mn in $Mn(Ca)CO_3$ precipitates. This could also be seen in the absence of particles with a detectable Ca to Mn ratio (Fig 14B, values for day 0 not shown). The Ca to Mn ratio in particles increased (Fig 14B, day 6) and rhombohedral $Mn(Ca)CO_3$ precipitates appeared with a mixed color of red and green in the NanoSIMS images. Apparently the $Mn(Ca)CO_3$ precipitates grew directly at the surface of MnO_2 particles. The needle shaped MnO_2 particles looked haggard in the time course of the experiment (Fig. 14, day 13, green rod). Analysis of approximately 1000 single particles at day 10, 13 and 17 using automated particle analysis with SEM-EDX revealed a homogenous Ca to Mn ratio among the precipitated particles (Fig. 14B). At day 3 and 6, the Ca to Mn ratio of the particles is more heterogeneous and the resulting slope like plot did not show a plateau as it can be seen at day 10, 13 and 17 (Fig. 14B). Because the $Mn(Ca)CO_3$ precipitates grew at the MnO_2 particle surfaces, the automated particle analysis might be unable

Table 20: Total inorganic carbon analysis of dried samples of the particulate phase at the end of the growth phase of *S. marisnigri* and calcite ($CaCO_3$) as reference material.

Sample	TIC (%)
$CaCO_3$ (control)	12.01
Culture sample 1	10.00
Culture sample 2	9.94

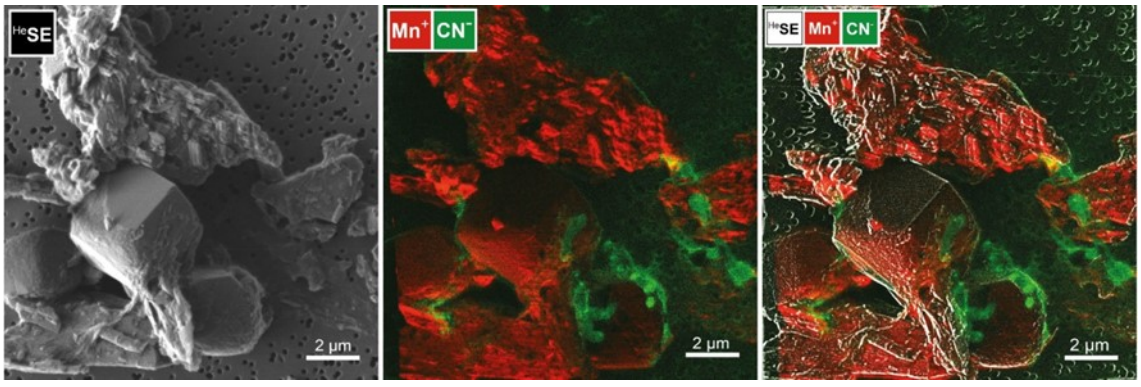

Figure 13: Scanning electron micrograph (left), overlay of HIM-SIMS analysis of the ion species Mn^+ (red) and CN^- (green) where CN is a reference to organic matter (middle), Laplacian pyramid image fusion of the scanning electron micrograph and ion signals of Mn^+ and CN^- (right). Cells and organic material (green) is attached to Mn containing particles. Copyright: Luxembourg Institute of Science and Technology, Advanced Instrumentation for Ion Nano-Analytics (AINA), Materials Research and Technology Department 41, rue du Brill, L-4422 Belvaux.

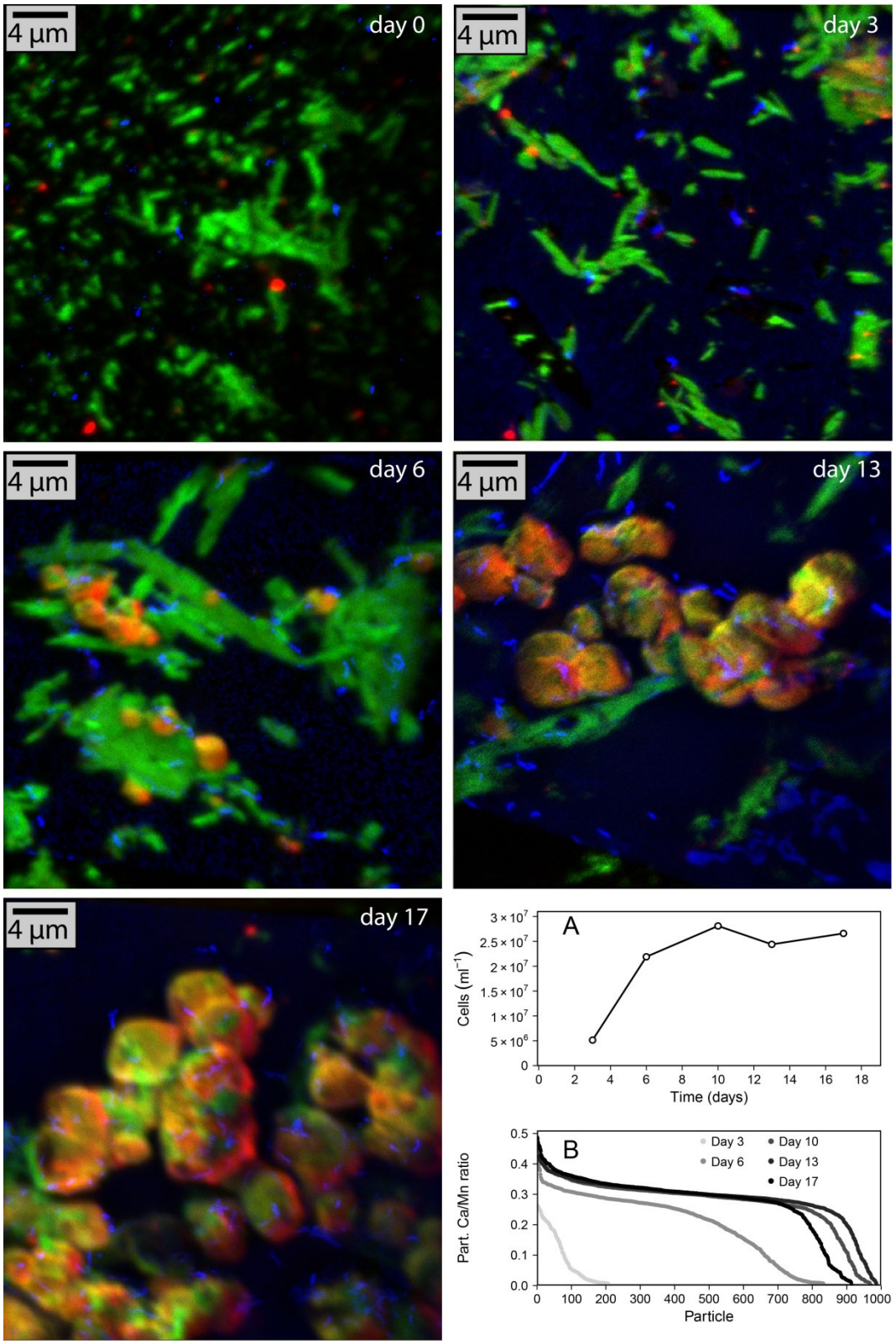

Figure 14: Mn particle dynamic in the growth phase of *S. marisnigri*. Growth of *S. marisnigri* (A, open circles, solid line) is accompanied with the increase of the Ca to Mn ratio in single particles (B) from day 3 to day 10 where growth stopped. Precipitation of cube shaped Mn(Ca)CO_3 precipitates can be traced in the NanoSIMS images by the portion of red (Ca) to green (Mn) color. *S. marisnigri* ($^{12}C^{14}N$ – blue) is more abundant at e.g. day 13 compared to day 0 as it can be expected by the direct cell counting (A). Analysis of up to 1000 single particles using SEM-EDX revealed the homogeneity of the Ca to Mn ratio in different particles at day 10 without major changes afterwards (B).

to distinguish between $Mn(Ca)CO_3$ precipitates and MnO_2 particles at day 3 and 6. After the complete growth of *S. marisnigri* at approximately day 10, no drastic change in the particulate Ca to Mn ratio was detectable (Fig. 14B). This indicates that the reduction of MnO_2 by *S. marisnigri* was fostering the succession of the observed Mn particles in this experiment, leading to the formation of $Mn(Ca)CO_3$ precipitates with a homogenous Ca to Mn ratio.

Cultivation of *S. marinsigri* with MnO_2 and $S_2O_3^{2-}$

The reduction of MnO_2 with $S_2O_3^{2-}$ as electron donor by *S. marisnigri* was accompanied by the complete oxidation of $S_2O_3^{2-}$ to SO_4^{2-} with a stoichiometry of 1:2 (Fig. 15A) following Eq. 3.12:

$$S_2O_3^{2-} + 5\,H_2O \longrightarrow 8\,e^- + 2\,SO_4^{2-} + 10\,H^+ \qquad 3.12$$

No detectable accumulation of S^0 or SO_3^{2-} was observed. The stoichiometry between $S_2O_3^{2-}$ and MnO_2 was 1:3.7, a bit lower than it would have been expected based on Eq. 3.13, but relatable because some reducing equivalents were needed to maintain CO_2 fixation according to Eq. 3.14.

$$4\,MnO_2 + S_2O_3^{2-} + 6\,H^+ \longrightarrow 4\,Mn^{2+} + 2\,SO_4^{2-} + 3\,H_2O \qquad 3.13$$

$$2\,CO_2 + S_2O_3^{2-} + 3\,H_2O \longrightarrow 2\,[CH_2O] + 2\,SO_4^{2-} + 2\,H^+ \qquad 3.14$$

Until day 6, the concentration of particulate Mn ($Mn_{part.}$) decreased concurrent with an equal increase in dissolved Mn ($Mn_{diss.}$) species (Fig. 15B). After 6-7 days, the precipitation of rhombohedral $Mn(Ca)CO_3$ was documented by a steady increase in the particulate Ca-content (Fig. 15B, bars) and again increasing concentration of $Mn_{part.}$. With a mean Ca to Mn ratio of 0.19 ± 0.03 (N = 77) in single rhombohedral $Mn(Ca)CO_3$ precipitates, the amount of reduced Mn in the particulate phase ($Mn_{part.(red)}$) was calculated with Eq. 2.8 (Fig. 15B, dashed blue line). No changes in Mn and S species were detectable in the abiotic control (Fig. 15C).

Thereby it was shown, that MnO_2 was almost completely reduced and transformed to $Mn(Ca)CO_3$, following the stoichiometry between $S_2O_3^{2-}$ oxidation and MnO_2 reduction. In

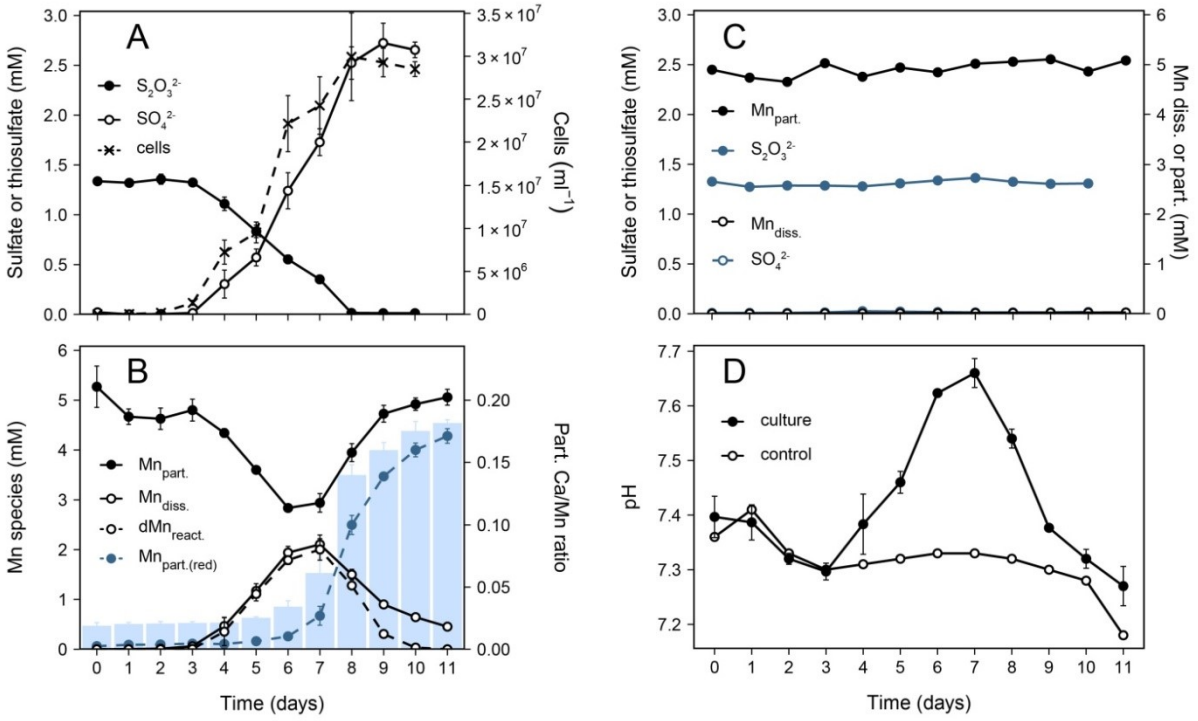

Figure 15: Growth of *S. marisnigri* with MnO_2 and $S_2O_3^{2-}$. A, oxidation of $S_2O_3^{2-}$ resulted in growth and accumulation of SO_4^{2-} in a final ratio of 1:2. B, reduction of MnO_2 results in the equal increase in dissolved Mn ($Mn_{diss.}$) until day 6, almost exclusively reactive Mn ($dMn_{react.}$, putative Mn^{3+}). With the precipitation of $Mn(Ca)CO_3$, indicated by the increase in particulate Mn and increasing particulate Ca to Mn ratio (bars). C, abiotic controls show no changes in the time course of the experiment. D, pH increase due to Mn reduction and decrease at the time $Mn(Ca)CO_3$ precipitates.

accordance to Eq. 3.13 and 3.15, the pH decreased from 7.65 at day 7 to 7.3 towards day 10-11 (Fig. 15D), due to the precipitation of $Mn(Ca)CO_3$.

$$Mn^{2+} + HCO_3^- \longrightarrow MnCO_3 + H^+ \qquad 3.15$$

In theory, results shown in Fig. 15 could also be attributed to a biological disproportionation of $S_2O_3^{2-}$ to H_2S and SO_4^{2-} (Eq. 3.16) with a subsequent chemical oxidation of H_2S with MnO_2 (Tab. 2).

$$S_2O_3^{2-} + H_2O \rightarrow SO_4^{2-} + HS^- + H^+ \qquad 3.16$$

This is unlikely and will be discussed in more details in chapter 3.3.3.

Cultivation of *S. marisnigri* with MnO_2 and a constant supply of H_2S

Growth of *S. marisnigri* with MnO_2 and a constant supply of H_2S resulted in the accumulation of SO_4^{2-} concurrent with increasing cell numbers, with negligible concentrations of S^0,

whereas in the sterile control S^0 accumulated with just minor concentrations of SO_4^{2-} (Fig. 16). In the biological treatment (Fig. 16B) 4 times more total dissolved Mn was produced compared to the sterile control (Fig. 16D), according to Eq. 3.17 and Eq. 3.18, respectively.

$$4\,MnO_2 + HS^- + 7\,H^+ \longrightarrow 4\,Mn^{2+} + SO_4^{2-} + 4\,H_2O \qquad 3.17$$

$$MnO_2 + HS^- + 3\,H^+ \longrightarrow Mn^{2+} + S^0 + 2\,H_2O \qquad 3.18$$

The summed concentration of S^0 and SO_4^{2-} between the biological treatment (Fig. 16A) and the sterile control (Fig. 16C) was unequal. Nevertheless, the filling levels of the bottles were equal and the setup of the experiment (see chapter 2.12.2) excluded dissimilarities regarding

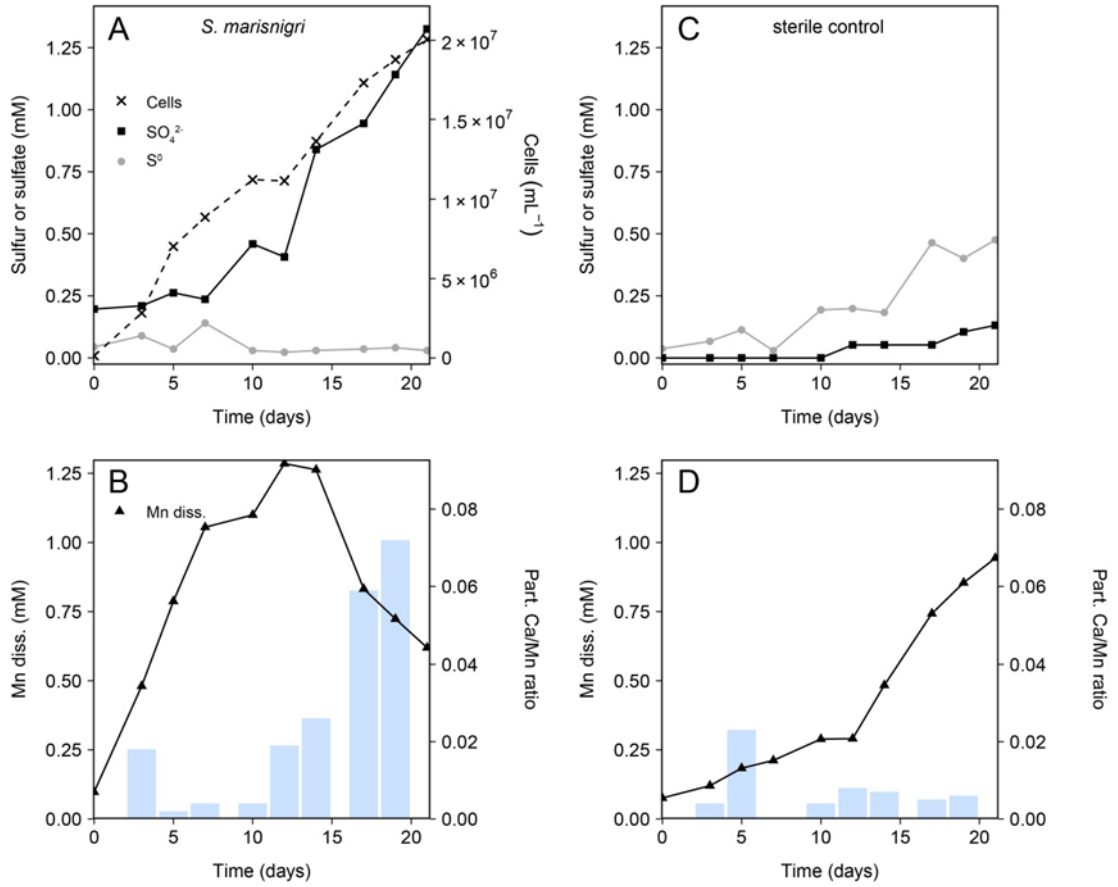

Figure 16: *S. marisnigri* and a sterile control were cultivated with MnO_2 and H_2S was constantly supplied via a peristaltic pump out of a Na_2S stock solution (Fig. 9). Growth of S. *marisnigri* was concurrent with the production of SO_4^{2-} (A) and the production of dissolved Mn (B), while the concentration of S^0 remained low. In the sterile control, S^0 instead of SO_4^{2-} accumulated (C) and the dissolved Mn is accumulating in a lower amount (D). Increasing Ca content in the particulate phase (B, bars) together with decreasing concentrations of dissolved Mn indicate the precipitation of $Mn(Ca)CO_3$.

H_2S addition between the bottles. Therefore, about 0.8 mM S was missing in S-pools others than S^0 and SO_4^{2-} in the sterile treatment. After day 5, the factor in the total dissolved Mn concentration between the biological and the sterile treatment exceeds 4 and reached 4.97 at day 7, which indicated the presence of a sulfur species with a redox state below 0, e.g. polysulfides (S_n^{2-}) or unreacted H_2S in the presence of MnO_2 in the sterile control.

The data resulted from growth of *S. marisnigri* with MnO_2 and a constant supply of H_2S (Fig. 16) could also be explained by an incomplete abiotic oxidation of H_2S with MnO_2 to e.g. S^0 (Tab. 2), followed by a biological oxidation to SO_4^{2-} or a disproportionation of S^0 to H_2S and SO_4^{2-}. To provide evidence, that *S. marisnigri* did not depend on S-compounds with intermediate oxidation state and is capable of oxidizing H_2S directly, several experiments were conducted.

Cultivation of *S. marisnigri* and *S. baltica* with NO_3^- and H_2S

S. marisnigri and *S. baltica* were cultivated with NO_3^- instead of MnO_2 as terminal electron acceptor. NO_3^- is non-reactive with H_2S and can be used as terminal electron acceptor by *S. marisnigri* and *S. baltica* (see chapter 3.3.1). H_2S was added several times a day in small amounts out of a Na_2S stock solution (Fig. 17, grey dots). Under these culturing conditions, *S. marisnigri* and *S. baltica* grew (Fig. 17, open circles, dashed line) and H_2S concentrations remained undetectable (open diamonds). In the corresponding controls H_2S accumulated steadily (solid diamonds) according to the additions of H_2S (grey dots).

Cultivation of *S. marinsigri* with MnO_2 and either H_2S or S-products of a chemical oxidation of H_2S with MnO_2

In another approach addressing the same question, *S. marisnigri* was cultivated with MnO_2 as terminal electron acceptor and the electron donor was supplied daily as described above by multiple small additions of different solutions. The first electron donor solution was a pure Na_2S stock solution (H_2S); the other was treated with MnO_2 to generate oxidation products of S with different oxidation states (Mn/H_2S) before it was added to *S. marisnigri*. Chemical

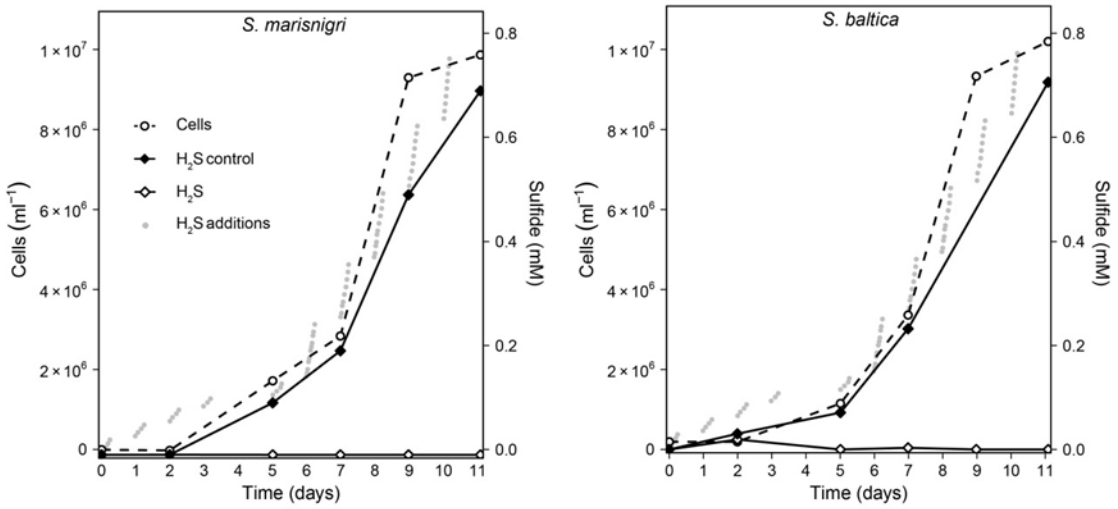

Figure 17: Cultivation of *S. marisnigri* and *S. baltica* with NO_3^- as terminal electron acceptor and H_2S as electron donor. H_2S was added in small single additions resulting in micromolar concentrations out of a Na_2S stock solution (grey dots). Both strains showed growth (open circles, dashed line) and H_2S remained constantly low (open diamonds, solid line). In the sterile controls, H_2S accumulated steadily according to the additions of H_2S (closed diamonds, solid line).

analysis of the two electron donor solutions showed the following composition. The H_2S solution had a concentration of 10.9 mM with no detectable S compounds with other oxidation state. The Mn/H_2S solution had a concentration of 9.5 mM and consisted of S^0 (96.1%), $S_2O_3^{2-}$ (3.6%) and SO_4^{2-} (0.3%). Growth of *S. marisnigri* was observed under both culturing conditions (Fig. 18). When H_2S was added directly as electron donor (left), growth rate and yield where increased in comparison to the parallels treated with pre-reacted H_2S

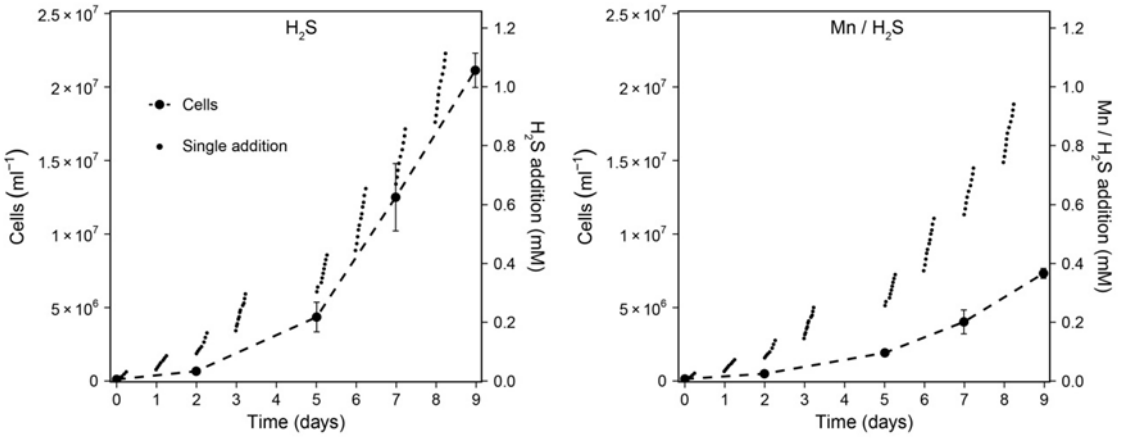

Figure 18: *S. marisnigri* in triplicates. Addition of H_2S, pre-reacted with MnO_2 (right) or not (left).

(right) within the 9 days of experiment. Samples for SO_4^{2-} were taken approximately 1 week after the end of the electron donor additions and SO_4^{2-} concentrations of 1.28 mM ± 0.04 (Mn/H_2S) and 1.54 mM ± 0.04 (H_2S) were measured. With pre-reacted H_2S (Fig. 18, right), the growth yield was approximately 60% lower compared to the parallel where H_2S was added directly (Fig. 18, left). This difference cannot be attributed to the overall lower addition of electron donor. Unfortunately, no cell numbers were estimated after day 9. Therefore it may be possible, that the growth rate of *S. marisnigri* was lower when pre-reacted H_2S was provided, but cell numbers kept increasing after day 9 reaching an overall comparable yield.

H_2S oxidation rates in a temperature gradient

Cell specific H_2S oxidation rate of *S. marisnigri* and H_2S oxidation rates in sterile controls in the presence of MnO_2 were estimated in a temperature gradient ranging from 3 °C to 18 °C (Fig. 19 – for more details see also chapter 3.2.1). The chemical oxidation rate responded linearly to changes in temperature, in contrast to the biological oxidation rate per cell, which responded in an exponential like decrease towards 3 °C, indicating an enzymatic related inhibition of the H_2S oxidizing activity due to low temperatures.

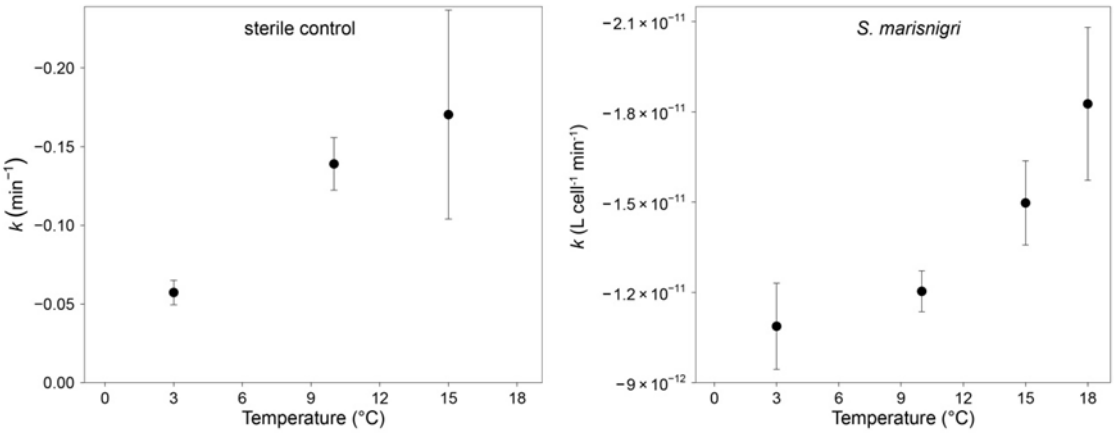

Figure 19: Reaction rate coefficient *k* in the temperature range from 3 to 18 °C for the oxidation of H_2S with or without *S. marisnigri*. In the sterile control, the reaction rate responded linearly to the change of the temperature. In the presence of *S. marisnigri* the reaction rate coefficient responded in an exponential like manner, reflecting a putative enzymatically catalyzed oxidation of H_2S.

3.2 Chapter II: Influence of a biological H_2S oxidation on the geochemical structure of the Black Sea suboxic zone.

In the Black Sea suboxic zone, H_2S is consumed up to tens of meters below the first detectable concentrations of O_2 or NO_3^-. The only available compound for H_2S oxidation would be MnO_2, which can be transported by gravitational sinking from the oxic, overlying water body, to the sulfidic water below.

3.2.1 Estimation of a biological H_2S oxidation rate in the presence of MnO_2

Experiments with *S. marisnigri* were done to obtain a H_2S-oxidation rate represented by a bacterium originating from the lower boundary of the Black Sea suboxic zone. To enable the measurement of a H_2S oxidation rate by *S. marisnigri* in the presence of MnO_2, the concurrent chemical oxidation of H_2S with MnO_2 had to be determinable and in best case constant to be subtracted from the overall oxidation rate. Therefore, the second order chemical reaction between MnO_2 and H_2S had to be simplified. By adding MnO_2 in excess, the reaction order was changed from a second order to a pseudo-first order reaction. Thereby, the reaction rate was only depending on the concentration of H_2S and not both, the surface area of MnO_2 and the concentration of H_2S.

This solved several difficulties:

i. The chemical reaction rate was only depending on the concentration of H_2S.

ii. The chemical oxidation of H_2S was proceeding with the maximum possible reaction rate at the given ambient conditions of pH, temperature and mineralogical structure of the provided MnO_2.

iii. Only the concentration of H_2S had to be recorded, which was possible with high resolution by the use of H_2S microsensors.

iv. The rate could be determined and subtracted from a rate which was determined in the presence of *S. marisnigri*.

S. marisnigri was cultivated with $S_2O_3^{2-}$ as electron donor and MnO_2 in 10-fold excess. During the growth phase of 12 days, the cell counts of *S. marisnigri* exceeded 10^7 cells mL^{-1}, $S_2O_3^{2-}$ was depleted and the remaining concentration of MnO_2 was high enough to result in pseudo-first order mode of reaction with single additions of H_2S (Tab.21 – compare sterile control with pasteurized culture treatment). Pulses of H_2S were added to the medium and the disappearance of H_2S was recorded with a H_2S microsensor (Fig. 20). Afterwards, the medium was pasteurized or poisoned with sodium azide to inhibit *S. marisnigri* and further pulses of H_2S were added. The concentration of H_2S was normalized to the initial concentration (Fig. 20A) of H_2S for each single addition and plotted against time. The reaction rate coefficient k ($time^{-1}$) was calculated for each addition of H_2S by fitting the equation in Fig. 20 to the respective plot (Fig. 20B and C), where $C_{H2S(t)}$ is the concentration of H_2S at time t, $C_{H2S(0)}$ is the initial concentration of H_2S, t the time in minutes and a the variable to adjust for the y-intercept. Consecutive additions of H_2S resulted in the reproducible exponential like disappearance of H_2S (Fig. 20, top) with comparable reaction rate coefficients, which are summarized in Tab. 21. Addition of sodium azide reduced the H_2S oxidation rate by approximately

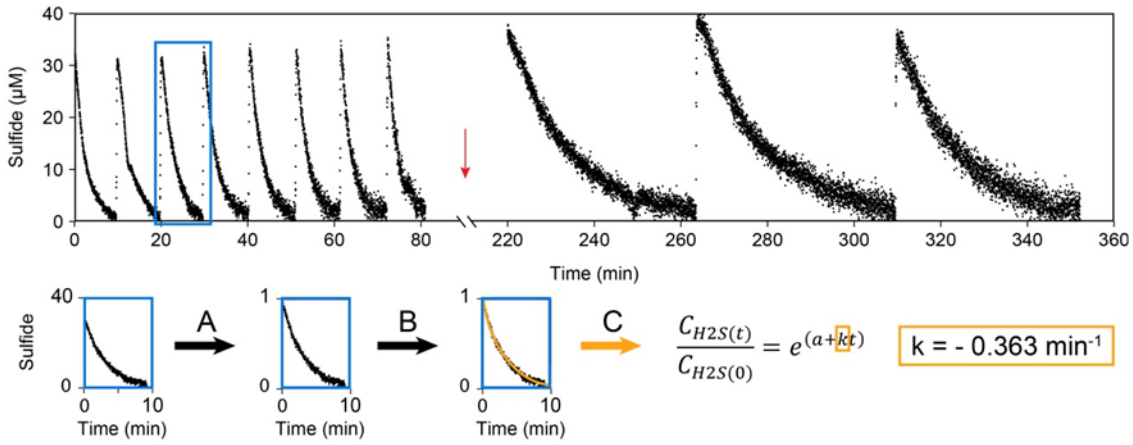

Figure 20: Experimental approach to determine H_2S oxidation rates. Chronological sequence of consecutive additions and adjacent consumptions of micromolar concentrations of H_2S (top). After several additions, the medium was either pasteurized or poisoned with sodium azide (red arrow) and another three additions were recorded subsequently. Each addition was evaluated separately. A, normalization of one addition to the initial value. B, non-linear least square fit to the shown equation. C, solving the equation after *k*.

Table 21: Reaction rate coefficient *k* as a function of different types of inhibition in the presence or absence of *S. marisnigri.* Cell numbers of *S. marisnigri* were 5.87 x 10^{10} L^{-1}, 4.71 x 10^{10} L^{-1} and 5.10 x 10^{10} L^{-1} in the parallels 1, 2 and 3, respectively. 0 = no inhibition; A = inhibition with sodium azide; P = inhibition with pasteurization.

	Inhibition	Parallel	*k* (min^{-1})	SD	N
S. marisnigri	0	1	-0.414	0.044	7
	A	1	-0.309	0.011	3
	0	2	-0.391	0.026	8
	P	2	-0.081	0.007	3
	0	3	-0.419	0.034	8
	P	3	-0.080	0.004	3
Sterile control	0	1	-0.090	0.004	5
	A	1	-0.071	0.003	2
	0	2	-0.098	0.009	5
	P	2	-0.077	0.001	3
	0	3	-0.073	0.005	5
	P	3	-0.079	0.004	3

25% while pasteurization reduced the oxidation rate to the level of the chemical background reaction (Tab. 21 - compare with the sterile control measurements). Little to no effect of the addition of sodium azide or pasteurization on the reaction rate of the sterile control was observed.

3.2.2 Numerical modeling

To implement these H_2S oxidation rates of *S. marisnigri* into a numerical model, a biological reaction rate coefficient k_{bio} had to be calculated according to Eq. 3.19,

$$k_0 - k_{\mathrm{A\ or\ P}} = k_{\mathrm{bio(A)or\ bio(P)}} \qquad 3.19$$

where k_0 is the reaction rate coefficient in the presence of *S. marisnigri* before inhibition, k_A the reaction rate coefficient after the addition of sodium azide, k_P the reaction rate coefficient after pasteurization and $k_{bio(A)}$ and $k_{bio(P)}$ the respective resulting biological reaction rate coefficients.

In the following, $k_{bio(A)}$ and $k_{bio(P)}$ were calculated per second and per cell to implement the value into the numerical model. Abundances of *Epsilonbacteraeota* in Black Sea waters of the

suboxic zone needed for the model were kindly provided by Klaus Jürgens. The cell abundances of *Epsilonbacteraeota* were estimated by fluorescence in situ hybridization (FISH) staining with probe EPS914. Cellular abundance of *Epsilonbacteraeota* did match the natural abundance of *Sulfurimonas* spp. in the Black Sea suboxic zone closely. This has been shown by Dr. Thomas Schott and Prof. Dr. Klaus Jürgens (personal communication). With 16S rRNA amplicon sequencing and metatranscriptomic analysis it was shown that over the entire suboxic zone up to 97% of all *Epsilonbacteraeota* reads belong to the genus *Sulfurimonas*, which is almost exclusively expressing the sulfide:quinone oxidoreductase gene (*sqr*) in the depth of H_2S removal. Therefore, applying the H_2S oxidation rates measured with *S. marisnigri* in pure culture to the abundance of *Epsilonbacteraeota* is reflecting the natural setting quite well.

For the model approach it is assumed that Mn oxides are constantly provided in sufficient amount by gravitational sinking. The H_2S profiles shown in Figure 21 (A and D) are obtained after a 3 year time run of the model. H_2S concentration profiles modeled with $k_{bio(A)}$ = -3.16 x 10^{-14} L cell^{-1} s^{-1} and $k_{bio(P)}$ = -1.05 x 10^{-13} L cell^{-1} s^{-1} (A and D, respectively) resulted in a sharp drop to 0 µM H_2S comparable to the measured H_2S profile in the Black Sea (Fig. 2A and B, Fig. 21, grey dots). The overall H_2S oxidation rate (Fig. 21B and E) exceeded 1 x 10^{-6} µM s^{-1} and 1.5 x 10^{-6} µM s^{-1} and the cell specific oxidation rate (Fig. 21C and F) exceeded 2 x 10^{-14} µM s^{-1} and 4 x 10^{-14} µM s^{-1} based on $k_{bio(A)}$ and $k_{bio(P)}$, respectively. Based on the work of Yao & Millero (1993) chemical reaction rates of MnO_2 and H_2S were calculated at 10 °C and pH 7. With 10 nM MnO_2 9.53 x 10^{-8} µM H_2S s^{-1} are oxidized at a constant H_2S concentration of 1 µM. The model was run with a chemical *k* value (k_{chem}) of -9.53 x 10^{-8} s^{-1}. Because the steep H_2S profile measured in situ by Schulz-Vogt et al. (2019) (Fig. 21, grey dots), oxidation rates were with k_{chem} were calculated at the chemocline and overlying waters (Fig. 21G). With these settings, the suboxic zone collapsed and H_2S was not retained at approx. 105 m water depth.

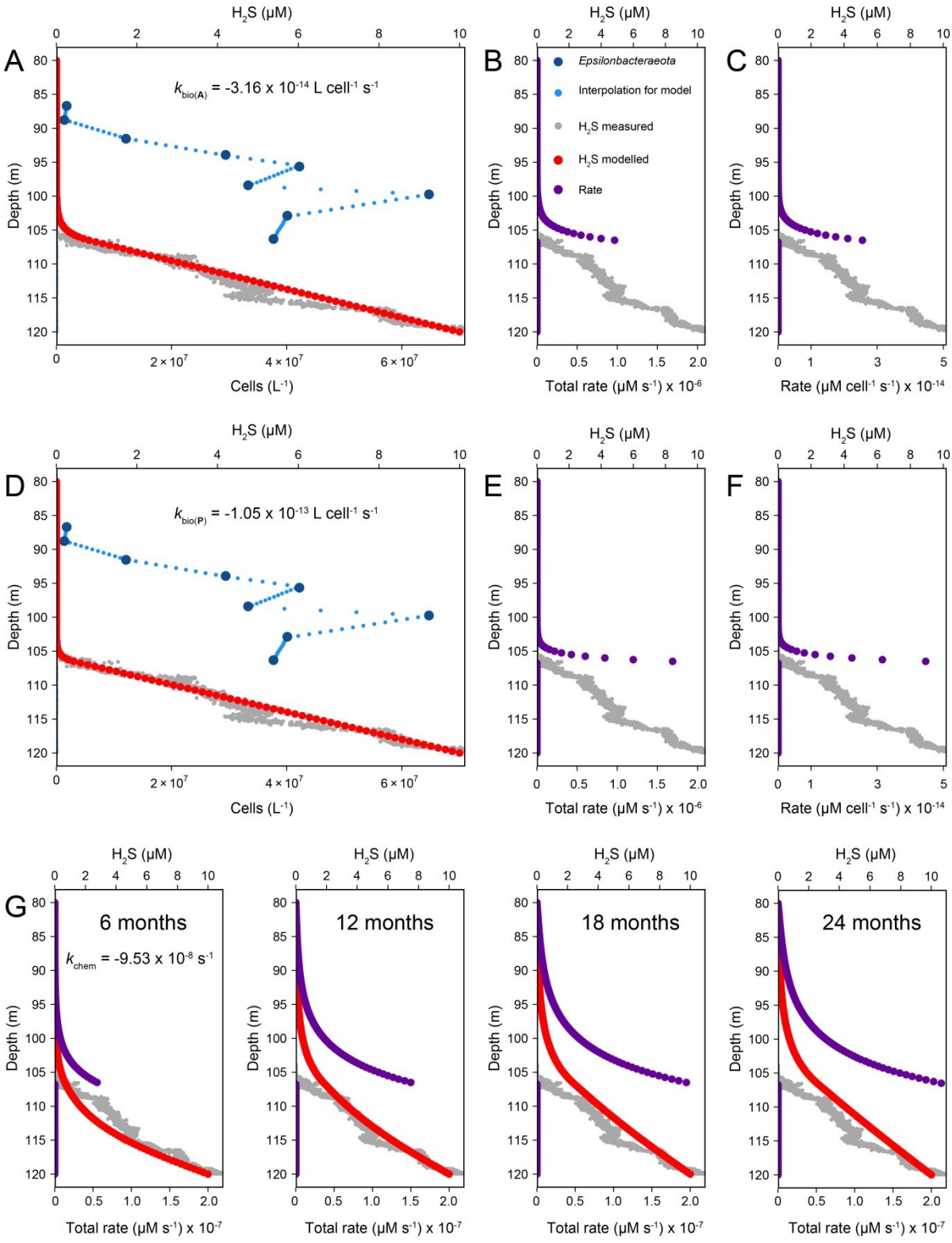

Figure 21: Modeled H_2S concentration (red dots) profiles based on $k_{bio(A)}$ (A), $k_{bio(P)}$ (D) and k_{chem} (G) and resulting total (B, E and G) and cell specific (C and F) H_2S oxidation rates (purple dots) in the suboxic zone of the Black Sea. Data for the in situ H_2S profile (grey dots) were taken from Schulz-Vogt et al. (2019). Abundances of *Epsilonbacteraeota* from the Black Sea (large blue dots) were kindly provided by Prof. Dr. Klaus Jürgens, and interpolated (small blue dots). Plots A to F are shown in steady state. Chemical H_2S oxidation rate (G) calculated at 10 °C, pH 7 and 10 nM MnO_2 (Yao & Millero, 1993).

3.3 Chapter III: Ecological niches of the newly isolated *Sulfurimonas* strains in comparison to *S. gotlandica*.

Two new isolates, one originating from the Black Sea named *Sulfurimonas marisnigri* and one from the Baltic Sea named *Sulfurimonas baltica,* together with the already validly described closely related species *Sulfurimonas gotlandica* GD1, were investigated regarding dissimilatory metabolism, assimilatory metabolism and abiotic factors influencing growth.

3.3.1 Dissimilatory metabolism - electron acceptors

Oxygen (O_2)

The ability to utilize O_2 as electron acceptor was tested along with the putative inhibiting effects of O_2 on growth of *S. marisnigri*, *S. baltica* and *S. gotlandica* by adjusting the O_2 content in the headspace of partially filled serum bottles, but no further electron acceptor was added. All strains showed growth with O_2 provided as electron acceptor (Fig. 22). In contrast to *S. gotlandica*, *S. marisnigri* and *S. baltica* were unable to grow at the highest O_2 content of 21%. No major difference in dissolved oxygen concentration at 21% O_2 in the headspace with *S. marisnigri* (-2 µM ± 22) or *S. baltica* (-6 µM ± 36) was detectable in comparison to the control, whereas the difference in dissolved O_2 concentration was clearly higher for *S. gotlandica* (-179 µM ± 81) shown in Tab. 22.

No visible differences in growth could be seen for 4% and 1% O_2 with *S. marisnigri* and *S. baltica*. *S. gotlandica* showed best growth at 4% followed by 1% and 21% O_2. At 0% O_2, all

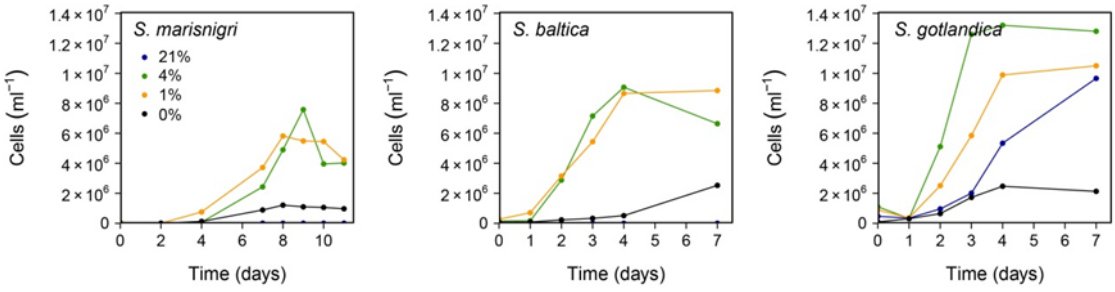

Figure 22: Growth of *S. marisnigri*, *S. baltica* and *S. gotlandica* with O_2 as electron acceptor at different O_2 contents in the headspace.

Table 22: Difference in the dissolved oxygen concentration after complete growth of *S. marisnigri*, *S. baltica* and *S. gotlandica* with O_2 as sole electron acceptor.

Strain	% O_2 (N)	ΔO_2 (µM)	SD
S. marisnigri	21 (3)	-2	22
	4 (3)	-45	1
	1 (3)	-30	1
	0 (2)	-2	0
S. baltica	21 (3)	-6	36
	4 (3)	-55	2
	1 (3)	-26	2
	0 (3)	-2	0
S. gotlandica	21 (3)	-179	81
	4 (3)	-49	1
	1 (3)	-21	1
	0 (3)	-2	1

strains showed increasing but overall lower cell numbers, which was supported by decreased dissolved oxygen concentrations in the serum bottles after growth. Because no reducing agent was used for the preparation of anoxic medium, small contaminations of O_2 could not be excluded. Between 1.5 and 10 µM dissolved O_2 were measured in un-inoculated serum bottles with 50 mL medium and 100 mL headspace volume.

Nitrate (NO_3^-)

All three strains showed growth with NO_3^- provided as electron acceptor (Fig. 23), but the overall growth yield of *S. marisnigri* and *S. baltica* is more than one order of magnitude lower compared to *S. gotlandica* under the same culturing conditions. In a more detailed approach, growth of *S. marisnigri* with $S_2O_3^{2-}$ and NO_3^- was shown to be concurrent with the production of NO_2^- and stoichiometric removal of NO_3^- (Fig. 24). The addition of MnO_2 at day 22, after growth stopped at day 8-9 due to the depletion of NO_3^- resulted in subsequent increasing cell numbers in the presence of approximately 4.5 mM NO_2^- indicating that *S. marisnigri* is not inhibited by about 4 mM NO_2^-.

Nitrite (NO_2^-)

No growth of *S. marisnigri, S. baltica* and *S. gotlandica* was observed with NO_2^- as electron acceptor within the time course of 7 days (Fig. 25). Because the growth yields of *S. baltica*

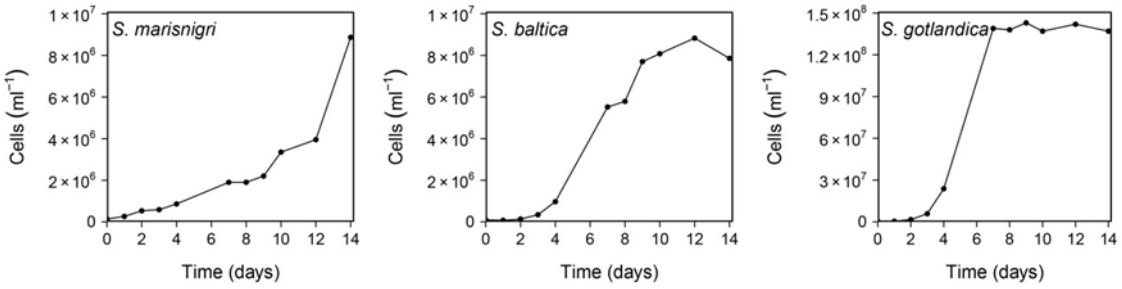

Figure 23: Growth of *S. marisnigri*, *S. baltica* and *S. gotlandica* with NO_3^- as sole electron acceptor.

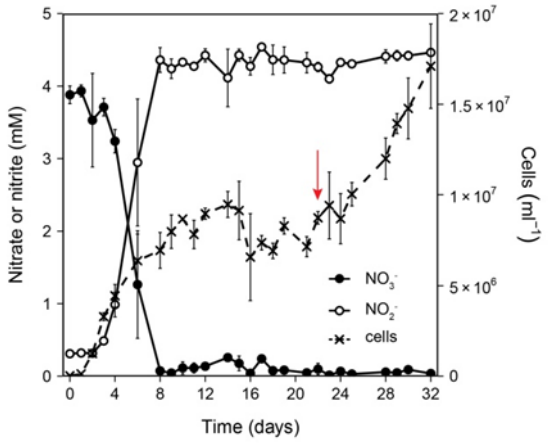

Figure 24 Growth of *S. marisnigri* with NO_3^- and a surplus of $S_2O_3^{2-}$ in triplicates. NO_3^- is stoichiometrically reduced to NO_2^-. Growth went on after MnO_2 was added at day 22 (red arrow).

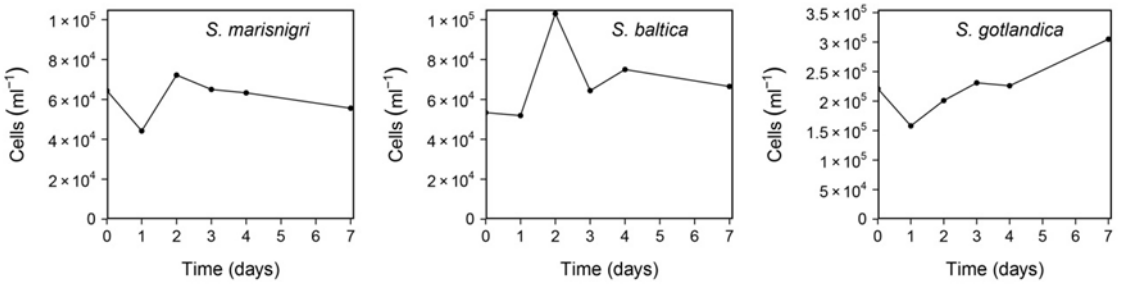

Figure 25: Growth of *S. marisnigri*, *S. baltica* and *S. gotlandica* with NO_2^- as sole electron acceptor. Mind the different y-axis and low values.

and *S. marisnigri* cultivated with NO_3^- and $S_2O_3^{2-}$ were comparable (Fig. 23), *S. baltica* might as well reduce NO_3^- to NO_2^- and not further to N_2. *S. gotlandica* might have started growing but a prolonged sampling would have been necessary to assure the trend towards day 7 (Fig. 25).

Metal oxides

All three strains were cultivated with different iron sources and *S. gotlandica* was additionally cultivated with MnO_2. As potential electron acceptor the iron oxides $FeCl_3$, Fe_2O_3, freshly precipitated amorphous FeOOH and goethite (α-FeOOH) together with $S_2O_3^{2-}$ as electron

donor were tested. In a first approach, all strains were cultivated with Fe_2O_3, $FeCl_3$ and *S. gotlandica* additionally with MnO_2 as electron acceptors (Fig. 26).

Unfortunately, no positive or negative controls were prepared for this experiment. All strains showed increasing cell numbers under these culturing conditions. Interestingly, cells of all three *Sulfurimonas* strains did not show attachment to any of the tested metal oxide particles examined by DAPI stained epifluorescence microscopy and SEM. To exclude a potential growth of the three strains with $S_2O_3^{2-}$ and O_2 contaminations in the medium, two bottles were prepared in parallel with just $S_2O_3^{2-}$. Putative O_2 contaminations were eliminated chemically in one bottle by the addition of cysteine 7 days before cells were added (Fig. 26, Control + Cys), the other remained untreated (Fig. 26, Control). This was done for *S. marisnigri* and *S. gotlandica*. Growth was detectable within 7 days when no cysteine was added in contrast to the parallel treated with cysteine, where no growth was observed. Additionally, concentrations of dissolved Fe and Mn were quantified since the reduction of metal oxides should have led to the increase in dissolved phases of the respective metal. No dissolved Fe could be detected in bottles cultivated with Fe_2O_3 and dissolved Mn concentration was below 25 µM, which is far too low to be attributed to a dissimilatory Mn reduction by *S. gotlandica*. Further, no indication of a particulate reduced Mn phase (see chapter 3.1) was observed by eye or

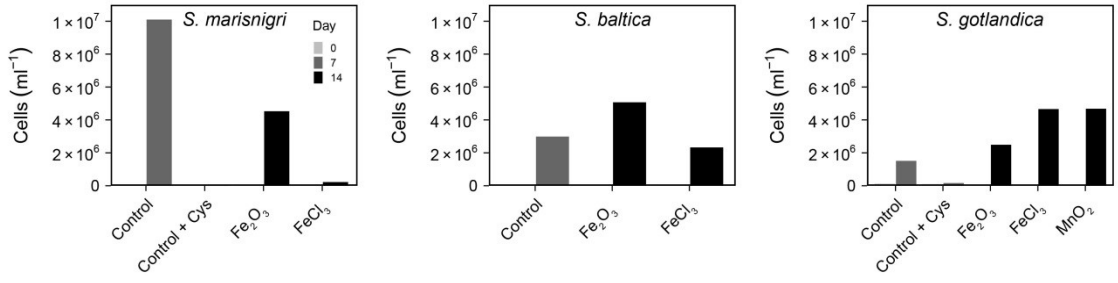

Figure 26: Growth of *S. marisnigri*, *S. baltica* and *S. gotlandica* cultivated with different metal oxides as electron acceptors. Control measurements were done without the addition of a metal oxide electron acceptor (Control) and cysteine was added to parallel control incubations (Control + Cys) to determine the influence of ambient O_2 contaminations on growth of *S. marisnigri* and *S. gotlandica*.

scanning electron microscopy when *S. gotlandica* was cultivated with MnO_2. In a second approach, all strains were cultivated with freshly precipitated amorphous FeOOH or goethite (α-FeOOH). No growth or attachment to the Fe oxide particles was observed.

3.3.2 Dissimilatory metabolism - electron donors

Elemental sulfur (S^0)

Freshly prepared colloidal elemental sulfur (S^0) was tested as potential electron donor for growth of *S. marisnigri*, *S. baltica* and *S. gotlandica*. All strains showed growth with S^0 as electron donor with a 1 day lag phase (Fig. 27) and the growth yield of all strains was comparable. No H_2S smell was noticeable at the end of the experiment after the bottles were opened.

Sulfite (SO_3^{2-})

Adding SO_3^{2-} as electron donor did not result in growth of *S. marisnigri* or *S. baltica* (Fig. 28). *S. gotlandica* showed growth until day 7 followed by an unexpected sharp drop from 8 x 10^7 cells mL^{-1} to 2-3 x 10^6 cells mL^{-1}.

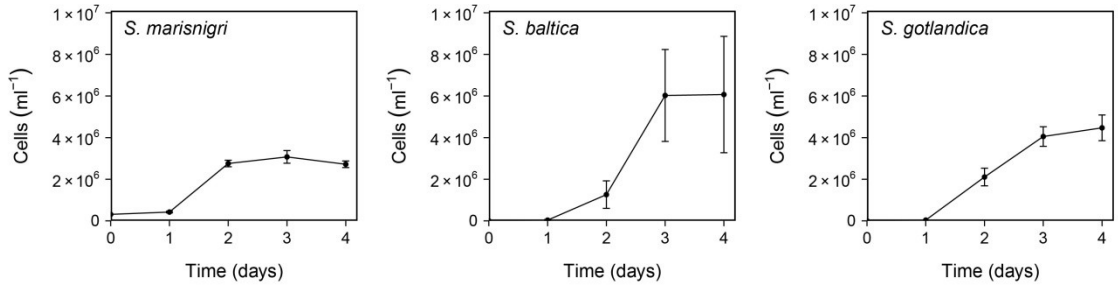

Figure 27: Growth of *S. marisnigri*, *S. baltica* and *S. gotlandica* in triplicates with colloidal sulfur (S^0) added as electron donor.

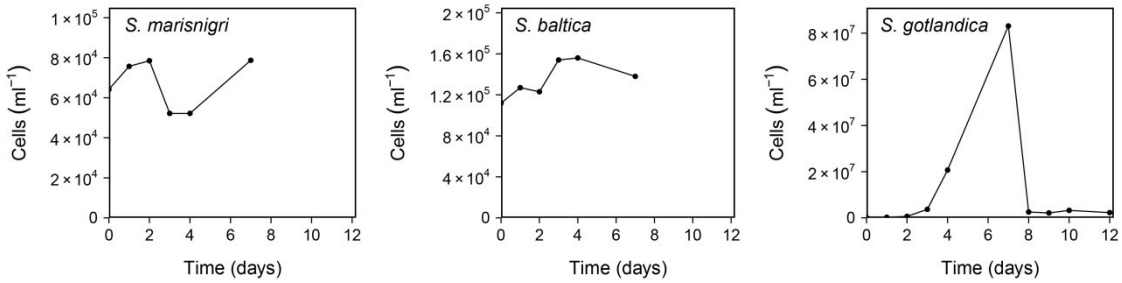

Figure 28: Growth of *S. marisnigri*, *S. baltica* and *S. gotlandica* with sulfite (SO_3^{2-}) added as electron donor.

Hydrogen (H_2)

Hydrogen was provided by flushing the bottle headspaces with H_2 gas. To exclude any negative effects of H_2 in the headspace on growth, a positive control containing a H_2 filled headspace as well as $S_2O_3^{2-}$ provided as electron donor in the medium was prepared. A negative control contained neither H_2 in the bottle headspace, nor $S_2O_3^{2-}$ was added as electron donor. All strains showed growth in the presence of H_2 in the bottle headspace (Fig. 29). Cell numbers of *S. gotlandica* were close to one magnitude higher than cell numbers of *S. marisnigri* and *S. baltica* after 14 days of growth. No growth was observed in negative controls.

Organic carbon

To test the ability of *S. marisnigri*, *S. baltica* and *S. gotlandica* to respire organic carbon, a mixture of acetate ($C_2H_4O_2$), propionate ($C_3H_6O_3$) and succinate ($C_4H_6O_4$) was supplied as electron donors (Fig. 30). Growth was not observed for *S. marisnigri* and *S. baltica*, and cell

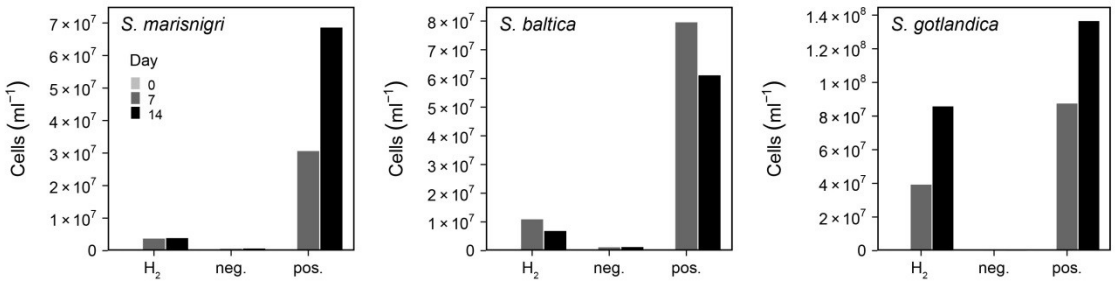

Figure 29: Growth of *S. marisnigri*, *S. baltica* and *S. gotlandica* with hydrogen (H_2) added as electron donor. Positive controls were prepared by adding $S_2O_3^{2-}$ as electron donor next to H_2. Negative controls were prepared by adding neither H_2 to the bottle head space nor $S_2O_3^{2-}$ as additional electron donor.

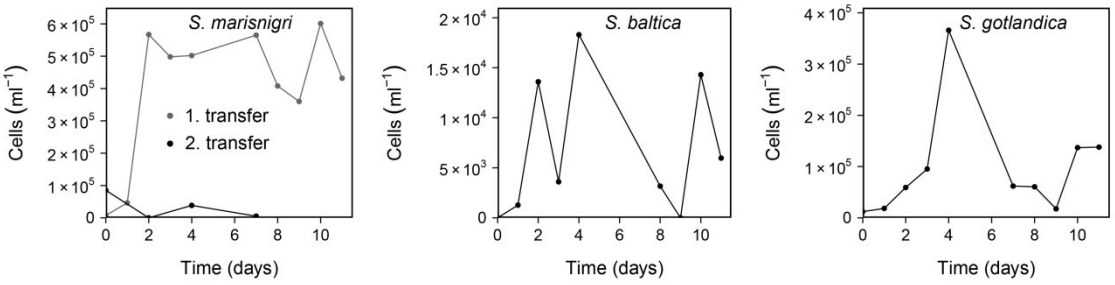

Figure 30: Growth of *S. marisnigri*, *S. baltica* and *S. gotlandica* with an organic carbon mixture containing acetate, propionate and succinate added as electron donor. With *S. marisnigri* as an example it can be seen, that multiple transfers might be necessary to exclude growth.

abundance remained low. *S. gotlandica* showed growth to a maximum of about 3.5 x 10^5 cells mL^{-1} at day 4, which is low compared to the growth yield on reduced sulfur species.

3.3.3 Disproportionation of S^0 and $S_2O_3^{2-}$

The disproportionation of S^0 or $S_2O_3^{2-}$ leads to the production of H_2S according to Eq. 3.20 and 3.21 (Finster et al., 1998), which itself can react chemically with MnO_2 (Yao and Millero, 1993, Tab. 2) used for cultivation as electron acceptor for *S. marisnigri* and *S. baltica*.

$$S_2O_3^{2-} + H_2O \rightarrow SO_4^{2-} + HS^- + H^+ \quad 3.20$$

$$S^0 + 4\,H_2O \rightarrow SO_4^{2-} + 3\,HS^- + 5\,H^+ \quad 3.21$$

To test the ability of the three strains to disproportionate $S_2O_3^{2-}$ and S^0 the respective compound was added without the addition of a further electron acceptor. All strains showed growth under these culturing conditions (Fig. 31).

However, the overall growth yield could also be attributed to the oxidation of S^0 and $S_2O_3^{2-}$ with ambient O_2 contaminations as electron acceptor, since the 0% O_2 negative control used

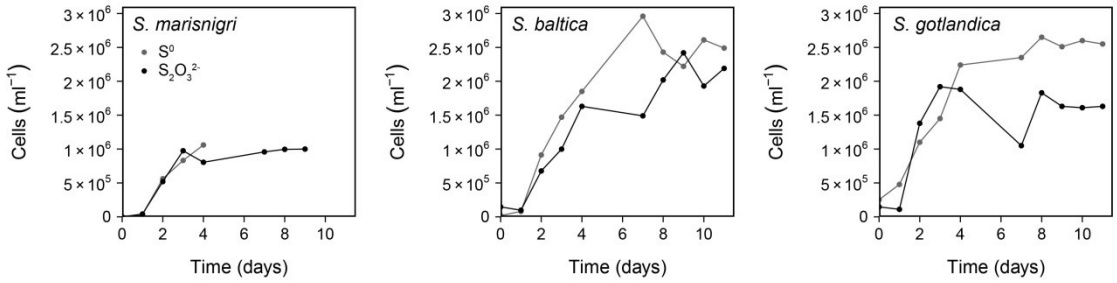

Figure 31: Growth of *S. marisnigri*, *S. baltica* and *S. gotlandica* cultivated with S^0 or $S_2O_3^{2-}$ and no further addition of an electron donor.

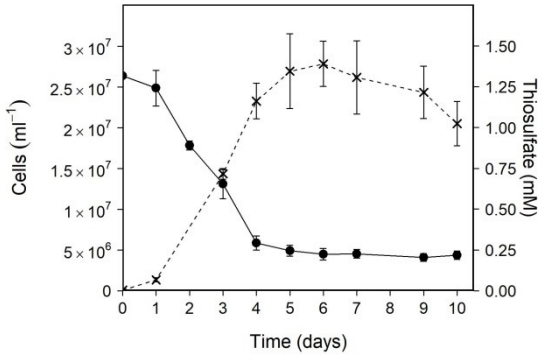

Figure 32: *S. marisnigri* grown with $S_2O_3^{2-}$ and MnO_2. Concentration of $S_2O_3^{2-}$ (black solid circles, solid line) remained unchanged after complete growth of *S. marisnigri* (crosses, dashed line) and depletion of MnO_2 approximately at day 4 to 5 according to the color shift to brownish-grey.

in the experiments with O_2 as potential electron acceptor shows comparable growth yields of 2-3 x 10^6 cells mL^{-1} (Fig. 22). Further, no smell of H_2S was noticeable after the bottles were opened at the end of growth. To address this critical issue in more detail, *S. marisnigri* was grown with MnO_2 and a slight surplus of $S_2O_3^{2-}$ (Fig. 32). At day 4 to 5 the color of the bottles changed from black to brown greyish which typically indicates the depletion of MnO_2 (see chapter 3.1). Concentrations of $S_2O_3^{2-}$ remained constant after the depletion of MnO_2 at approximately day 5-6 indicating no disproportionation of $S_2O_3^{2-}$.

3.3.4 Sulfate (SO_4^{2-}) - reduction

To test for SO_4^{2-} reduction a mixture of acetate, propionate and succinate was added to standard medium enriched in SO_4^{2-} added as $MgSO_4$. No growth of *S. baltica* and *S. gotlandica* was observed (Fig. 33). Increasing but overall low cell numbers of *S. marisnigri* were observed. No smell of H_2S was noticeable after the bottles were opened.

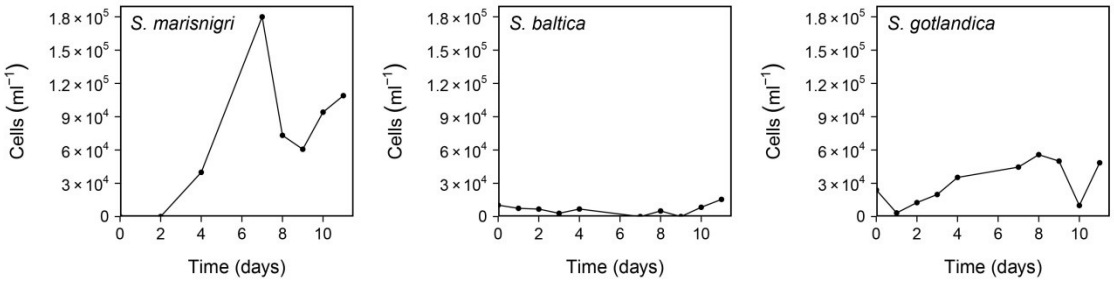

Figure 33: Growth of *S. marisnigri*, *S. baltica* and *S. gotlandica* cultivated with SO_4^{2-} and an organic carbon mixture of acetate, propionate and succinate.

3.3.5 Fermentation

To test for fermentation of organic C, a mixture of acetate, propionate and succinate was added to standard medium. All three strains showed little to no growth under these culturing conditions (Fig. 34). For *S. marisnigri* the first transfer and for *S. baltica* and *S. gotlandica* the second transfer is displayed. The first transfers of *S. baltica* and *S. gotlandica* resulted in cell numbers one magnitude higher compared to the second transfer, which might have also been the case for *S. marisnigri*, if another transfer would have been made.

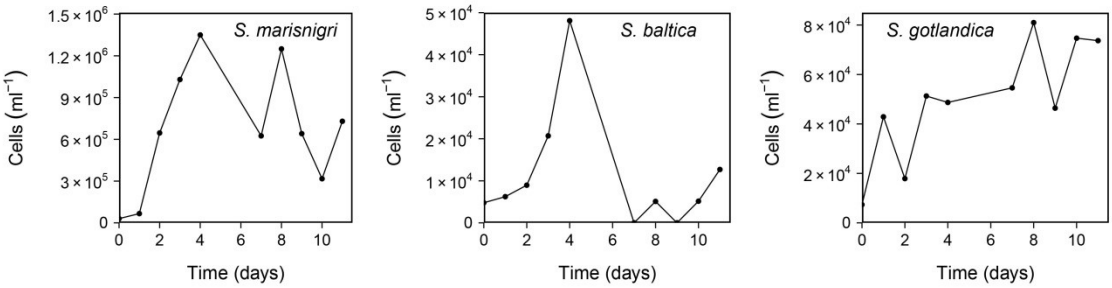

Figure 34: Growth of *S. marisnigri*, *S. baltica* and *S. gotlandica* cultivated with a mixture of acetate, propionate and succinate without any further electron acceptor or donor. Cellular abundance of *S. marisnigri* of the first transfer is shown. For *S. baltica* and *S. gotlandica* the second transfer in the respective growth medium is shown.

3.3.6 Assimilatory metabolism

N_2 - fixation

The ability of *S. marisnigri*, *S. baltica* and *S. gotlandica* to fix molecular N_2 as N-source was investigated by omitting the addition of NH_4Cl as N-source to the medium (Fig. 35). N_2 should have been available in sufficient amounts, because the gas mixture used to purge O_2 during medium preparation and to prevent O_2 contamination in the bottling process consists of 80 vol.% N_2. No NO_3^- was added as electron acceptor for the growth of *S. gotlandica* because it could be used as nitrogen source, too. Thus, O_2 was provided as electron acceptor by replacing the headspace volume with normal breathing air. *S. gotlandica* showed growth in the respective experiment when NH_4Cl was present and O_2 was provided as sole electron acceptor (Fig. 40 and 22). *S. marisnigri* and *S. baltica* showed growth under these culturing conditions in the absence of NH_4Cl (Fig. 35, blue graphs). No growth of *S. gotlandica* was observed under these culturing conditions.

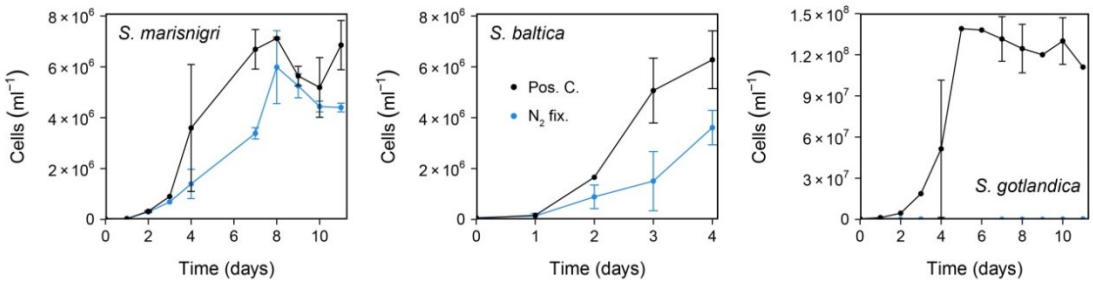

Figure 35: Growth of *S. marisnigri*, *S. baltica* and *S. gotlandica* in the absence of NH_4Cl with only N_2 provided as the N source. For *S. gotlandica*, NO_3^- was substituted with O_2 as electron acceptor by exchanging the headspace with sterile breathing air.

Organic carbon (C-org) assimilation

To test for the ability to use organic carbon as C-source (C-heterotroph) growth medium was prepared with N_2 or Ar gas instead of a gas mixture containing CO_2 and HEPES was used as pH buffer. As potential C-sources acetate, propionate and succinate were tested next to a positive control where HCO_3^- was added and a negative control where no carbon source was provided (Fig. 36). *S. marisnigri* did not show growth with acetate and propionate in the growth phase of 7 days. In the treatment containing succinate the cell numbers were slightly higher compared to the negative control (6.03 x 10^5 cells mL^{-1} to 4.84 x 10^5 cells mL^{-1}, respectively). Therefore, the difference can be considered as too low to decide whether growth was positive or not. *S. baltica* showed growth with all tested carbon sources. Highest cell numbers after the growth period of 7 days were measured with acetate (4.10 x 10^7 cells mL^{-1}) and succinate (3.81 x 10^7 cells mL^{-1}) about 30% more compared to the positive control (2.93 x 10^7 cells mL^{-1}). Cell numbers with propionate were slightly lower after 7 days of growth (1.19 x 10^7 cells mL^{-1}). *S. gotlandica* did not show growth with the tested carbon sources.

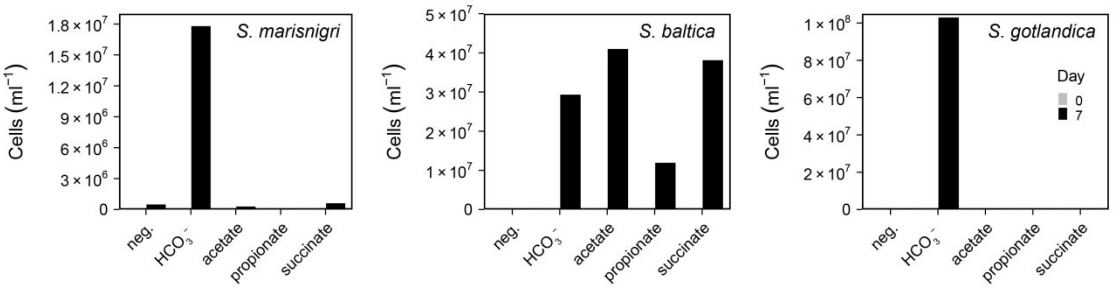

Figure 36: Growth of *S. marisnigri*, *S. baltica* and *S. gotlandica* with C provided exclusively in the form or organic carbon compounds.

Polyphosphate (polyP) accumulation

To quantify the amount of phosphorus accumulated as polyP in *S. marisnigri*, cells of a grown culture were separated into polyP bearing (polyP+) and polyP free (polyP-) cells by specific staining with the antibiotic tetracycline and fluorescence-activated cell sorting. The P content of the sorted samples with known cell concentrations was estimated with ICP-MS. The quan-

tity of P accumulated as polyP in a polyP+ cell was calculated by subtracting the mean P content of a polyP- cell from the mean P content of a polyP bearing cell. With this approach a content of 7.54 x 10^{-18} kg P $cell^{-1}$ (7.54 fg P $cell^{-1}$) or 2.43 x 10^{-16} mol P $cell^{-1}$ (0.243 fmol P $cell^{-1}$) stored as polyP was estimated for *S. marisnigri*.

3.3.7 Abiotic factors influencing growth

In a natural environment, bacteria often have to face geochemical gradients which in some cases are changing on short time scales. Next to the availability of energy sources and nutrients, many abiotic factors influence growth of bacteria. In the following, the influence of temperature (0 °C – 40 °C), salinity (5 – 60), pH (4 – 9) and the presence of O_2 on growth of *S. marisnigri*, *S. baltica* and *S. gotlandica* were investigated. The standard conditions for experiments shown here, if not mentioned otherwise, were anoxic medium prepared as described in the material and methods section 2.1, addition of thiosulfate ($S_2O_3^{2-}$) as electron donor, manganese oxide (MnO_2) for *S. marisnigri* and *S. baltica* or nitrate (NO_3^-) for *S. gotlandica* as electron acceptor, and dark incubation at 10 °C.

Temperature

S. marisnigri and *S. gotlandica* grew from 0 °C to 25 °C, with optimal growth at 20 °C. *S. baltica* grew from 0 °C to 20 °C and optimal growth was observed at 15 °C, slightly lower in comparison to *S. marisnigri* and *S. gotlandica*. All three strains can be considered as psychrotolerant species (Fig. 37).

Salinity

All three strains treated in this work were isolated from brackish environments. *S. marisnigri* was isolated from the Black Sea and *S. baltica* and *S. gotlandica* from the Baltic Sea, at salinities of 21, 14 and 13, respectively. Growth of all strains between a salinity of 5 and 60 was tested (Fig. 38). *S. baltica* and *S. gotlandica* grew from salinities of 5 to 40 with optimal growth at rates of 1.66 d^{-1} and 1.13 d^{-1} at a salinity of 21 and 14, respectively. *S. marisnigri*

grew from salinity 10 to 40 with optimal growth at a rate of 1.01 d^{-1} at a salinity of 25. No growth was observed at a salinity of 60.

pH

To investigate the influence of a different pH on growth of the three strains, medium was prepared with a defined pH from pH 4 to pH 9 (Fig. 39). *S. marisnigri* showed growth from pH 6.5 to 9 with the highest growth rates at pH 7.5 and 8. *S. baltica* showed growth from pH 7 to pH 8 with an optimum between pH 7 and 7.5 and *S. gotlandica* showed growth from pH 6.5 to pH 8 with highest growth rates between pH 7 and 8.

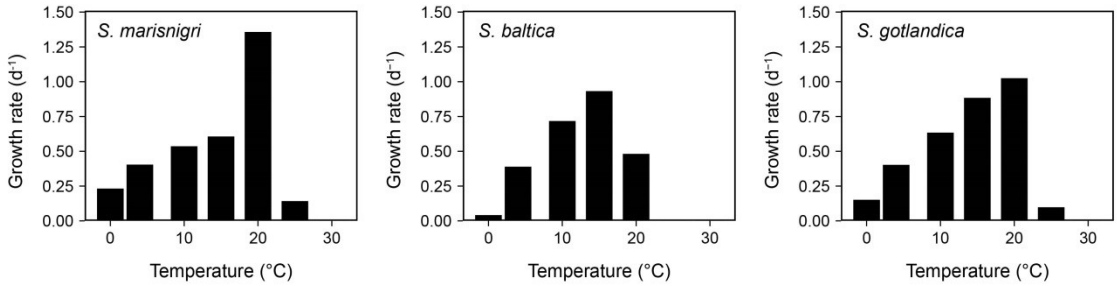

Figure 37: Growth rates of *S. marisnigri*, *S. baltica* and *S. gotlandica* in the temperature range from 0 °C to 30 °C. No growth was observed with temperature exceeding 25 °C.

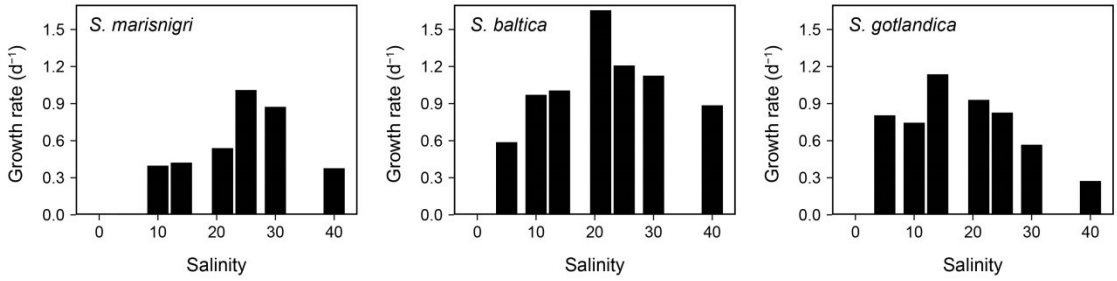

Figure 38: Growth rates of *S. marisnigri*, *S. baltica* and *S. gotlandica* in the salinity range from 5 to 40. No growth was observed at a salinity of 60.

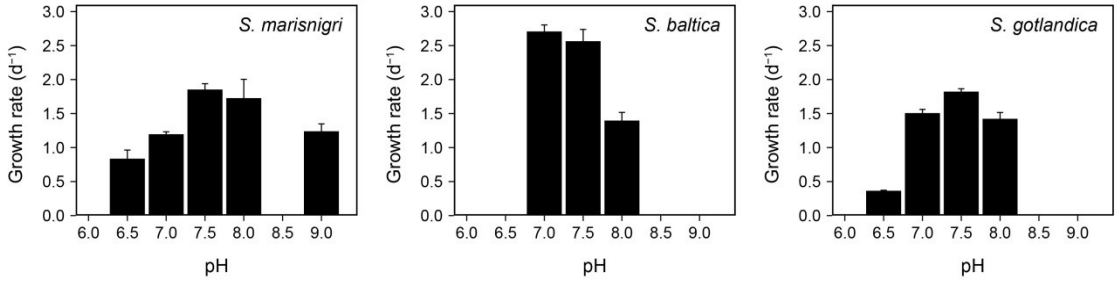

Figure 39: Growth rates of *S. marisnigri*, *S. baltica* and *S. gotlandica* in the pH range from 6 to 9 in triplicates. One replicate of *S. gotlandica* at pH 6.5 did not grow and the bar represents the mean value and standard deviation of 2 values. No growth was observed below pH 6.5.

Oxygen tolerance

Species of the genus *Sulfurimonas* are commonly found in or next to sulfidic environments with often frequently changing redoxconditions. Cultured representatives of the genus *Sulfurimonas* are to the most extent tolerant to oxygen and predominantly capable of utilizing O_2 as terminal electron acceptor for growth (Han and Perner, 2015).

To investigate whether the presence of dissolved O_2 influences the growth of the three strains, serum bottles were partially filled and the O_2 content in the headspace was adjusted by exchanging a portion of the headspace with sterile filtered air. By this, headspaces with 0%, 1%, 4% and 21% vol.% O_2 were established. In contrast to chapter 3.3.1, MnO_2 or NO_3^- was added as the standard electron acceptor. *S. marisnigri* and *S. gotlandica* showed growth under all tested headspace O_2 contents (Fig. 40). Growth of *S. baltica* was observed at 0%, 1% and 4% O_2, but in contrast to *S. marisnigri* and *S. gotlandica*, no growth could be detected at 21% O_2. Elevated O_2 content in the headspace had no effect on doubling time and growth rate of *S. marisnigri*, which were overall very low in this experiment (24 to 29 h and 0.72 to 0.59 d^{-1}, respectively) with high variation (Tab. 23). Low headspace O_2 contents of 0% and 1% had no effect on the doubling time of *S. baltica* (12

h ± 0 and 12 h ± 2, respectively) but a 4% O_2 content reduced growth to doubling times of 16 h ± 5. A low O_2 content had a positive effect on growth of *S. gotlandica*.

S. gotlandica grew faster with an O_2 content of 1% compared to 0%, 4% and 21% resulting in doubling times of 12 h ± 0 compared to 17 to 20 h, respectively. The growth yield of *S. marisnigri* in the presence of all tested headspace O_2 contents was higher than in the 0% treatment. Concentration of dissolved O_2 was decreasing to sterile control bottles when growth was detectable (Tab. 24). No change in dissolved O_2 concentration was observed in the 21% headspace O_2 treatment with *S. baltica*, where no growth was detectable. Leftover concentrations of NO_3^- were higher after growth of *S. gotlandica* when O_2 was present in the bottle headspace (Tab.24), indicating that O_2 was utilized concurrent with NO_3^-. About 4 mM

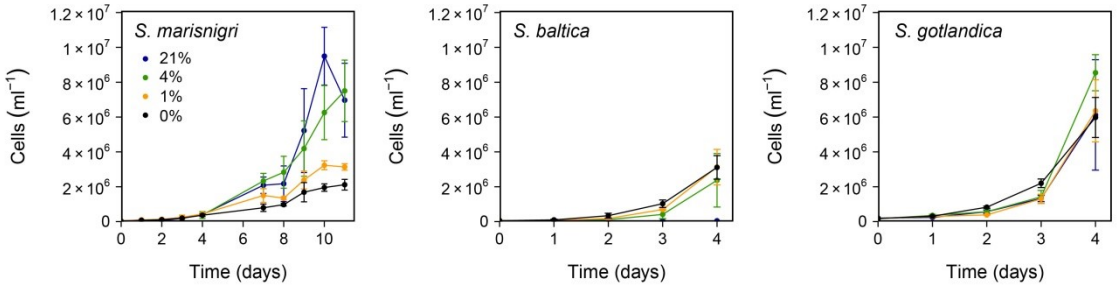

Figure 40: Growth of *S. marisnigri*, *S. baltica* and *S. gotlandica* inoculated with varying oxygen contents in the headspace and the addition of either MnO_2 or NO_3^-.

Table 23: Doubling times (g) and growth rates (k) of *S. marisnigri*, *S. baltica* and *S. gotlandica* cultivated with varying headspace oxygen contents in the presence of either MnO_2 or NO_3^-.

Strain	% O_2	g (h)	SD	k (d^{-1})	SD
S. marisnigri	21	27	4	0.63	0.09
	4	24	5	0.72	0.13
	1	26	8	0.72	0.28
	0	29	5	0.59	0.11
S. baltica	21	-	-	-	-
	4	16	5	1.16	0.46
	1	12	2	1.40	0.03
	0	12	0	1.43	0.19
S. gotlandica	21	20	1	0.85	0.05
	4	19	4	0.89	0.17
	1	12	0	1.45	0.02
	0	17	1	0.99	0.05

Table 24: Difference in the dissolved oxygen concentration after complete growth of *S. marisnigri*, *S. baltica* and *S. gotlandica* compared to un-inoculated controls and leftover concentrations of NO_3^- after growth of *S. gotlandica*.

Strain	% O_2	ΔO_2 (µM)	SD	NO_3^- (mM)	SD
S. marisnigri	21	-86	21	-	-
	4	-36	2	-	-
	1	-26	1	-	-
	0	0	0	-	-
S. baltica	21	+5	2	-	-
	4	-46	8	-	-
	1	-23	2	-	-
	0	-4	1	-	-
S. gotlandica	21	-73	5	4.1	0.9
	4	-22	3	2.7	0.2
	1	-18	2	3.0	0.6
	0	-2	0	1.8	0.4

NO_3^- out of approximately 10 mM NO_3^- added initially remained in the parallel with the highest headspace O_2 content of 21% compared to 1.8 mM NO_3^- when no O_2 was introduced into the headspace (Tab. 24). Nitrite (NO_2^-) was not detectable (< 50 µM). Unfortunately, no complete growth curve was recorded for *S. baltica* and *S. gotlandica* and no conclusion towards an overall growth yield can be made.

Cell morphology of *S. marisnigri*

Cells of *S. marisnigri* (Fig 41 and 42) possess one polar flagellum (Fig. 42C, red arrows) and showed movement under phase contrast microscopy. Mn-particles are often covered with threads (Fig. 42D), but whether these threads are somehow similar to the periplasmic exten-

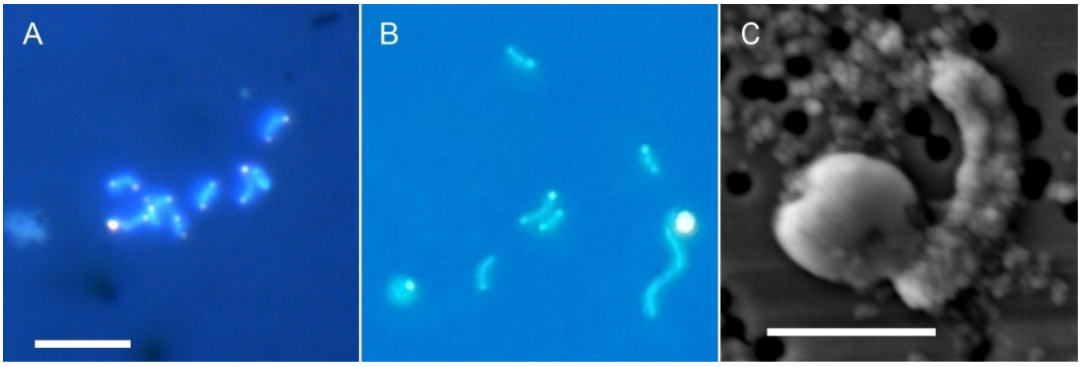

Figure 41: DAPI stained fluorescence images (A and B) and scanning electron micrograph (C) of *S. marisnigri*. Scale bars: A, 5 µm. B, photograph trough the eyepiece of the microscope, compare size to A. C, 1 µm.

sions of the metal reducing bacterium *Shewanella oneidensis* MR-1, so called nano-wires, and if they are of bacterial origin is so far unknown. Cells contained either no, one or two polyphosphate(PolyP)- inclusions indicated by the yellow color at the cell poles (Fig. 41A and B) when stained with the DNA dye DAPI. At late stages of growth, coccoid cells appear frequently (Fig. 41B and C), especially when the electron donor is oversupplied (or the electron acceptor is limited, respectively), but whether there is a causal relation to these observations was not investigated.

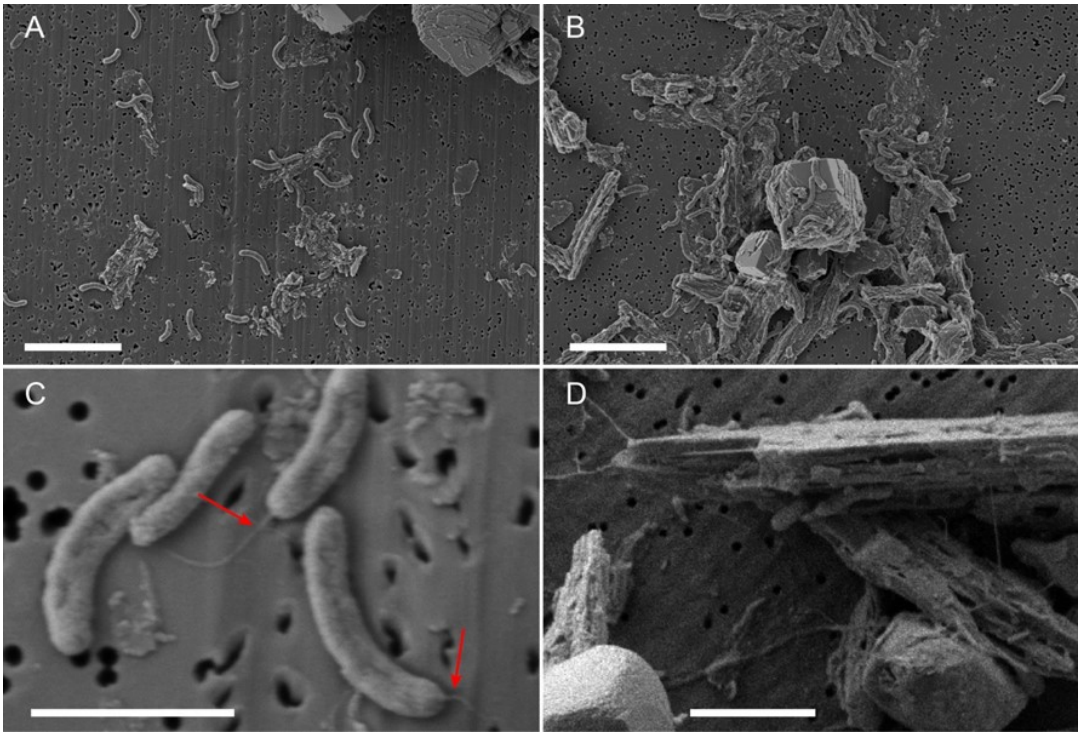

Figure 42: Scanning electron micrographs of a *S. marisnigri* culture grown with MnO_2 and $S_2O_3^{2-}$. Scale bars: A and B, 5µm. C and D, 2 µm.

Genomic potential of *S. marisnigri*

The annotated genome of *S. marisnigri* was screened for marker genes involved in carbon, nitrogen, oxygen and sulfur metabolism (Tab. 25). Genes detected by the automated annotation from RAST were marked with † and genes detected via the comparison to the genome of the closely related species *S. gotlandica* (Grote et al., 2012) were marked with *. Three marker genes for CO_2 fixation via the reverse tricarbolic acid cycle (rTCA) were detected by RAST annotation as well as comparison to the annotated genome of *S. gotlandica*. Genes involved in the fixation of N_2: *nifD*, *nifK* and *nifH* were detected by RAST annotation. A *ccoNOQP* cluster involved in the reduction of O_2 was detected via RAST annotation and comparison to *S. gotlandica*. NO_3^- reduction via a periplasmatic nitrate reductase (Nap) was found with the gene cluster *napAGHBFLD*, but further genes encoding for NO_2^- reductases were not detectable. Interestingly, genes for a putative nitric oxide (NO) reductase (Nos) might be present, but no statement whether this is a functioning gene or a false annotation can be made. Sulfur oxidation is represented by a functional sox gene cluster (*soxXYZAB*) together with multiple copies of a sulfide:quinone oxidoreductase (*sqr*). Genes involved in the accumulation and degradation of polyphosphates by polyphosphate kinase (*ppk*) and exopolyphosphatase (*ppx*) were identified by RAST annotation.

Table 25: Presence of specific marker genes involved in carbon, nitrogen and sulfur metabolism in the genome of *S. marisnigri*. *Mapped to the genome of *S. gotlandica*. †By RAST annotation.

Genes	Location	Genes	Location	Genes	Location
CO_2 fixation		**O_2 reduction*†**		**Sulfur oxidation*†**	
2-oxoglutarate:ferredoxin oxidoreductase*†		*ccoN*	peg. 640	*soxX*	peg. 1253
oorC	peg. 1784	*ccoO*	peg. 641	*soxY*	peg. 1254
oorB	peg. 1785	*ccoQ*	peg. 642	*soxZ*	peg. 1255
oorA	peg. 1786	*ccoP*	peg. 643	*soxA*	peg. 1256
oorD	peg. 1787	**NO_3^- reduction*†**		*soxB*	peg. 1257
Pyruvate:ferredoxin oxidoreductase*		*napA*	peg. 242	**Sulfide:quinone oxidoreductase**	
porC	peg. 655	*napG*	peg. 243	*sqr1**	peg. 384
porD	peg. 656	*napH*	peg. 244	*sqr2*†*	peg. 1056
porA	peg. 657	*napB*	peg. 245	*sqr3*, *4* or *5**	peg. 1638
porB	peg. 658	*napF*	peg. 246	**Polyphosphatekinases†**	
Pyruvate:ferredoxin oxidoreductase†	peg. 1206 – 1208	*napL*	peg. 247	*ppk1*	peg. 306
ATP-dependent citrate lyase*†		*napD*	peg. 249	*ppx*	peg. 1175
acly (α-subunit)	peg. 977	**NO reduction**			
acly (β-subunit)	peg. 976	*norC*†*	peg. 2453		
N_2 fixation†		*norB*†*	peg. 2454		
nifD	peg. 2005	*norDQ*†*	peg. 2455, 2456		
nifK	peg. 2006	**Assimilatory NO_3^- reduction (*nar*/*nos*)?†**			
nifH	peg. 2008		Peg. 1508, 2481		
nifUBTQXEZN	peg. 1319, 1988, 1998, 2009, 2010, 2014, 2024, 2029, 2030				

4 Discussion

4.1 Bacterial sulfur oxidation coupled to Mn reduction and a general view onto pelagic redoxclines with focus on the Black Sea

Since decades dark CO_2 fixation rates together with H_2S oxidation in the absence of O_2 and NO_3^- were observed (e.g. Taylor et al., 2001; Grote et al., 2008). Although earlier attempts to cultivate organisms with the ability to utilize MnO_2 for H_2S oxidation have failed (Jannasch et al., 1991), even in more recent literature this metabolic pathway was suggested (Taylor et al., 2001; Jost et al., 2010), but evidence was so far missing. With the isolation of *S. marisnigri* and *S. baltica*, representative species from the Black Sea and the Baltic Sea have been shown to grow with reduced sulfur compounds provided as electron donor and MnO_2 provided as electron acceptor (e.g. Fig. 15, 16 and chapter 3.3.7). Both organisms belong to the genus *Sulfurimonas*, which is globally abundant in environments with strong redox gradients, such as pelagic redoxclines, marine sediments and hydrothermal deep-sea vents (Han & Perner, 2015). *Sulfurimonas* belongs to the group of *Epsilonbacteraeota*, which is suggested to be of significant importance for biogeochemical and geological processes throughout Earth's history as primary colonizers by generation of organic carbon via dark CO_2 fixation and e.g. acid dissolution of limestone via biological H_2S oxidation (Campbell et al., 2006). In pelagic redoxclines of e.g. the Black Sea, the Baltic Sea or the Cariaco Trench, up to 30% of the total bacterial community is actively fixing CO_2 (Ho et al., 2004; Grote et al., 2007, 2008; Jost et al., 2010). Among these autotrophic bacteria, *Epsilonbacteraeota* were found as the dominant group representing up to 70% of the CO_2 fixing bacteria of the Baltic Sea and up to 100% of the CO_2 fixing bacteria in the Black Sea (Grote et al., 2008). In the Baltic Sea, *Sulfurimonas* subgroup GD17 was further shown to be the dominant group within the group of *Epsilon-bacteraeota* (Grote et al., 2008) and cells of the genus *Sulfurimonas* were almost exclusively representing the group of *Epsilonbacteraeota* in the Black Sea (Prof. Dr. Klaus Jürgens, pers.

communication – see also chapter 3.2.2), providing strong evidence, that *Epsilonbacteraeota* and the genus *Sulfurimonas* in particular may have a strong influence on the biogeochemistry of the respective habitat and may offer together with the results of this thesis a plausible explanation for dark CO_2 fixation rates in the absence of O_2 and NO_3^- (Taylor et al., 2001; Ho et al., 2004; X. Lin et al., 2006; Jost et al., 2010).

S. marisnigri oxidized H_2S and $S_2O_3^{2-}$ to SO_4^{2-} with MnO_2 as terminal electron acceptor. The oxidation proceeded without the accumulation of S compounds with intermediate oxidation state, e.g.: S^0, $S_2O_3^{2-}$ or SO_3^{2-}. Alike, at the bottom boundary of the suboxic zone where H_2S is consumed, no pronounced accumulation of these intermediates was observed (Jørgensen et al., 1991; Luther III et al., 1991; Glazer et al., 2006). A purely abiotic oxidation of H_2S would result in a variety of sulfur species, e.g. S^0, $S_2O_3^{2-}$ and SO_4^{2-} depending on the pH and the ratio of MnO_2 to H_2S (Yao & Millero, 1996; Herszage & dos Santos Afonso, 2003). For example, at near neutral pH with a MnO_2/H_2S ratio of 1, S^0 is the important reaction product with a yield of approximately 80 to 90%. Lower MnO_2/H_2S ratios and higher pH foster S^0 as reaction product, while higher MnO_2/H_2S ratios and lower pH result in increasing quota of SO_4^{2-} and to a minor extent $S_2O_3^{2-}$ (Yao & Millero, 1996; Herszage & dos Santos Afonso, 2003). In the Black Sea, the MnO_2/H_2S ratio is about 0.04 (Schulz-Vogt et al., 2019) at a pH of 7 to 8, favoring S^0 as the product of abiotic oxidation of H_2S. Thus, the missing accumulation of sulfur intermediates in the Black Sea suboxic zone strongly suggests a biological mode of H_2S oxidation.

H_2S oxidation rates appeared to be of significant importance for the retention of H_2S at the bottom boundary of the suboxic zone (Fig. 21) and the formation of linear concentration profiles of H_2S measured in-situ [e.g. Schulz-Vogt et al. (2019)]. A lower reaction rate coefficient based on chemical oxidation of H_2S by MnO_2 (k_{chem}) calculated after Yao & Millero (1993) with a constant MnO_2 concentration of 10 nM (Schulz-Vogt et al., 2019) resulted in the collapse of the suboxic zone. Apparently, a local high H_2S oxidation rate is essential for

the formation and maintenance of the suboxic zone and H_2S concentration profile of the Black Sea which coincides with a local maximum in the transcription of *sqr* by *Sulfurimonas* spp. (Prof. Dr. Klaus Jürgens, personal communication). Next to the absence of sulfur intermediates, this also strongly suggests a biological mode of H_2S oxidation at the chemocline of the Black Sea.

The H_2S oxidation rates per cell which where estimated in the present study are based on the difference in the H_2S oxidation rate before and after treatment with either sodium azide ($k_{bio(A)}$) or heat pasteurization ($k_{bio(P)}$). While heat pasteurization reduced the overall reaction rate to the chemical background, sodium azide had an inhibitory effect of approximately 25% (Tab. 21). Also Myers and Nealson (1988) reported a partial inhibition of organotrophic Mn reduction for *Shewanella oneidensis* MR-1 with sodium azide of 37%. Therefore, $k_{bio(P)}$ can be assumed as the more realistic value for H_2S oxidation by *S. marisnigri* than $k_{bio(A)}$.

Together with the cell abundance of *Epsilonbacteraeota* in Black Sea waters, which were represented by over 90% *Sulfurimonas* spp. (Prof. Dr. Klaus Jürgens, pers. communication), estimated H_2S oxidation rates by *S. marisnigri* are high enough to counterbalance H_2S fluxes from the euxinic bottom waters (Fig. 21). In-situ H_2S oxidation rates measured by Jørgensen et al. (1991) were compared to rates estimated with *S. marisnigri* in lab experiments in Tab. 26. Jørgensen et al. (1991) reported an abrupt decrease in H_2S oxidation below the Black Sea chemocline. Likewise, depth profile of the expression of the *sqr*, which is almost exclusively affiliated to species of the genus *Sulfurimonas*, shows a sharp drop to 0 below the chemocline (Prof. Dr. Klaus Jürgens, personal communication). Assuming a cellular abundance of 4×10^7 cells L^{-1}, reflecting the abundance of *Epsilonbacteraeota* (Fig. 21), a potential H_2S oxidation rate by *Sulfurimonas* can be calculated at ambient concentrations of H_2S, which are in the same order of magnitude and comparable to in-situ H_2S oxidation rates estimated by Jørgensen et al. (1991) shown in Tab. 26.

Table 26: H_2S oxidation rates estimated in pure culture with *S. marisnigri* compared to in situ H_2S oxidation rates measured by Jørgensen et al. (1991).

C_{H2S} (µM)	Cells (L^{-1})	H_2S_{ox} (µM s^{-1}) k_{bioA}/k_{bioP}	H_2S_{ox} (µM s^{-1}) Jørgensen et al. (1991)
2.5	~ 4 x 10^7	3.16 x 10^{-6} / 1.05 x 10^{-5}	~ 1.3 x 10^{-5}
4	~ 4 x 10^7	5.05 x 10^{-6} / 1.68 x 10^{-5}	~ 3.5 x 10^{-5}
8.5	~ 4 x 10^7	1.07 x 10^{-5} / 3.57 x 10^{-5}	~ 6.6 x 10^{-5}

H_2S oxidation rates can be transformed and compared to Mn reduction rates measured in the Black Sea by assuming that 4 mole of MnO_2 can be reduced to Mn^{2+} for every mole H_2S oxidized to SO_4^{2-} according to Tab. 2. Lewis & Landing (1991) modeled Mn reduction rates at the lower boundary of the Black Sea suboxic zone, which were 3.7 x 10^{-8} µM s^{-1} and 1.2 x 10^{-8} µM s^{-1} at two different stations. Assuming a cellular abundance of 4 x 10^7 cells L^{-1}, H_2S concentrations as low as 7 nM and 2 nM based on $k_{bio(A)*4}$ and 2 nM and 0.7 nM based on $k_{bio(P)*4}$ would be sufficient to account for the modeled Mn reduction rates, respectively.

Based on the assumption that the suboxic zone is a tens of meter thick layer that shuttles oxidation potential from the oxic surface water layer to the sulfidic bottom water by e.g. a Mn cycle (Burdige & Nealson, 1986; Lewis & Landing, 1991; Yao & Millero, 1993; Dellwig et al., 2010), fluxes of O_2 into the suboxic zone from surface waters and fluxes of H_2S from euxinic waters have to be stoichiometric to result in a stable formation of the suboxic zone. Fluxes of O_2 from oxygenated surface waters into the suboxic zone and fluxes of H_2S from the euxinic water body into the suobxic zone were calculated based on Fick's first law of diffusion (Eq. 4.22),

$$J = -D \frac{\Delta c}{\Delta x} \qquad 4.22$$

with J as the flux, D as the diapycnal diffusivity coefficient derived from (Gregg & Yakushev, 2005), c as concentration of the respective compound and x as distance (depth). With data collected by Schulz-Vogt et al. (2019), an O_2 flux of 1.66 x 10^{-6} mmol O_2 m^{-2} s^{-1} and a H_2S flux of 1.34 x 10^{-6} mmol H_2S m^{-2} s^{-1} was calculated (Tab. 27). Assuming a reduction of O_2 to H_2O and an oxidation of H_2S to SO_4^{2-}, 4 moles of e^- are transferred per mole O_2 reduced and 8 e^-

are transferred per mole of H_2S oxidized (Tab. 28). The fluxes of O_2 and H_2S can therefore be multiplied by 4 and 8 to calculate the flux of electron accepting potential ($J_{e- acc.}$) and electron donating potential ($J_{e- don.}$) into the suboxic zone. The accepting flux derived from the O_2 flux is 6.64 x 10^{-6} mmol electrons m^{-2} s^{-1} and the donating flux derived from H_2S flux is 1.07 x 10^{-5} mmol electrons m^{-2} s^{-1}. The bottom boundary of the suboxic zone is thereby missing 4.08 x 10^{-6} mmol electron accepting potential m^{-2} s^{-1} or 4.08 nmol m^{-2} s^{-1} of oxidation potential to balance the net flux of electrons across the suboxic zone (Tab. 27, bold).

Potentially, riverine input of MnO_2 could be an external source of electron accepting potential which may explain this discrepancy. To evaluate the magnitude of a potential impact on the water column geochemistry of riverine discharge, an example calculation will be carried out with the Danube River, which represents 50 – 71% of the total riverine input into the Black Sea (Özsoy & Ünlüata, 1997; Jaoshvili, 2002; Murray & Yakushev, 2006). The Danube Rover discharges 190 – 250 km^3 yr^{-1} ≙ 6025 – 7927 m^3 s^{-1} of water into the Black Sea (Bondar, 1991; Jaoshvili, 2002; Murray & Yakushev, 2006), which contains 20 mg L^{-1} sus-

Table 27: Data used for the calculation of electron fluxes across the suboxic zone of the Black Sea

Term	Value
$\Delta c/\Delta x\ O_2^{\dagger}$	0.83 mmol m^{-3} m^{-1}
$\Delta c/\Delta x\ H_2S^{\dagger}$	0.67 mmol m^{-3} m^{-1}
$D_{O2/H2S}^{*}$	2 x 10^{-6} m^2 s^{-1}
J_{O2}	1.66 x 10^{-6} mmol m^{-2} s^{-1}
$J_{e- acc.}$	6.64 x 10^{-6} mmol m^{-2} s^{-1}
J_{H2S}	1.34 x 10^{-6} mmol m^{-2} s^{-1}
$J_{e- don.}$	1.07 x 10^{-5} mmol m^{-2} s^{-1}
$J_{e- don} - J_{e- acc.}$	**4.08 x 10^{-6} mmol m^{-2} s^{-1}**

Table 28: Electron difference between oxidized and reduced O, S, N and Mn compounds.

Educt	Product	Δe^-
O_2	2 H_2O	+ 4 e^-
H_2S	SO_4^{2-}	- 8e^-
MnO_2	Mn^{2+}	+ 2 e^-

pended matter (Guieu et al., 1998). In the suspended matter Mn contents of 1704 ppm are reported (Guieu et al., 1998), which equates to 620 µmol Mn m^{-3}. The annual input of Mn into the Black Sea with a surface area of 4.2 x 10^5 km^2 (Özsoy & Ünlüata, 1997) from the Danube is 6.47 x 10^3 – 8.51 x 10^3 t Mn, which equates to 8.9 x 10^{-3} –11.7 x 10^{-3} nmol Mn m^{-2} s^{-1}. Assuming that each MnO_2 can accept two electrons (Tab. 28), 17.8 x 10^{-3} – 23.4 x 10^{-3} nmol electrons m^{-2} s^{-1} can be accepted by the flux of Mn, only providing 0.44 – 0.57% of the calculated need of 4.08 nmol m^{-2} s^{-1}. The real fluxes might be even smaller because shelf areas may influence the amount of Mn reaching central parts of the Black Sea from the rivers and counterclockwise circulation around the deep basins will affect the dispersal of the riverine Mn, too (Oguz et al., 1993). Even though the Danube River is not the only external source of oxidative potential for the Black Sea, the overall input of Mn is likely too low to compensate the discrepancy between O_2 and H_2S fluxes into the suboxic zone.

A fraction of the electrons, donated by the H_2S flux ($J_{e\text{- don.}}$), is used by chemo-lithoautotrophic bacteria to fix CO_2. The fixation of one mole inorganic CO_2 is accepting 4 mole e^- (Eq. 1.1). Based on the Mn(IV)/Mn(II) to $S_2O_3^{2-}/SO_4^{2-}$ ratio of 3.7 in the growth experiment with *S. marisnigri* (Fig. 15), an e^- demand of 7.5% from the bulk of electrons provided by the electron donor can be calculated which is most probably used for the reduction of CO_2 to organic C. Applying this percentage to the Black Sea and assuming a H_2S oxidation by chemolithoautotrophic bacteria, CO_2 fixation could account for 8.03 x 10^{-7} mmol electron m^{-2} s^{-1} or 19.7% of the missing electron accepting budget ($J_{e\text{- don.}} – J_{e\text{- acc.}}$). From literature, values up to 20% are reported for the fixation of CO_2 by chemolithoautotrophic bacteria (Kelly, 1982), which would explain about 50% of the discrepancy between $J_{e\text{- acc.}}$ and $J_{e\text{- don.}}$. CO_2 fixation rates of up to 2.32 x 10^{-6} mmol m^{-3} s^{-1} estimated by Jørgensen et al. (1991) or 9.26 x 10^{-6} mmol m^{-3} electrons accepted s^{-1} may balance the excess flux of 4.08 mmol m^{-3} s^{-1} electrons from $J_{e\text{- don.}}$.

Just recently, Schulz-Vogt et al. (2019) showed that large magnetotactic bacteria are moving through the complete suboxic zone displacing phosphate vertically by internal storage of polyP. The authors suggested that these bacteria might store NO_3^- internally in vacuoles for the oxidation of H_2S at the lower boundary of the suboxic zone. To account for the missing 4.08 x 10^{-6} mmol e^-_{acc} m^{-2} s^{-1}, 8.16 x 10^{-7} mmol NO_3^- m^{-2} s^{-1} would have to be displaced by large magnetotactic bacteria. Because the concentration profile of NO_3^- is approaching zero together with the concentration profile of NH_4^+ and turned into N_2 by anaerobic ammonium oxidation (anammox) [Kuypers et al. (2003)], it may be assumed that NO_3^- is completely exhausted due to the reduction to NO_2^- and subsequently to N_2 by anammox, but Kuypers et al. (2003) showed that the flux of NO_3^- is 2 µmol m^{-2} h^{-1} larger than the flux of NH_4^+. The remaining 2 µmol NO_3^- m^{-2} h^{-1} are equal to 5.56 mmol NO_3^- m^{-2} s^{-1} which could explain 68% of the missing electron accepting potential at the chemocline. No loss of NO_3^- for the degradation of organic matter can be expected, because no heterotrophic denitrification was detectable in the depth of NO_3^- removal (Jensen et al., 2008).

In summary, concentration gradients and the resulting fluxes of O_2 and H_2S directly above and below the suboxic zone are unbalanced. External input of oxidized compounds, e.g. by riverine input, may not have a big impact on the stoichiometry of the suboxic zone. Internal sinks for e^- might be the fixation of CO_2 by chemolithoautotrophic bacteria and the displacement of NO_3^- by large magnetotactic bacteria. However the mechanism of intracellular transport of NO_3^- by large magnetotactic bacteria remains to be proven.

4.2 Mechanism of MnO_2 reduction and potential implications for $Mn(Ca)CO_3$ authigenesis

4.2.1 Biological MnO_2 reduction and competition with an abiotic reaction

The reduction of particulate electron acceptors like Mn of Fe is a challenging task for bacteria. Electrons from an electron donor have to be transferred from the cytoplasmic membrane to the cell outside onto the particulate electron acceptor. On the basis of microscopic inspection and SIMS analysis, it appeared that *S. marisnigri* is depending on physical contact with the Mn particle surface (Fig. 12, 13 and 14). This is in agreement with considerations of Canfield et al. (2005), because in contrast to Fe oxides MnO_2 is practically insoluble at near neutral pH and a direct electron transfer should be necessary for the reduction. Physical contact, however, can be either direct via the cell surface (Myers & Myers, 2003), periplasmmatic extensions of the outer membrane (El-Naggar et al., 2010; Pirbadian et al., 2014), conductive pili (Bond & Lovley, 2003) or the transfer of e^- with molecules e.g. flavine, quinone or humic acids (Nevin & Lovley, 2002; Marsili et al., 2008; Canstein et al., 2008 - Fe). Whether *S. marisnigri* transfers electrons with the above mentioned systems or in a different way remains to be elucidated.

Biological oxidation of H_2S in the presence of MnO_2 has to face similar difficulties as the biological oxidation of H_2S with O_2 as terminal electron acceptor. In contrast to e.g. the oxidation of H_2S with NO_3^-, H_2S reacts abiotically with O_2 and MnO_2 (Chen & Morris, 1972; Burdige & Nealson, 1986; Yao & Millero, 1993) which is a loss of potential energy for the organism. Strategies to minimize the loss of potential energy to a chemical reaction are e.g. the spatial separation of the oxidation and the reduction reaction or to compete with the chemical reaction by a faster biological reaction rate. Species of the *Desulfobulbaceae* form long filaments with a conductive outer envelope at sedimentary redoxclines and perform the oxidation of H_2S and the reduction of O_2 at the respective poles of the filament and shuttle the electrons over centimeter wide distances (Nielsen & Risgaard-Petersen, 2014). As pointed out

in the introduction, local high reaction rates by *Beggiatoa* result in low local concentrations or even depletion of the reactants (Jørgensen & Revsbech, 1983). As a further advantage, this local depletion increases the concentration gradient and increases the net flux of the reactants and thus the input of potential energy.

The same may apply for the biological oxidation of H_2S with MnO_2 (Fig. 43). The chemical reaction rate of H_2S with MnO_2 follows a chemical reaction of second order and depends on the concentration of H_2S and the surface area of MnO_2 (Yao & Millero, 1993). Low reactant concentrations result in low reaction rates. Because H_2S needs to have contact to the MnO_2 particle surface to react chemically, the visible attachment and proliferation of *S. marisnigri* on the MnO_2 particle surface (Fig. 12) might hamper the chemical reaction by blocking reactive surface sites of the MnO_2 particle [like *Geobacter sulfurreducens* (Fig. 5 in Bond & Lovley, (2003))]. Additionally, active biological H_2S oxidation keeps the H_2S concentration at the particle surface low, thereby suppressing the chemical reaction. The chemical two e^- transfer oxidation of H_2S to S^0 with MnO_2 (Tab. 2, Eq. 3.18) is surface controlled, pH depend and the reactivity decreases with increasing pH (Yao & Millero, 1993, 1996; Luther III, 2010). As shown in Tab. 2, Eq. 3.17, 3.18 and Fig. 15D, the pH increases due to MnO_2 reduction with reduced sulfur compounds, which should also inhibit the competing chemical reaction of H_2S and MnO_2.

4.2.2 Theoretical implications for the authigenesis of $Mn(Ca)CO_3$

The activity of *S. marisnigri* at the particle surface may also offer a plausible explanation for the precipitation of $Mn(Ca)CO_3$, which was observed at MnO_2 particles (Fig. 13 and 14). The precipitation of $Mn(Ca)CO_3$ is an interesting finding, because Ca-rich $MnCO_3$ layers occur frequently in geological records (Neumann et al., 2002; Dellwig et al., 2018, 2019; Häusler et al., 2018; Hermans et al., 2019), but the mechanism of formation is still under debate. Chemical studies of Middelburg et al. (1987) suggested a precipitation of Ca-rich $MnCO_3$ when dis-

solved Mn reaches supersaturation, but oversaturated porewater profiles did not show precipitation (Carman & Rahm, 1997; Lenz et al., 2015; Dellwig et al., 2018; Häusler et al., 2018). Experiments of Mucci (1988) and Böttcher (1998) showed that precipitation is depending on the kinetic of precipitation and Böttcher (1998) suggested a putative microbial involvement in the precipitation process. Böttcher (1998) was able to chemically precipitate the complete solid solution series of $Mn_xCa_{1-x}CO_3$ with x = 0.25 to 0.75 chemically. In contrast to this, Ca-rich $MnCO_3$ found in the Baltic Sea sediments shows a distinct Ca content analogue to the $Mn(Ca)CO_3$ precipitated in this study (Fig. 14 and 15, Patricia Roeser, personal communication).

In the Baltic Sea, Ca-rich $MnCO_3$ layers are often observed concurrent with major baltic inflow (MBI) events (Häusler et al., 2018). MBI's are intrusions of dense, oxygen rich waters from the North Sea into the anoxic and often euxinic basins of the Baltic Sea (Matthäus & Franck, 1992). Dissolved Mn^{2+} in the euxinic waters is oxidized and transported to the sediment surface as MnO_2 where it accumulates in the deeper basins (Sulu-gambari et al., 2017; Häusler et al., 2018; Hermans et al., 2019). Hermans et al. (2019) showed the formation of Ca-rich $MnCO_3$ at the sediment surface in June 2016 after a MBI at the end of 2015 to beginning of 2016. Ca-rich $MnCO_3$ precipitation was also observed in the Baltic Sea sediments near the surface and the difference in $\delta^{18}O$ between $MnCO_3$ precipitates and porewaters emphasized a role of microbial MnO_2 reduction during Ca-rich $MnCO_3$ authigenesis (Neumann et al., 2002). High MnO_2 content together with ongoing sulfate reduction resulting in H_2S fluxes from deeper sediment layers are analogue to the culturing conditions of *S. marisnigri* shown in Fig. 16, where $Mn(Ca)CO_3$ precipitated as indicated by an increasing Ca content in the particulate phase.

In the experiments shown in the present work with precipitation of $Mn(Ca)CO_3$ (e.g. Fig. 14 and 15), precipitation might be fostered by the high alkalinity of approximately 30 mM due to pH buffering with HCO_3^- and pH adjustment with N_2 gas with 10-30% CO_2. However, also in

culturing approaches with pH buffering based on HEPES and pH adjustment with H_2SO_4 (Fig. 39) a color change implying $Mn(Ca)CO_3$ precipitation was observed. This may indicate that the artificial high alkalinity might not be the major factor controlling $Mn(Ca)CO_3$ precipitation in the presented experiments. In theory, concentration of Mn^{2+} and CO_3^{2-} should be the major factor controlling the precipitation of $Mn(Ca)CO_3$. Hypothetical implications of bacterial proliferation on MnO_2 particles which may result in the precipitation of $Mn(Ca)CO_3$ are visualized in Fig. 43. The reduction of MnO_2 and oxidation of H_2S is increasing the con-

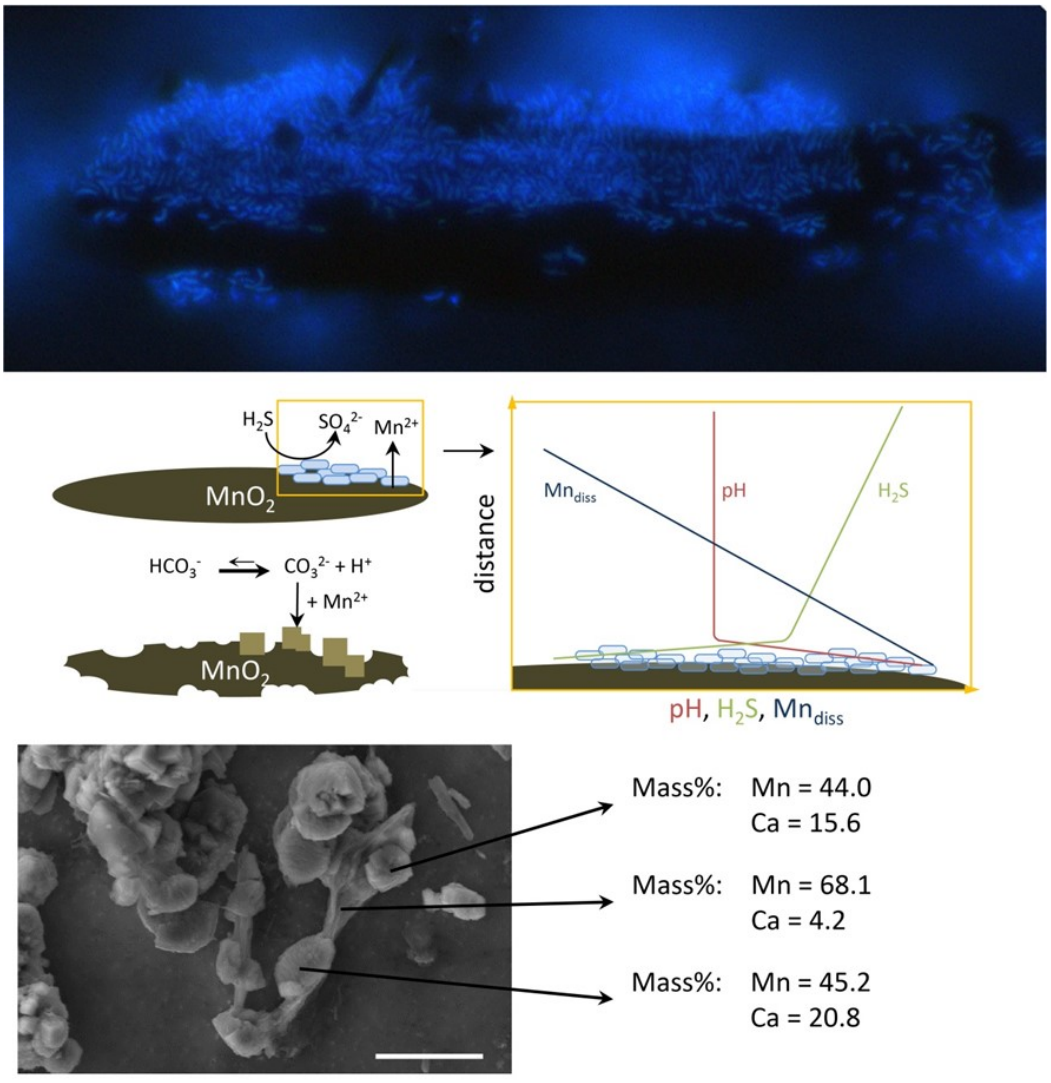

Figure 43: Hypothetical implications of bacterial proliferation on MnO_2 particles. MnO_2 dependent H_2S oxidation leads to the production of dissolved Mn^{2+}, increasing pH and low concentrations of H_2S near the particle surface. Thereby, the chemical oxidation of H_2S is suppressed and the flux of H_2S is increased due to a steeper concentration gradient. The increase in pH in the microenvironment of the Mn particle stimulates the precipitation of Mn-carbonate due to the higher proportion of CO_3^{2-} at higher pH together with high concentrations of Mn^{2+}.

centration of Mn^{2+} at the particle surface and the pH according to Eq. 3.17. According to Glasby & Schulz (1999), $MnCO_3$ is the stable form of Mn(II) under sweater conditions with a pH of 9 to 12.Increased pH shifts Eq. 4.23 to the right,

$$HCO_3^- \leftrightarrow H^+ + {CO_3}^{2-} \quad 4.23$$

which increases the portion of free CO_3^{2-} ions and stimulates the formation of carbonate precipitates (Brown et al., 1989). This may be a plausible explanation for observed Ca-rich $MnCO_3$ precipitates in Baltic Sea sediments after a major Baltic inflow event by altering the micro-environment around a MnO_2 particle.

4.3 Ecological potential of *S. marisnigri*, *S. baltica* and *S. gotlandica* in comparison to other species of the genus *Sulfurimonas*

4.3.1 Electron acceptors

Oxygen

S. marisnigri, *S. baltica* and *S. gotlandica* showed growth with O_2 as electron acceptor under the described culturing conditions (Fig. 22). This is in contrast to Labrenz et al. (2013), who stated, that *S. gotlandica* is unable to utilize O_2 as electron acceptor. So far, all other isolated strains of the genus *Sulfurimonas*: *S. denitrificans*, *S. hongkongensis*, *S. autotrophica* and *S. paralvinellae* were reported to utilize O_2 as terminal electron acceptor (See references in Tab. 29). Han & Perner (2015) argued that the absence of growth with O_2 as electron acceptor reported by Labrenz et al. (2013) may not have been detected with the respective growth experiments. Labrenz et al. (2013) also stated that the growth rates under the tested conditions might just have been too low to be detectable. The observed growth of *S. gotlandica* in this work is supported by the decreasing O_2 concentrations in the medium (Fig. 22 and Tab. 22). Further, NO_3^- seemed to be substituted by O_2 as electron acceptor by *S. gotlandica* when cultivated with NO_3^- and O_2 to test for O_2 tolerance (Fig. 40, Tab. 24). Leftover concentrations of NO_3^- were higher at the end of growth when higher O_2 concentrations were present in the

Table 29: Ecological potential of *S. marisnigri*, *S. baltica* and *S. gotlandica* (in the present study) in comparison to other cultivated species of the genus *Sulfurimonas*. + = yes, - = no, n.d. = not determined, ( ) = uncertain, ‡ = on the basis of cultivation and genome, * = only to NO_2^-, † = Acetate, propionate and succinate.

	S. marisnigri	*S. baltica*	*S. gotlandica* (this study)	*S. gotlandica*	*S. denitrificans*	*S. hongkongensis*	*S. autotrophica*	*S. paralvinellae*
Electron donors								
Red. Inorg. S comp.								
Sulfide (H_2S)	+ ‡	+	n.d.	+	+	+	+	-
Elemental sulfur (S^0)	+	+	+	+	+	n.d.	+	+
Thiosulfate ($S_2O_3^{2-}$)	+	+	+	+	+	+	+	+
Sulfite (SO_3^{2-})	-	-	+	+	-	n.d.	-	-
Hydrogen	+ ‡	+	+	+	+	+	-	+
Organic comp.†	(-)	-	(+)	+	+	-	-	+
Electron acceptors								
Manganese oxide (MnO_2)	+	+	-	-	n.d.	n.d.	n.d.	n.d.
Fe_2O_3, $FeCl_3$, amorphous FeOOH, α-goethite	-	-	-	-	n.d.	n.d.	n.d.	n.d.
Nitrate (NO_3^-)	+* ‡	+(*)	+	+	+	+	-	+
Nitrite (NO_2^-)	-	-	(-)	+	+	-	-	-
Oxygen (O_2)	+ ‡	+	+	(+)	+	n.d.	+	+
Carbon source								
CO_2 / HCO_3^-	+ ‡	+	+	+	+	+	+	+
Acetate	-	+	-	+	n.d.	n.d.	-	-
Propionate	-	+	-	n.d.	n.d.	n.d.	n.d.	n.d.
Succinate	-	+	-	n.d.	n.d.	n.d.	n.d.	n.d.
N_2 fixation	+ ‡	+	(-)	n.d.	n.d.	n.d.	n.d.	n.d.
Disproportionation								
S^0	(-)	(-)	(-)	+	n.d.	n.d.	n.d.	n.d.
$S_2O_3^{2-}$	(-)	(-)	(-)	+	n.d.	n.d.	n.d.	n.d.
SO_4^{2-} reduction†	(-) ‡	-	-	n.d.	n.d.	n.d.	n.d.	n.d.
Fermentation†	(+)	(+)	(+)	n.d.	n.d.	n.d.	n.d.	n.d.
PolyP inclusions	+	+	+	+	n.d.	n.d.		n.d.
Factors influencing growth								
Temperature range	0 – 25	0 – 20	0 – 25	4 – 20	10 – 30	15 – 35	10 – 40	4 – 35
Temperature optimum	20	15	15 – 20	15	22	30	23 – 26	30
Salinity range	10-40	5-40	5-40	n.d.	n.d.	10 – 60	16 – 60	n.d.
Salinity optimum	25	21	14	n.d.	n.d.	30	40	n.d.
Oxygen tolerance	0 – 21%	0 – 4%	0 – 21%	0 – 20%	n.d.	n.d.	n.d.	n.d.
pH range	6.5 – 9.0	7.0 – 8.0	6.5 – 8.0	6.5 – 8.4	n.d.	6.5 – 8.5	4.5 – 9.0	5.4 – 8.6
pH optimum	7.5 – 8.0	7.0 – 7.5	7.5	6.7 – 8.0	7.0	7.0 – 7.5	6.0 – 7.5	6.1
Motility	+	+	+	+	-	n.d.	+	+
References				Grote et al. (2012) Labrenz et al. (2013) Han and Perner (2015)	Timmer-ten Hoor (1975) Timmer-ten Hoor (1981) Labrenz et al. (2013)	Cai et al. (2014)	Inagaki et al. (2003) Sikorski et al. (2010)	Takai et al. (2006) Takai et al. (2005)

bottles (Tab. 24). This is in agreement with the genetic potential of *S. gotlandica* and all of the so far sequenced *Sulfurimonas* species: *S. denitrificans*, *S. hongkongensis*, *S. autotrophica*, *S. gotlandica* and *S. marisnigri*. All genomes of these strains contain a *ccoNOQP* operon. The *ccoNOQP* operon encodes for a cbb3-type cytochrome c oxidase (Han & Perner, 2015) and is responsible for the reduction of O_2 to H_2O by transferring e^- from cytochrome c to O_2, thereby generating a proton gradient (Pitcher & Watmough, 2004).

Denitrification in the presence of O_2 is a subject of ongoing discussion. Marchant et al. (2017) reported denitrification from intertidal flats in the Wadden Sea at O_2 concentration above 100 µM. In contrast to that, O_2 concentrations as low as 2 µM were shown to inhibit denitrification in O_2 minimum zones (Dalsgaard et al., 2014), but did also show that the tested O_2 concentrations had little to no effect on the expression of *narG,* catalyzing NO_3^- reduction, but expression of *norB*, catalyzing nitric oxide reduction, was strongly affected. Therefore, decreasing concentrations of NO_3^- in the presence of approximately 200 µM O_2 with *S. gotlandica* (Fig. 40 and Tab. 24) may not have resulted in the formation of N_2 but intermediates, which were not investigated. This finding is worth to be tested in a separate experiment in pure culture with *S. gotlandica*.

For *S. marisnigri* and *S. baltica*, no concentrations of MnO_2 or total dissolved Mn in the presence of O_2 were measured. Thus, no reduction of MnO_2 in the presence of O_2 could be demonstrated directly. The growth yield of *S. marisnigri* after 11 days with 21% O_2 and 4% O_2 headspace content was comparable (Fig. 40). Because the difference in the dissolved O_2 concentration was larger in the 21% O_2 treatment (Tab. 24), the comparable growth yield may indicate the reduction of MnO_2 in the presence of 4% O_2 in the bottle headspace, which does not exclude MnO_2 reduction by *S. marisnigri* in the presence of higher O_2 concentrations.

Nitrate

S. marisnigri, *S. baltica* and *S. gotlandica* showed growth with NO_3^- as terminal electron acceptor but the growth yield differed strongly (Fig. 23). *S. marisnigri* reduced NO_3^- to NO_2^-

and not further to N_2 as it is described for *S. gotlandica* (Labrenz et al., 2013), which is probably the reason for the lower growth yield (Fig. 23). *S. gotlandica* produced overpressure due to N_2 formation while growing. No overpressure was produced by *S. marisnigri* and *S. baltica* and the growth yields of these strains was comparable (Fig. 23). Thus it can be speculated that *S. baltica* reduced NO_3^- to NO_2^- like *S. marisnigri*, even though it was not investigated for *S. baltica*. This is supported by the absence of growth, when *S. marisnigri* and *S. baltica* are cultivated with NO_2^- as terminal electron acceptor (Fig. 25). This is in accordance with the genome of *S. marisnigri*. A periplasmatic nitrate reductase (Nap) was detected (Tab. 25) responsible for the reduction of NO_3^- to NO_2^-, but in contrast to the genome of *S. gotlandica* (Grote et al., 2012), no genes for the dissimilatory reduction of NO_2^- (*nir*) have been found. This is supporting the observed results in pure culture growth experiments. Interestingly, a nitric oxide reductase (Nor) is present in the genome of *S. marisnigri*, but whether this gene is functional remains to be tested in growth experiments.

Metal oxides

The test for growth on Fe and Mn oxides was difficult, because all strains showed growth with O_2 as terminal electron acceptor (Fig. 22) and cultivation was performed without reducing agents and redox indicators, because preliminary test showed inhibiting effects of these compounds on growth of *S. marisnigri*. Due to the lack of a reducing agent, O_2 contaminations of < 10 µM are likely present in all cultivation attempts. Therefore, as described in the results part, visualization with SEM and DAPI staining epifluorescence microscopy was performed to look for cell attachment of all three strains to Fe and Mn oxide particles. Attachment of *S. marisnigri* and *S. baltica* with MnO_2 as it is shown in Fig. 12, 13 and 14 was not observed when Fe oxides were provided as electron acceptor. No attachment of *S. gotlandica* with either Fe or Mn oxides was observed. Because the essential genes involved in the reduction of MnO_2 by *S. marisnigri* and *S. baltica* are currently unknown, this cannot be supported by the presence or absence of specific genes in the genome of *S. gotlandica*. The ability to re-

duce MnO_2 together with the inability to reduce Fe oxides by *S. marisnigri* and *S. baltica* is an important finding because it differs from the so far described organisms capable of organotrophic metal oxide reduction, which typically grow on different particulate electron acceptors like Fe, Cr, U or Tc (Lovley, 1991; Marshall et al., 2008; H. Lin et al., 2012). For *Shewanella oneidensis* MR-1, an organotrophic Mn reducing bacterium able to reduce Mn and Fe, it was shown, that different protein components are active for the reduction of either Fe or Mn (H. Lin et al., 2012). Thus, the inability for Fe reduction might just be a result of gene loss due to repeated cultivation with solely Mn. Nonetheless, similar findings were reported from anoxic sediments. SO_4^{2-} was formed in anoxic sediment slurries when MnO_2 was added, apparently based on biological activity, which could not be induced by the addition of Fe oxides (Aller & Rude, 1988; G. M. King, 1990). This may indicate a biological metabolism based on MnO_2 reduction without the ability to reduce Fe oxides. Interestingly, the authors of the respective works also reported the formation of Ca-rich $MnCO_3$.

4.3.2 Disproportionation

Whether disproportionation of S^0 and $S_2O_3^{2-}$ by *S. marisnigri*, *S. baltica* and *S. gotlandica* can support slow growth is difficult, as low amounts of O_2 contaminations could not be completely avoided, as described for metal oxide reduction. Nevertheless, in comparison with the well described disproportioning bacteria *Desulfocapsa sulfoexigens* (Finster et al., 1998), several differences appeared. *D. sulfoexigens* produced millimolar concentrations of H_2S with $S_2O_3^{2-}$ or S^0 as the sole energy source in the absence of Fe oxides, which are shown to oxidize H_2S chemically and precipitate as FeS and FeS_2 when they are provided (Finster et al., 1998). A production of millimolar concentrations of H_2S by *Sulfurimonas* would eliminate micromolar concentrations of O_2 and result in free H_2S, which would be detectable by H_2S microsensors and smell. This was not the case and even with higher cell numbers after an exponential growth phase exceeding 10^7 cells mL^{-1} (Fig. 33) $S_2O_3^{2-}$ concentrations remained constant.

Finally, *S. marisnigri* showed growth with $S_2O_3^{2-}$ as electron donor and NO_3^- as electron acceptor (Fig. 23 and 24). Growth was concurrent with the stoichiometric reduction of NO_3^- to NO_2^-, which cannot be attributed to $S_2O_3^{2-}$ disproportionation, because NO_3^- would not react chemically with H_2S as it might proceed in the presence of O_2 and MnO_2.

4.3.3 Electron donors

Sulfur oxidation

The ability to oxidize reduced sulfur compounds of *S. marisnigri*, *S. baltica* and *S. gotlandica* has been shown. *S. gotlandica* showed growth with S^0, $S_2O_3^{2-}$ and SO_3^{2-} (e.g. Fig. 23, 27 and 28) and *S. marisnigri* and *S. baltica* with H_2S, S^0 and $S_2O_3^{2-}$ (e.g. Fig. 17, 23, 27 and 37). Growth of *S. gotlandica* on H_2S is well known and has therefore not been tested in this study (Grote et al., 2012; Labrenz et al., 2013). *S. marisnigri* and *S. baltica* were unable to grow on SO_3^{2-}. The lack of the sulfite dehydrogenase (Sor) in the genome of *S. marisnigri*, encoded by *sorA* and *sorB,* may be responsible for the observed result (Fig. 28 and Tab. 29). A similar lack of metabolic potential has been reported for *S. denitrificans*, which also lacks the genes *sorA* and *sorB* and did not grow with SO_3^{2-} as electron donor (Timmer-ten Hoor, 1981; Sievert et al., 2008). SO_4^{2-} was the terminal end product of S oxidation by *S. marisnigri* in this study. Complete oxidation to SO_4^{2-} was already shown for *S. gotlandica* (Grote et al., 2012; Labrenz et al., 2013). Terminal oxidation product of H_2S, S^0 and $S_2O_3^{2-}$ of *S. baltica* was not investigated, but it can be presumed to be SO_4^{2-} based on the growth yields in comparison to *S. marisnigri* and *S. gotlandica*.

In the genome of *S. marisnigri* and all so far sequenced *Sulfurimonas* species a s*oxXYZAB* cluster, which is the basic configuration for the oxidation of reduced sulfur to SO_4^{2-} with a sox-cluster (Frigaard & Dahl, 2008) is present (see references in Tab 29). It is suggested, that residues of short chain polysulfides enter the sox system bound to SoxYZ and are oxidized to SO_4^{2-} in multiple steps (Frigaard & Dahl, 2008). For the phototrophic bacterium *Rhodovulum*

sulfidophilum, the sox system also seems to be essential for the utilization of H_2S as electron donor (Appia-Ayme et al., 2001), but sox deficient mutants of *Allochromatium vinosum* show wild-type rates of H_2S oxidation, suggesting different pathways for H_2S oxidation (Han & Perner, 2015).

In species of the genus *Sulfurimonas*, oxidation of H_2S is most probably catalyzed by the enzyme sulfide:quinone oxidoreductase (SQR). So far all sequenced *Sulfurimonas* species contain several types of *sqr*, potentially adapted to different levels of H_2S with varying H_2S affinities (Marcia et al., 2010). It is unclear, whether all types of SQR form the same sulfur intermediates, but short chains of polysulfides (S_n^{2-}) were thought to be the most likely product (Marcia et al., 2010; Han & Perner, 2015). Unlike hypothesized earlier (Steudel, 1996), the formation of S_n^{2-} is considered to be a product of biological H_2S oxidation rather than the product of the abiotical reaction of H_2S and S^0 (Frigaard & Dahl, 2008), and has been reported for *Sulfurimonas* sp. in cultures (Han & Perner, 2015). S_n^{2-} can enter the Sox pathway as described earlier (Frigaard & Dahl, 2008).

Next to a functional sox-operon (*soxXYZAB*), *S. gotlandica* also contains *soxCD* (Grote et al., 2012), which was not found in the genome of *S. marisnigri*. The absence of *soxCD* in *Paracoccus pantotrophus* resulted in the decreased yield of just two electrons when $S_2O_3^{2-}$ was provided as electron donor in contrast to an eight e^- yield when s*oxCD* was present (Friedrich et al., 2000, 2005). It is not stated whether these six electrons are used for the reduction of the respective electron acceptor without energy generation for cell metabolism or not. This could explain the difference in the growth yield between *S. gotlandica* and *S. marisnigri* (e.g. Fig. 26, positive controls), which will be demonstrated with a short calculation. The strains were cultivated as positive controls in the experiment to test for the assimilation of organic C with $S_2O_3^{2-}$ and MnO_2 for *S. marisnigri* and NO_3^- for *S. gotlandica* (Fig. 36). Because MnO_2 was limited in cultivation of *S. marisnigri* with $S_2O_3^{2-}$ and $S_2O_3^{2-}$ was limited in cultivation of *S. gotlandica* with NO_3^-, the respective limiting compound concentration was

chosen for the following calculation. 20 mM of electrons can be accepted by 10 mM of MnO_2 provided as electron acceptor for *S. marisnigri*. With a total yield of 1.7 x 10^{10} cells L^{-1}, 8.5 x 10^8 cells per millimol accepted e^- were generated. For *S. gotlandica*, 32 mM of e^- can be donated by the 4 mM $S_2O_3^{2-}$ provided. With a total yield of 1 x 10^{11} cells L^{-1}, 3.13 x 10^9 cells per millimol donated e^- are generated. Dividing the 3.13 x 10^9 by 8.5 x 10^8 gives a factor of 3.68, which may reflect the loss of electrons due to the lack of *soxCD* as shown by Friedrich et al. (2000) for *P. pantotrophus*. This difference is not observed when S^0 instead of $S_2O_3^{2-}$ is supplied as electron donor (Fig. 27). Further, based on experiments with *S. marisnigri* and *S. baltica* on NO_3^- as electron acceptor and successive additions of H_2S (Fig. 17), 1.67 x 10^9 cells per millimol donated e^- from H_2S are generated by both strains, a doubled growth yield compared to cultivation with $S_2O_3^{2-}$. Cultivation of *S. marisnigri* on MnO_2 and a constant supply of H_2S via a peristaltic pump (Fig. 16) resulted in the generation of 1.92 x 10^9 cells per millimol e^- based on the produced concentration of SO_4^{2-}, an even higher growth yield than in cultivations with NO_3^-.

4.3.4 Organic carbon oxidation, fermentation and sulfate reduction

The reduction of MnO_2 or NO_3^- by the utilization of organic carbon was not observed or far less important than inorganic electron donors, which results in an uncertain evaluation of this electron donor. Studies focusing on the consumption of educts and production of the metabolites would be necessary to provide evidence regarding organotrophic Mn reduction or denitrification under these culturing conditions. Further, pyruvate, amino acids and yeast extracts might also be worth to be tested as they can be utilized by *S. gotlandica* as shown by Labrenz et al. (2013). As pointed out before, dynamics of the metabolites would need to be recorded along with cell growth to address a potential activity with fermentation or sulfate reduction by *S. marisnigri*, *S. baltica* and *S. gotlandica*. Sulfate reduction seems unlikely, because *dsr* genes are not present in the genome of *S. marisnigri* and *S. gotlandica*.

4.3.5 Assimilatory metabolism

N_2 fixation

One of the most interesting findings is the ability of *S. marisnigri* and *S. baltica* to grow without the addition of NH_4^+ as N-source, apparently fixing molecular N_2. This has so far not been reported for the genus *Sulfurimonas*, but it is supported by the presence of genes encoding for nitrogen fixation (*nifUBTHQXEZN)* and by genes encoding for a Mo-Fe nitrogenase α- and β-chain (peg. 2006 and 2005, respectively) which are orthologue to *nifK* and *nifD*, which form the reaction center for N_2- fixation together with *nifH* (Mus et al., 2018). Compared to the respective positive controls (Fig. 35, black), growth was slower and the overall growth yield might be interpreted as lower, which could be explained by the high energy demand to break up the N≡N covalent bonds for the assimilation of molecular N (Havelka et al., 1982).

It is arguable whether this complex is used for the assimilation of nitrogen, because NH_4^+ is present in micromolar concentrations at the bottom boundary of the Black Sea suboxic zone, where *S. marisnigri* was isolated from and N_2 fixation is a highly energy demanding process.

CO_2 fixation

All tested *Sulfurimonas* strains are able to fix CO_2. Autotrophic CO_2 fixation by members of the *Epsilonbaceraeota* (Hügler et al., 2005) and the genus *Sulfurimonas* is done via the reductive tricarbolic acid cycle (rTCA). Key enzymes for the rTCA are 2-oxoglutarate:ferredoxin oxidoreductase (*oor*), pyruvate:ferredoxin oxidoreductase (*por*) and ATP-dependent citrate lyase (*acly*) (Aoshima, 2007), which are found in all sequenced *Sulfurimonas* genomes (See references in Tab. 29) and were also detected in *S. marisnigri* (Tab. 25).

Polyphosphate

Polyphosphate is a storage molecule linking phosphate residues with energy-rich phosphoranhydride bonds. Although polyP is found in every cell, the physiological function next to responsible genes for the accumulation or degradation of polyP is under debate and often

poorly understood (Kornberg et al., 1999). PolyP was observed in cells of *S. marisnigri* (Fig. 41), *S. baltica* (not shown) and *S. gotlandica* (Möller et al., 2019). Typically, two inclusions of polyP were located at the cell poles of rod shapes cells (Fig. 41), but cells with just one inclusion or without any polyP inclusions were also observed. Sometimes cells where noticeably longer and had more than two polyP inclusions, which was also reported by Lars Möller (Master thesis) for *S. gotlandica*. Next to the visible accumulation of polyP, genes involved in the formation (polyphosphate kinase, peg. 306) and degradation (exopolyphosphatase, peg. 1175) of polyP were found in the genome of *S. marisnigri*. Functions of polyP were reported to be manifold, ranging from energy (Brock & Schulz-Vogt, 2011; Möller et al., 2019) and P storage (Harold, 1962) to regulation of the cell metabolism (Kornberg et al., 1999). PolyP in *S. marisnigri* and *S. baltica* might also serve as energy storage for motility when electron donors or acceptors become limited and to survive under unfavorable conditions, as it is reported for *S. gotlandica* (Möller et al., 2019). Accumulation of polyP during high metabolic activity together with changing cell morphology when the electron donor is becoming limited might be an adaptation for small scale migration when Mn oxides are getting depleted while sinking into euxinic waters. Because the expression of polyphosphate kinases throughout the suboxic zone is most frequently done by the genus *Sulfurimonas* (Schulz-Vogt et al., 2019), polyP might have an important role for the live strategy of *Sulfurimonas* spp. in the Black Sea.

5 Conclusion and outlook

Growth of *S. marisnigri*, *S. baltica* and *S. gotlandica* was documented with the electron acceptors O_2 and NO_3^-, *S. marisnigri* and *S. baltica* showed growth also with MnO_2. This is the first report of manganese reduction within the genus *Sulfurimonas* and the first documented manganese reducing species able to oxidize reduced sulfur species in general. No growth was observed when Fe oxides were provided as terminal electron acceptors. Growth of all three strains with O_2 was supported by decreasing dissolved O_2 concentrations and the presence of *ccoNOQP* in the genome of *S. marisnigri* and *S. gotlandica*. In contrast to the denitrifying organism *S. gotlandica*, *S. marisnigri* reduced NO_3^- to NO_2^- without further reduction to N_2. Based on the growth yield, the absence of an overpressure at the end of the growth phase and the absence of growth with NO_2^- as electron acceptor, it is assumed, that *S. baltica* reduces NO_3^- to NO_2^- as it was shown for *S. marisnigri*. The inorganic electron donors H_2, H_2S, S^0 and $S_2O_3^{2-}$ supported growth of *S. marisnigri*, *S. baltica* and *S. gotlandica*, whereas SO_3^{2-} only supported growth of *S. gotlandica*. This was supported by the absence of *sorA* and *sorB* in the genome of *S. marisnigri* analogous to growth experiments and the genome reported for *S. denitrificans*. For the oxidation of reduced sulfur, *soxXYZAB* and multiple copies of *sqr* were found in the genome of *S. marisnigri*. The absence of *soxCD* might explain different growth yields in comparison with *S. gotlandica* when $S_2O_3^{2-}$ was provided as electron donor, which was not detectable when H_2S or S^0 were provided instead of $S_2O_3^{2-}$.

In the present study, *S. marisnigri* and *S. gotlandica* grew autotrophically, while *S. baltica* was able to grow also with acetate, succinate and propionate. Autotrophic growth by *S. marisnigri* with the reverse tricarboxylic acid cycle was confirmed by the presence of the three marker genes 2-oxoglutarate:ferredoxin oxidoreductase, pyruvate:ferredoxin oxidoreductase and ATP-dependent citrate lyase, similar to all so far sequenced *Sulfurimonas* strains. *S. marisnigri* and *S. baltica* showed growth in the absence of NH_4^+ with N_2 as the only

N source. The ability to fix molecular N_2 was so far not reported from species of the genus *Sulfurimonas* and should be confirmed with isotopically labeled incubation experiments. Nevertheless, a set of *nif* genes including *nifD*, *nifK* and *nifH* was detected in the genome of *S. marisnigri*, supporting the finding from the cultivation experiment. No sulfate reducing activity, fermentation or respiration of organic carbon was observed. No *dsr* genes were found in the genome of *S. marisnigri*, supporting the results from cultivation experiments. Respiration of organic material is reported for *S. gotlandica* but was not observed in this study. Disproportionation of S^0 and $S_2O_3^{2-}$ could not be completely ruled out but appeares unlikely. *S. marisnigri* and *S. baltica* grew from 0 °C to 25°C and 0 °C to 20 °C, respectively. Next to *S. gotlandica*, these are the only cultured psychrotolerant species of the genus *Sulfurimonas*. Growth was observed at near neutral pH with small differences between the three species. The presence of O_2 did not result in the absence of growth.

With this finding, the high abundance of *Sulfurimonas* spp. in the pelagic redoxcline of the Black Sea in the absence of O_2, NO_3^- and light offers a plausible explanation for measured CO_2 fixation rates in the depth of H_2S removal. The described energy metabolism is potentially of general importance for the interpretation of pelagic and sediment redox environments with implications for the biogeochemical formation and maintenance, respectively. It was shown, that the oxidation rate of H_2S is a major factor for the retention of H_2S at the lower boundary of the Black Sea suboxic zone and determines the shape of the concentration profile, indicating the importance of biological H_2S oxidation for the expansion of suboxic zones with undetectable concentrations of O_2 and H_2S.

The formation of $Mn(Ca)CO_3$ in experiments with *S. marisnigri* and *S. baltica*, even though it might be fostered by artificial culturing conditions, should be investigated in more detail. Biological reduction of Mn might facilitate the formation of Mn-carbonate precipitates by influencing the ambient concentration of dissolved Mn and CO_3^{2-} by sulfur oxidation with MnO_2 and concurrent increase in pH. Interestingly, the Ca content of the Mn(Ca)CO3 precipitates in

this study is analogue to precipitates found in Baltic Sea sediments. The reduction of MnO_2 by *S. marisnigri* lead to the formation of dissolved reactive Mn, putative Mn^{3+}, which is reported as an important intermediate in the pelagic and the sedimentary Mn cycle.

Finally, the change in the cell morphology of *S. marisnigri* when the electron acceptor is becoming limited, which was also reported from *S. gotlandica*, might be an important adaptation for survival in pelagic redoxclines together with polyphosphate as redox independent energy supply. A further study examining external factors such as stoichiometry of electron acceptor and donor and the influence onto polyphosphate metabolism and cell morphology might give an insight into the extraordinary live strategy of *Sulfurimonas* spp.

6 References

Aller, R. C., & Rude, P. D. (1988). Complete oxidation of solid phase sulfides by manganese and bacteria in anoxic marine sediments. *Geochimica et Cosmochimica Acta*, *52*(3), 751–765.

Aoshima, M. (2007). Novel enzyme reactions related to the tricarboxylic acid cycle: phylogenetic/functional implications and biotechnological applications. *Applied Microbiologie and Biotechnology*, *75*(2), 249–255.

Appia-Ayme, C., Little, P. J., Matsumoto, Y., Leech, A. P., & Berks, B. C. (2001). Cytochrome complex essential for photosynthetic oxidation of both thiosulfate and sulfide in *Rhodovulum sulfidophilum*. *Journal of Bacteriology*, *183*(20), 6107–6118.

Aziz, R. K., Bartels, D., Best, A. A., DeJongh, M., Disz, T., Edwards, R. A., Formsma, K., Gerdes, S., Glass, E. M., Kubal, M., & others. (2008). The RAST Server: rapid annotations using subsystems technology. *BMC Genomics*, *9*(1), 75.

Blumentals, I. I., Itoh, M., Olson, G. J., & Kelly, R. M. (1990). Role of polysulfides in reduction of elemental sulfur by the hyperthermophilic archaebacterium *Pyrococcus furiosus*. *Applied and Environmental Microbiology*, *56*(5), 1255–1262.

Bond, D. R., & Lovley, D. R. (2003). Electricity production by *Geobacter sulfurreducens* attached to electrodes. *Applied and Environmental Microbiology*, *69*(3), 1548–1555.

Bondar, C. (1991). Water flow and sediment transport of the Danube at its outlet into the Black Sea. *Meteorology and Hydrology*, *21*(1), 21–25.

Bonfield, J. K., & Whitwham, A. (2010). Gap5-editing the billion fragment sequence assembly. *Bioinformatics*, *26*(14), 1699–1703.

Böttcher, M. E. (1998). Manganese(II) partitioning during experimental precipitation of rhodochrosite-calcite solid solutions from aqueous solutions. *Marine Chemistry*, *62*, 287–297.

Brock, J., & Schulz-Vogt, H. N. (2011). Sulfide induces phosphate release from

polyphosphate in cultures of a marine *Beggiatoa* strain. *ISME Journal*, *5*, 497–506.

Brown, J., Colling, A., Park, D., Phillips, J., Rothery, D., & Wright, J. (1989). *Ocean chemistry and deep-sea sediments*. (G. Bearman, Ed.). Pergamon Press.

Burdige, D. J., & Nealson, K. H. (1985). Microbial manganese reduction by enrichment cultures from coastal marine sediments. *Applied and Environmental Microbiology*, *50*(2), 491–497.

Burdige, D. J., & Nealson, K. H. (1986). Chemical and microbiological studies of sulfide-mediated manganese reduction. *Geomicrobiology Journal*, *4*(4), 361–387.

Cai, L., Shao, M.-F., & Zhang, T. (2014). Non-contiguous finished genome sequence and description of *Sulfurimonas hongkongensis* sp. nov., a strictly anaerobic denitrifying, hydrogen- and sulfur-oxidizing chemolithoautotroph isolated from marine sediment. *Standards in Genomic Sciences*, *9*(3), 1302–1310.

Campbell, B. J., Engel, A. S., Porter, M. L., & Takai, K. (2006). The versatile ε-proteobacteria: key players in sulphidic habitats. *Nature Reviews*, *4*, 458–468.

Canfield, D. E., & Thamdrup, B. (2009). Towards a consistent classification scheme for geochemical environments, or, why we wish the term 'suboxic' would go away. *Geobiology*, *7*(4), 385–392.

Canfield, D. E., Thamdrup, B., & Kristensen, E. (2005). *Aquatic geomicrobiology*. (A. J. Southward, P. A. Tyler, C. M. Young, & L. A. Fuiman, Eds.). Gulf Professional Publishing.

Canstein, H. Von, Ogawa, J., Shimizu, S., & Lloyd, J. R. (2008). Secretion of flavins by *Shewanella* species and their role in extracellular electron transfer. *Applied and Environmental Microbiology*, *74*(3), 615–623.

Carman, R., & Rahm, L. (1997). Early diagenesis and chemical characteristics of interstitial water and sediments in the deep deposition bottoms of the Baltic proper. *Journal of Sea Research*, *37*, 25–47.

Chen, K. Y., & Morris, J. C. (1972). Kinetics of oxidation of aqueous sulfide by O_2. *Environmental Science & Technology*, *6*(6), 529–537.

Chevreux, B., Wetter, T., Suhai, S., & others. (1999). Genome sequence assembly using trace signals and additional sequence information. In *German conference on bioinformatics* (Vol. 99, pp. 45–56).

Cline, J. D. (1969). Spectrophotometric determination of hydrogen sulfide in natural waters. *Limnology and Oceanography*, *14*(3), 454–458.

Conrad, R., Schink, B., & Phelps, T. J. (1986). Thermodynamics of H_2-consuming and H_2-producing metabolic reactions in diverse methanogenic environments under in situ conditions. *FEMS Microbiology Ecology*, *38*, 353–360.

Dalsgaard, T., Stewart, F. J., Thamdrup, B., De Brabandere, L., Revsbech, N. P., Ulloa, O., Canfield, D. E., & DeLong, E. F. (2014). Oxygen at nanomolar levels reversibly suppresses process rates and gene expression in anammox and denitrification in the oxygen minimum zone of northern Chile. *mBio*, *5*(3), 1–14.

Dellwig, O., Leipe, T., März, C., Glockzin, M., Pollehne, F., Schnetger, B., Yakushev, E. V., Böttcher, M. E., & Brumsack, H. J. (2010). A new particulate Mn-Fe-P-shuttle at the redoxcline of anoxic basins. *Geochimica et Cosmochimica Acta*, *74*(24), 7100–7115.

Dellwig, O., Schnetger, B., Brumsack, H. J., Grossart, H. P., & Umlauf, L. (2012). Dissolved reactive manganese at pelagic redoxclines (part II): Hydrodynamic conditions for accumulation. *Journal of Marine Systems*, *90*(1), 31–41.

Dellwig, O., Schnetger, B., Meyer, D., Pollehne, F., Häusler, K., & Arz, H. W. (2018). Impact of the Major Baltic Inflow in 2014 on manganese cycling in the Gotland Deep (Baltic Sea). *Frontiers in Marine Science*, *5*, 1–20.

Dellwig, O., Wegwerth, A., Schnetger, B., Schulz, H., & Arz, H. W. (2019). Dissimilar behaviors of the geochemical twins W and Mo in hypoxic-euxinic marine basins. *Earth-Science Reviews*, *193*, 1–23.

Diaz, R. J., & Rosenberg, R. (2008). Spreading dead zones and consequences for marine ecosystems. *Science*, *321*(5891), 926–929.

Dowsett, D., Wirtz, T., & Yedra, L. (2017). HIM-SIMS: Correlative SE/chemical imaging at the limits of resolution. *Microscopy and Microanalysis*, *23*, 278–279.

El-Naggar, M. Y., Wanger, G., Leung, K. M., Yuzvinsky, T. D., Southam, G., Yang, J., Lau, W. M., Nealson, K. H., & Gorby, Y. A. (2010). Electrical transport along bacterial nanowires from *Shewanella oneidensis* MR-1. *Proceedings of the National Academy of Sciences of the United States of America*, *107*(42), 18127–18131.

Evans, C. L. (1967). The toxicity of hydrogen sulphide and other sulphides. *Quarterly Journal of Experimental Physiology and Cognate Medical Sciences*, *52*(3), 231–248.

Finster, K., Liesack, W., & Thamdrup, B. (1998). Elemental sulfur and thiosulfate disproportionation by *Desulfocapsa sulfoexigens* sp. nov., a new anaerobic bacterium isolated from marine surface sediment. *Applied and Environmental Microbiology*, *64*(1), 119–125.

Friedrich, C. G., Bardischewsky, F., Rother, D., Quentmeier, A., & Fischer, J. (2005). Prokaryotic sulfur oxidation. *Current Opinion in Microbiology*, *8*, 253–259.

Friedrich, C. G., Quentmeier, A., Bardischewsky, F., Rother, D., Kraft, R., Kostka, S., & Prinz, H. (2000). Novel genes coding for lithotrophic sulfur oxidation of *Paracoccus pantotrophus* GB17. *Journal of Bacteriology*, *182*(17), 4677–4687.

Frigaard, N.-U., & Dahl, C. (2008). Sulfur metabolism in phototrophic sulfur bacteria. *Advances in Microbial Physiology*, *54*, 103–200.

Froelich, P. N., Klinkhammer, G. P., Bender, M. L., Luedtke, N. A., Heath, G. R., Cullen, D., Dauphin, P., Hammond, D., Hartman, B., & Maynard, V. (1979). Early oxidation of organic matter in pelagic sediments of the eastern equatorial Atlantic: suboxic diagenesis. *Geochimica et Cosmochimica Acta*, *43*(7), 1075–1090.

García-Robledo, E., Corzo, A., & Papaspyrou, S. (2014). A fast and direct spectrophotometric

method for the sequential determination of nitrate and nitrite at low concentrations in small volumes. *Marine Chemistry*, *162*, 30–36.

Glasby, G. P., & Schulz, H. D. (1999). EH, pH diagrams for Mn, Fe, Co, Ni, Cu and As under seawater conditions: Application of two new types of EH, pH diagrams to the study of specific problems in marine geochemistry. *Aquatic Geochemistry*, *5*, 227–248.

Glazer, B. T., Luther, G. W., Konovalov, S. K., Friederich, G. E., Nuzzio, D. B., Trouwborst, R. E., Tebo, B. M., Clement, B., Murray, K., & Romanov, A. S. (2006). Documenting the suboxic zone of the Black Sea via high-resolution real-time redox profiling. *Deep-Sea Research Part II: Topical Studies in Oceanography*, *53*, 1740–1755.

Gregg, M. C., & Yakushev, E. (2005). Surface ventilation of the Black Sea's cold intermediate layer in the middle of the western gyre. *Geophysical Research Letters*, *32*, 1–4.

Grote, J., Jost, G., Labrenz, M., Herndl, G. J., & Jürgens, K. (2008). *Epsilonproteobacteria* represent the major portion of chemoautotrophic bacteria in sulfidic waters of pelagic redoxclines of the Baltic and Black Seas. *Applied and Environmental Microbiology*, *74*(24), 7546–7551.

Grote, J., Labrenz, M., Pfeiffer, B., Jost, G., & Jürgens, K. (2007). Quantitative distributions of *Epsilonproteobacteria* and a *Sulfurimonas* subgroup in pelagic redoxclines of the central Baltic Sea. *Applied and Environmental Microbiology*, *73*(22), 7155–7161.

Grote, J., Schott, T., Bruckner, C. G., Glöckner, F. O., Jost, G., Teeling, H., Labrenz, M., & Jürgens, K. (2012). Genome and physiology of a model Epsilonproteobacterium responsible for sulfide detoxification in marine oxygen depletion zones. *Proceedings of the National Academy of Sciences of the United States of America*, *109*(2), 506–510.

Guieu, C., Martin, J.-M., Tankéré, S. P. C., Mousty, F., Trincherini, P., Bazot, M., & Dai, M. H. (1998). On trace metal geochemistry in the Danube River and western Black Sea. *Estuarine, Coastal and Shelf Science*, *47*, 471–485.

Han, Y., & Perner, M. (2015). The globally widespread genus *Sulfurimonas*: versatile energy metabolisms and adaptations to redox clines. *Frontiers in Microbiology*, *6*, 1–17.

Harold, F. M. (1962). Depletion and replenishment of the inorganic polyphosphate pool in *Neurospora crassa*. *Journal of Bacteriology*.

Häusler, K., Dellwig, O., Schnetger, B., Feldens, P., Leipe, T., Moros, M., Pollehne, F., Schönke, M., Wegwerth, A., & Arz, H. W. (2018). Massive Mn carbonate formation in the Landsort Deep (Baltic Sea): Hydrographic conditions, temporal succession, and Mn budget calculations. *Marine Geology*, *395*, 260–270.

Havelka, U. D., Boyle, M. G., & Hardy, R. W. F. (1982). Biological nitrogen fixation. *Nitrogen in Agricultural Soils*, 365–422.

Henkel, J. V, Dellwig, O., Pollehne, F., Herlemann, D. P. R., Leipe, T., & Schulz-Vogt, H. N. (2019). A bacterial isolate from the Black Sea oxidizes sulfide with manganese(IV) oxide. *Proceedings of the National Academy of Sciences of the United States of America*, *116*(25), 12153–12155.

Hermans, M., Lenstra, W. K., Helmond, N. A. G. M. Van, Behrends, T., Egger, M., Séguret, M. J. M., Gustafsson, B. G., & Slomp, C. P. (2019). Impact of natural re-oxygenation on the sediment dynamics of manganese, iron and phosphorus in a euxinic Baltic Sea basin. *Geochimica et Cosmochimica Acta*, *246*, 174–196.

Herszage, J., & dos Santos Afonso, M. (2003). Mechanism of hydrogen sulfide oxidation by manganese(IV) oxide in aqueous solutions. *Langmuir*, *19*, 9684–9692.

Ho, T. Y., Taylor, G. T., Astor, Y., Varela, R., Müller-Karger, F., & Scranton, M. I. (2004). Vertical and temporal variability of redox zonation in the water column of the Cariaco Basin: Implications for organic carbon oxidation pathways. *Marine Chemistry*, *86*, 89–104.

Hügler, M., Wirsen, C. O., Fuchs, G., Taylor, C. D., & Sievert, S. M. (2005). Evidence for autotrophic CO_2 fixation via the reductive tricarboxylic acid cycle by members of the ε

subdivision of proteobacteria. *Journal of Bacteriology*, *187*(9), 3020–3027.

Inagaki, F., Takai, K., Kobayashi, H., Nealson, K. H., & Horikoshi, K. (2003). *Sulfurimonas autrotrophica* gen. nov., sp. nov., a novel sulfur-oxidizing ε-proteobacterium isolated from hydrothermal sediments in the Mid-Okinawa Trough. *International Journal of Systematic and Evolutionary Microbiology*, *53*(6), 1801–1805.

Jannasch, H. W., Wirsen, C. O., & Molyneaux, S. J. (1991). Chemoautotrophic sulfur-oxidizing bacteria from the Black Sea. *Deep Sea Research Part A. Oceanographic Research Papers*, *38*, S1105–S1120.

Jaoshvili, S. (2002). *The rivers of the Black Sea*. (I. Khomerki, G. Gigineishvili, & A. Kordzadze, Eds.). European Environment Agency Copenhagen.

Jensen, M. M., Kuypers, M. M. M., Lavik, G., & Thamdrup, B. (2008). Rates and regulation of anaerobic ammonium oxidation and denitrification in the Black Sea. *Limnology and Oceanography*, *53*(1), 23–36.

Jørgensen, B. B. (1982). Mineralization of organic matter in the sea bed – the role of sulphate reduction. *Nature*.

Jørgensen, B. B. (2000). Bacteria and marine biogeochemistry. *Marine Geochemistry*, 173–207.

Jørgensen, B. B., Findlay, A. J., & Pellerin, A. (2019). The biogeochemical sulfur cycle of marine sediments. *Frontiers in Microbiology*, *10*, 1–27.

Jørgensen, B. B., Fossing, H., Wirsen, C. O., & Jannasch, H. W. (1991). Sulfide oxidation in the anoxic Black Sea chemocline. *Deep Sea Research Part A. Oceanographic Research Papers*, *38*, 1083–1103.

Jørgensen, B. B., & Revsbech, N. P. (1983). Colorless sulfur bacteria, Beggiatoa sp. and Thiovulum sp. in O2 and H2S microgradients. *Applied and Environmental Microbiology*, *45*(4), 1261–1270.

Jost, G., Martens-Habbena, W., Pollehne, F., Schnetger, B., & Labrenz, M. (2010). Anaerobic

sulfur oxidation in the absence of nitrate dominates microbial chemoautotrophy beneath the pelagic chemocline of the eastern Gotland Basin, Baltic Sea. *FEMS Microbiology Ecology*, *71*, 226–236.

Kelly, D. P. (1982). Biochemistry of the chemolithotrophic oxidation of inorganic sulphur. *Philosophical Transactions of the Royal Society B*, *298*, 499–528.

King, C. (2004). *The Black Sea: A history*. Oxford University Press, USA.

King, G. M. (1990). Effects of added manganic and ferric oxides on sulfate reduction and sulfide oxidation in intertidal sediments. *FEMS Microbiology Ecology*, *73*, 131–138.

Kirchman, D. L. (1999). Bacterial biogeochemistry: The ecophysiology of mineral cycling. *Limnology and Oceanography*. Elsevier, San Diego.

Koch, C., Günther, S., Desta, A. F., Hübschmann, T., & Müller, S. (2013). Cytometric fingerprinting for analyzing microbial intracommunity structure variation and identifying subcommunity function. *Nature Protocols*, *8*(1), 190.

Kornberg, A., Rao, N. N., & Ault-Riché, D. (1999). Inorganic polyphosphate: A molecule of many functions. *Annu. Rev. Biochem.*, *68*, 89–125.

Kuypers, M. M. M., Sliekers, A. O., Lavik, G., Schmid, M., Jørgensen, B. B., Kuenen, J. G., S., S. D. J., Strous, M., & Jetten, M. S. M. (2003). Anaerobic ammonium oxidation by anammox bacteria in the Black Sea. *Nature*, *422*(6932), 608–611.

Labrenz, M., Grote, J., Mammitzsch, K., Boschker, H. T. S., Laue, M., Jost, G., Glaubitz, S., & Jurgens, K. (2013). *Sulfurimonas gotlandica* sp. nov., a chemoautotrophic and psychrotolerant epsilonproteobacterium isolated from a pelagic redoxcline, and an emended description of the genus *Sulfurimonas*. *International Journal of Systematic and Evolutionary Microbiology*, *63*, 4141–4148.

Lenz, C., Jilbert, T., Conley, D. J., & Slomp, C. P. (2015). Hypoxia-driven variations in iron and manganese shuttling in the Baltic Sea over the past 8 kyr. *Geochemistry, Geophysics, Geosystems*, *16*, 3754–3766.

Lewis, B. L., & Landing, W. M. (1991). The biogeochemistry of manganese and iron in the Black Sea. *Deep Sea Research Part A. Oceanographic Research Papers*, *38*, 773–803.

Lin, H., Szeinbaum, N. H., DiChristina, T. J., & Taillefert, M. (2012). Microbial Mn(IV) reduction requires an initial one-electron reductive solubilization step. *Geochimica et Cosmochimica Acta*, *99*, 179–192.

Lin, X., Wakeham, S. G., Putnam, I. F., Yrene, M., Scranton, M. I., Chistoserdov, A. Y., Taylor, T., Astor, Y. M., & Taylor, G. T. (2006). Comparison of vertical distributions of prokaryotic assemblages in the anoxic Cariaco Basin and Black Sea by use of fluorescence in situ hybridization. *Applied and Environmental Microbiology*, *72*(4), 2679–2690.

Lovley, D. R. (1991). Dissimilatory Fe(III) and Mn(IV) reduction. *Microbiological Reviews*, *55*(2), 259–287.

Lovley, D. R., & Phillips, E. J. P. (1986). Organic matter mineralization with reduction of ferric iron in anaerobic sediments. *Applied and Environmental Microbiology*, *51*(4), 683–689.

Luther III, G. W. (2010). The role of one- and two-electron transfer reactions in forming thermodynamically unstable intermediates as barriers in multi-electron redox reactions. *Aquatic Geochemistry*, *16*, 395–420.

Luther III, G. W., Church, T. M., & Powell, D. (1991). Sulfur speciation and sulfide oxidation in the water column of the Black Sea. *Deep Sea Research Part A. Oceanographic Research Papers*, *38*, 1121–1137.

Mandernack, K. W., & Tebo, B. M. (1999). In situ sulfide removal and CO_2 fixation rates at deep-sea hydrothermal vents and the oxic/anoxic interface in Framvaren Fjord, Norway. *Marine Chemistry*, *66*(3–4), 201–213.

Marchant, H. K., Ahmerkamp, S., Lavik, G., Tegetmeyer, H. E., Graf, J., Klatt, J. M., Holtappels, M., Walpersdorf, E., & Kuypers, M. M. M. (2017). Denitrifying community

in coastal sediments performs aerobic and anaerobic respiration simultaneously. *ISME Journal*, *11*(8), 1799–1812.

Marcia, M., Ermler, U., Peng, G., & Michel, H. (2010). A new structure based classification of sulfide:quinone oxidoreductases. *Proteins: Structure, Function, and Bioinformatics*, *78*(5), 1073–1083.

Marie, D., Partensky, F., Jacquet, S., & Vaulot, D. (1997). Enumeration and cell cycle analysis of natural populations of marine picoplankton by flow cytometry using the nucleic acid stain SYBR Green I. *Applied and Environmental Microbiology*, *63*(1), 186–193.

Marshall, M. J., Plymale, A. E., Kennedy, D. W., Shi, L., Wang, Z., Reed, S. B., Dohnalkova, A. C., Simonson, C. J., Liu, C., Saffarini, D. A., Romine, M. F., Zachara, J. M., Beliaev, A. S., & Fredrickson, J. K. (2008). Hydrogenase- and outer membrane c -type cytochrome-facilitated reduction of technetium (VII) by *Shewanella oneidensis* MR-1. *Environmental Microbiology*, *10*, 125–136.

Marsili, E., Baron, D. B., Shikhare, I. D., Coursolle, D., Gralnick, J. A., & Bond, D. R. (2008). *Shewanella* secretes flavins that mediate extracellular electron transfer. *Proceedings of the National Academy of Sciences of the United States of America*, *105*(10), 3968–3973.

Matthäus, W., & Franck, H. (1992). Characteristics of major Baltic inflows - a statistical analysis. *Continental Shelf Research*, *12*(12), 1375–1400.

Middelburg, J. J., De Lange, G. J., & van Der Weijden, C. H. (1987). Manganese solubility control in marine pore waters. *Geochimica et Cosmochimica Acta*, *51*(3), 759–763.

Möller, L., Laas, P., Rogge, A., Goetz, F., Bahlo, R., Leipe, T., & Labrenz, M. (2019). *Sulfurimonas* subgroup GD17 cells accumulate polyphosphate under fluctuating redox conditions in the Baltic Sea: possible implications for their ecology. *The ISME Journal*, *13*, 482–493.

Mucci, A. (1988). Manganese uptake during calcite precipitation from seawater: Conditions leading to the formation of a pseudokutnahorite. *Geochimica et Cosmochimica Acta*, *52*(7), 1859–1868.

Murray, J. W., Jannasch, H. W., Honjo, S., Anderson, R. F., Reeburgh, W. S., Top, Z., Friederich, G. E., Codispoti, L. A., & Izdar, E. (1989). Unexpected changes in the oxic/anoxic interface in the Black Sea. *Nature*, *338*(6214), 411–413.

Murray, J. W., Top, Z., & Özsoy, E. (1991). Hydrographic properties and ventilation of the Black Sea. *Deep Sea Research Part A. Oceanographic Research Papers*, *38*, 663–689.

Murray, J. W., & Yakushev, E. V. (2006). The suboxic transition zone in the Black Sea. In L. N. Neretin (Ed.), *Past and Present Water Column Anoxia* (Vol. 64, pp. 105–138). Kluwer Academic Publishers.

Mus, F., Alleman, A. B., Pence, N., Seefeldt, L. C., & Peters, J. W. (2018). Exploring the alternatives of biological nitrogen fixation. *Metallomics*, *10*, 523–538.

Myers, C. R., & Myers, J. . M. (2003). Cell surface exposure of the outer membrane cytochromes of *Shewanella oneidensis* MR-1. *Letters in Applied Microbiology*, *37*, 254–258.

Myers, C. R., & Nealson, K. H. (1988). Bacterial manganese reduction and growth with manganese oxide as the sole electron acceptor. *Science*, *240*, 1319–1321.

Nelson, D. C., Jørgensen, B. B., & Revsbech, N. P. (1986). Growth pattern and yield of a chemoautotrophic *Beggiatoa* sp. in oxygen-sulfide microgradients. *Applied and Environmental Microbiology*, *52*(2), 225–233.

Neretin, L. N., Volkov, I. I., Rozanov, A. G., Demidova, T. P., & Falina, A. S. (2006). Biogeochemistry of the Black Sea anoxic zone with a reference to the sulphur cycle. In L. N. Neretin (Ed.), *Past and Present Water Column Anoxia* (pp. 67–104). Dordrecht: Springer Netherlands.

Neumann, T., Heiser, U., Leosson, M. A., & Kersten, M. (2002). Early diagenetic processes

during Mn-carbonate formation: Evidence from the isotopic composition of authigenic Ca-rhodochrosites of the Baltic Sea. *Geochimica et Cosmochimica Acta*, *66*(5), 867–879.

Nevin, K. P., & Lovley, D. R. (2002). Mechanisms for accessing insoluble Fe (III) oxide during dissimilatory Fe (III) reduction by *Geothrix fermentans*. *Applied and Environmental Microbiology*, *68*(5), 2294–2299.

Nielsen, L. P., & Risgaard-Petersen, N. (2014). Rethinking sediment biogeochemistry after the discovery of electric currents. *Annual Review of Marine Science*, *7*(1), 425–442.

Nurk, S., Bankevich, A., Antipov, D., Gurevich, A., Korobeynikov, A., Lapidus, A., Prjibelsky, A., Pyshkin, A., Sirotkin, A., Sirotkin, Y., Stepanauskas, R., McLean, J., Lasken, R., Clingenpeel, S. R., Woyke, T., Tesler, G., Alekseyev, M. A., & Pevzner, P. A. (2013). Assembling genomes and mini-metagenomes from highly chimeric reads. In M. Deng, R. Jiang, F. Sun, & X. Zhang (Eds.), *Research in Computational Molecular Biology* (pp. 158–170). Berlin, Heidelberg: Springer Berlin Heidelberg.

Oguz, T., Latun, V. S., Latif, M. A., Vladimirov, V. V., Sur, H. I., Markov, A. A., Özsoy, I. E., Kotovshchikov, B. B., Egemeev, V. V, & Ünlüata, Ü. (1993). Circulation in the surface and intermediate layers of the Black Sea. *Deep Sea Research Part I*, *40*(8), 1597–1612.

Overmann, J., Cypionka, H., & Pfennig, N. (1992). An extremely low-light-adapted phototrophic sulfur bacterium from the Black Sea. *Limnology and Oceanography*, *37*(l), 150–155.

Özsoy, E., & Ünlüata, Ü. (1997). Oceanography of the Black Sea: a review of some recent results. *Earth-Science Reviews*, *42*, 231–272.

Pirbadian, S., Barchinger, S. E., Leung, K. M., Byun, H. S., Jangir, Y., Bouhenni, R. A., Reed, S. B., Romine, M. F., Saffarini, D. A., Shi, L., Gorby, Y. A., Golbeck, J. H., & El-Naggar, M. Y. (2014). *Shewanella oneidensis* MR-1 nanowires are outer membrane and periplasmic extensions of the extracellular electron transport components. *Proceedings*

of the National Academy of Sciences of the United States of America, *111*(35), 12883–12888.

Pitcher, R. S., & Watmough, N. J. (2004). The bacterial cytochrome *cbb*$_3$ oxidases. *Biochimica et Biophysica Acta*, *1655*, 388–399.

Polerecky, L., Adam, B., Milucka, J., Musat, N., Vagner, T., & Kuypers, M. M. M. (2012). Look@NanoSIMS – a tool for the analysis of nanoSIMS data in environmental microbiology. *Environmental Microbiology*, *14*(4), 1009–1023.

Ramsing, N., & Gundersen, J. (2011). Seawater and gases. *Limnol. Oceanogr*, *37*, 1307–1312.

Rickard, D., & Luther III, G. W. (2007). Chemistry of iron sulfides. *Chemical Reviews*, *107*(2), 514–562.

Schmidtko, S., Stramma, L., & Visbeck, M. (2017). Decline in global oceanic oxygen content during the past five decades. *Nature*, *542*(7641), 335–339.

Schnetger, B., & Dellwig, O. (2012). Dissolved reactive manganese at pelagic redoxclines (part I): A method for determination based on field experiments. *Journal of Marine Systems*, *90*, 23–30.

Schulz-Vogt, H. N., Pollehne, F., Jürgens, K., Arz, H. W., Bahlo, R., Dellwig, O., Henkel, J. V, Herlemann, D. P. R., Krüger, S., Leipe, T., & Schott, T. (2019). Effect of large magnetotactic bacteria with polyphosphate inclusions on the phosphate profile of the suboxic zone in the Black Sea. *ISME Journal*, *13*, 1198–1208.

Schulz, H. D. (2006). Conceptual models and computer models. In H. D. Schulz & M. Zabel (Eds.), *Marine Geochemistry* (pp. 513–547). Springer.

Sievert, S. M., Scott, K. M., Klotz, M. G., Chain, P. S. G., Hauser, L. J., Hemp, J., Hu, M., Land, M., Lapidus, A., Larimer, F. W., Lucas, S., Malfatti, S. A., Meyer, F., Paulsen, I. T., Ren, Q., Simon, J., & Class, U. G. (2008). Genome of the Epsilonproteobacterial chemolithoautotroph *Sulfurimonas denitrificans*. *Applied and Environmental*

Microbiology, *74*(4), 1145–1156.

Sikorski, J., Munk, C., Lapidus, A., Djao, O. D. N., Lucas, S., Glavina Del Rio, T., Nolan, M., Tice, H., Han, C., Cheng, J.-F., Tapia, R., Goodwin, L., Pitluck, S., Liolios, K., Ivanova, N., Mavromatis, K., Mikhailova, N., … Klenk, H.-P. (2010). Complete genome sequence of *Sulfurimonas autotrophica* type strain (OK10T). *Standards in Genomic Sciences*, *3*(2), 194–202.

Siu, T., & Jia, C. Q. (1999). Kinetics of reaction of sulfide with thiosulfate in aqueous solution. *Industrial & Engineering Chemistry Research*, *38*, 1306–1309.

Steudel, R. (1996). Mechanism for the formation of elemental Sulfur from aqueous sulfide in chemical and microbiological desulfurization processes. *Industrial and Engineering Chemistry Research*, *35*(4), 1417–1423.

Stramma, L., Johnson, G. C., Sprintall, J., & Mohrholz, V. (2008). Expanding oxygen-minimum zones in the tropical oceans. *Science*, *320*(5876), 655–658.

Stumm, W., & Morgan, J. J. (1996). *Aquatic Chemistry: Chemical equilibria and rates in natural waters*. Wiley.

Sulu-gambari, F., Roepert, A., Jilbert, T., Hagens, M., Meysman, F. J. R., & Slomp, C. P. (2017). Molybdenum dynamics in sediments of a seasonally-hypoxic coastal marine basin. *Chemical Geology*, *466*, 627–640.

Takai, K., Campbell, B. J., Cary, S. C., Suzuki, M., Oida, H., Nunoura, T., Hirayama, H., Nakagawa, S., Suzuki, Y., Inagaki, F., & Horikoshi, K. (2005). Enzymatic and genetic characterization of carbon and energy metabolisms by deep-sea hydrothermal chemolithoautotrophic isolates of *Epsilonproteobacteria*. *Applied and Environmental Microbiology*, *71*(11), 7310–7320.

Takai, K., Suzuki, M., Nakagawa, S., Miyazaki, M., Suzuki, Y., Inagaki, F., & Horikoshi, K. (2006). *Sulfurimonas paralvinellae* sp. nov., a novel mesophilic, hydrogen- and sulfur-oxidizing chemolithoautotroph within the *Epsilonproteobacteria* isolated from a deep-

sea hydrothermal vent polychaete nest, reclassification of *Thiomicrospira denitrificans* as *Sulfurimonas denitrificans* comb. nov. and emended description of the genus *Sulfurimonas*. *International Journal of Systematic and Evolutionary Microbiology*, *56*(8), 1725–1733.

Taylor, G. T., Iabichella, M., Ho, T., Scranton, M. I., Thunell, R. C., Muller-Karger, F., & Varela, R. (2001). Chemoautotrophy in the redox transition zone of the Cariaco Basin: A significant midwater source of organic carbon production. *Limnology and Oceanography*, *46*(1), 148–163.

Tebo, B. M. (1991). Manganese(II) oxidation in the suboxic zone of the Black Sea. *Deep Sea Research Part A. Oceanographic Research Papers*, *38*, 883–905.

Tebo, B. M., Bargar, J. R., Clement, B. G., Dick, G. J., Murray, K. J., Parker, D., Verity, R., & Webb, S. M. (2004). Biogenic manganese oxides: Properties and mechanisms of formation. *Annual Review of Earth and Planetary Sciences*, *32*, 287–328.

Thamdrup, B. (2000). Bacterial manganese and iron reduction in aquatic sediments. In *Advances in microbial ecology* (pp. 41–84). Springer.

Thauer, R. K., Jungermann, K., & Decker, K. (1977). Energy conservation in chemotrophic anaerobic bacteria. *Bacteriological Reviews*, *41*(1), 100–180.

Timmer-ten Hoor, A. (1975). A new type of thiosulphate oxidizing, nitrate reducing microorganism: *Thiomicrospira denitrificans* sp. nov. *Netherlands Journal of Sea Research*, *9*(3–4), 344–350.

Timmer-ten Hoor, A. (1981). Cell yield and bioenergetics of *Thiomicrospira denitrificans* comapred with *Thiobacillus denitrificans*. *Antonie van Leeuwenhoek*, *47*, 231–243.

Vollnhals, F., Audinot, J.-N., Wirtz, T., Mercier-Bonin, M., Fourquaux, I., Schroeppel, B., Kraushaar, U., Lev-Ram, V., Ellisman, M. H., & Eswara, S. (2017). Correlative microscopy combining secondary ion mass spectrometry and electron microscopy: Comparison of intensity–hue–saturation and laplacian pyramid methods for image

fusion. *Analytical Chemistry*, *89*(20), 10702–10710.

Widdel, F., & Pfennig, N. (1981). Studies on dissimilatory sulfate-reducing bacteria that decompose fatty acids - I. Isolation of new sulfate-reducing bacteria enriched with acetate from saline environments. Description of *Desulfobacter postgatei* gen. nov., sp. nov. *Archives of Microbiology*, *129*(5), 395–400.

Wirtz, T., Philipp, P., Audinot, J.-N., Dowsett, D., & Eswara, S. (2015). High-resolution high-sensitivity elemental imaging by secondary ion mass spectrometry: from traditional 2D and 3D imaging to correlative microscopy. *Nanotechnology*, *26*(43) doi:10.1088/0957-4484/26/43/434001.

Yakushev, E. V., Chasovnikov, V. K., Debolskaya, E. I., Egorov, A. V., Makkaveev, P. N., Pakhomova, S. V., Podymov, O. I., & Yakubenko, V. G. (2006). The northeastern Black Sea redox zone: Hydrochemical structure and its temporal variability. *Deep-Sea Research Part II: Topical Studies in Oceanography*, *53*(17–19), 1769–1786.

Yao, W., & Millero, F. H. (1996). Oxidation of hydrogen sulfide by Mn(IV) and Fe(III) (hydr)oxides in seawater. *Marine Chemistry*, *52*, 1–16.

Yao, W., & Millero, F. J. (1993). The rate of sulfide oxidation by δMnO_2 in seawater. *Geochimica et Cosmochimica Acta*, *57*, 3359–3365.

Zaikova, E., Walsh, D. A., Stilwell, C. P., Mohn, W. W., Tortell, P. D., & Hallam, S. J. (2010). Microbial community dynamics in a seasonally anoxic fjord: Saanich Inlet, British Columbia. *Environmental Microbiology*, *12*(1), 172–191.

Zopfi, J., Ferdelman, T. G., & Fossing, H. (2004). Distribution and fate of sulfur intermediates - sulfite, tetrathionate, thiosulfate and elemental sulfur - in marine sediments. *Special Paper of the Geological Society of America*, *379*, 17–34.

7 Acknowledgements

I thank **Prof. Dr. Heide Schulz-Vogt** for several years of support and supervision. An always open door, an open mind for discussion at eye level and openness for new and not always bearing fruit ideas are exceptional and not taken for granted.

I thank my thesis committee including **Prof. Dr. Heide Schulz-Vogt**, **Dr. Falk Pollehne**, **Dr. Olaf Dellwig**, **Dr. Kai Finster**, **Dr. Matthias Labrenz** and **Prof. Dr. Friedrich Widdel** for assistance and guidance throughout the time of the dissertation.

I thank the **Deutsche Forschungsgemeinschaft (DfG)** for funding the project ANAMARE (grant number SCHU1416/5-1).

I thank the **working group 'Geomikrobiologie'** and the **working group 'Mikrobielle Prozesse und Phosphorkreislauf'** at the IOW for several years of discussion even though I missed a lot of the meetings.

I thank **Prof. Dr. Klaus Jürgens** for the permission to use environmental data of bacterial abundances and molecular data of *Epsilonbacteraeota* and *Sulfurimonas* of the Black Sea.

I thank **Christin Laudan** for years of help and joy in- and outside the lab.

I thank **Christian Burmeister**, **Christian Meeske**, **Anne Köhler**, **Katja Käding**, **Ronny Baaske**, **Sascha Plewe, Bolle** and **Stefan Otto** for lab assistance and help with methodology.

I thank **Dr. Olaf Dellwig** for important contribution in the work concerning manganese analysis, general criticism and discussion.

I thank **Dr. Falk Pollehne** for helpful discussion regarding the complex biogeochemical system of the Black Sea.

I thank **Dr. Thomas Schott** for the bioinformatics procession of the genomic sequence data of *S. marisnigri* and *S. gotlandica.*

I thank **Dr. Patricia Roeser** for providing helpful comments, discussion and information regarding natural manganese-carbonate depositories.

I thank **Dr. Angela Vogts** and **Annett Grüttmüller** for Nano-SIMS analysis and help with the look@NanoSIMS tool.

I thank **Dr. Thomas Leipe** for the analysis of TIC.

I thank **Prof. Dr. Klaus Jürgens**, **Prof. Dr. Daniel Herlemann, Dr. Matthias Labrenz** and **Dr. Peter Holtermann** for discussion, ideas in the office and the corridors of the IOW.

I thank **Jelena Lovric** for HIM-SIMS analysis of the *S. marisnigri* culture.

I thank the **workshop of the IOW** for providing fast and useful handmade tools for experimental setups.

I thank the **EDV of the IOW** for immediate help with technical problems of the PC.

I thank the **R** and **Stack Overflow community** for offering an inexhaustible amount of information free of charge.

I thank **Tobias Apelt** for the permission to include some results of his Bachelor Thesis.

I thank **Solveig Kühl** for an always open door and help with every part of bureaucracy I had to struggle with.

I thank **Philipp Braun**, **René Janßen**, **Katharina Kesy, Simon Langer**, **Lars Möller** and **Mirco Haseler** as fellow sufferers to the aim of receiving a doctor's degree.

I thank **Franziska**, **Lina**, **Falk**, **Hendrik**, **NV**, and **Franziska** for the daily conversations about work and private life.

I thank **Jakob**, **Vivi**, **Dajana**, **Stege**, **Matze**, **Moritz**, **Katrin**, **Ron**, **Wolfer**, **Anne**, **Basti**, **Frank**, **Björni**, **Schelly**, **Lukas** und **Flo**.

I thank **Patrick**, **Bat**, **Felix**, **Manuel** and **Oizo**.

I thank **Christian Stolle**, **Judith Piontek**, **Dandan Shen** and **Jenny Fabian** for a great working atmosphere and an open ear for complaints concerning technical issues in the office.

I thank my **family** for support in every imaginable situation.

I thank **Laura Fuchs** for the last years and especially the patience throughout the last months writing this thesis.

Erklärung

Hiermit versichere ich, dass ich die vorliegende Arbeit selbstständig angefertigt und ohne fremde Hilfe verfasst habe, keine außer den von mir angegebenen Hilfsmitteln und Quellen dazu verwendet habe und die den benutzten Werken inhaltlich und wörtlich entnommenen Stellen als solche kenntlich gemacht habe.

Rostock, _____ _____

Unterschrift